$SU(3)$ Squeezing: Quantum and Semiclassical Evolutions

by

Hossein Tavakoli Dinani

A thesis
submitted in conformity with the requirements for the degree of
Master of Science
in
Department of Physics
Lakehead University

June 4, 2012

ABSTRACT

In this thesis we describe a squeezing for $SU(3)$ systems and compare squeezing in the phase space in the semiclassical approximation with squeezing obtained by the full quantum mechanical calculation. We show that the equations of motion in phase space for $SU(3)$ Wigner function are given in terms of the Poisson bracket plus quantum correction terms which depend on the inverse dimension of the system. In the semiclassical approximation, for large values of the $SU(3)$ representation label λ, we can ignore the quantum correction terms and use the truncated Liouville equation; squeezing in $SU(3)$ systems is well described by this truncated Liouville equation. Finally, we find some scaling behaviors associated with squeezing in $SU(3)$ and compare these with the corresponding $SU(2)$ calculations.

ACKNOWLEDGEMENTS

CONTENTS

1. INTRODUCTION AND MOTIVATION

The idea of developing a quantum theory that could easily be understood using the tools of classical mechanics has attracted significant attention since the early days of quantum mechanics. A very important development came with the work of Moyal [1], who realized that Weyl quantization [2] could be inverted by the Wigner transform [3] from an operator on the Hilbert space to a function on the phase space. The quantum expectation value of an operator can then be represented by the statistical like average of the corresponding phase space function with the statistical density given by the Wigner function. This formal resemblance of quantum mechanics in the phase space formulation to classical mechanics provides deeper understanding of differences between the quantum and classical phenomena.

The objective of this thesis is to investigate squeezing properties of $SU(3)$ states using fully quantum and semiclassical methods. The basic ingredients of the thesis are the quantum evolution equation and its semiclassical counterpart, the concept of coherent states, the concept of squeezing, and some notions regarding the group $SU(3)$.

In this introduction, we will use the example of position and momentum space to illustrate the basic principle and terminology of the phase space approach to quantum mechanics, and some of the resulting surprises of this approach. One such surprise is that quantum probability distributions in phase space can be locally negative. We will also review coherent states for the harmonic oscillator and illustrate squeezing of such a coherent state. In the later chapters , these notions will be generalized to $SU(2)$ and $SU(3)$ systems, which describe 2-level and 3-level atoms. The chapter on $SU(2)$ is a bridge between the more familiar position-momentum space and the more abstract setting of the $su(3)$ algebra. The new and main results of this thesis are found in Chapter 5, which deals with squeezing in $SU(3)$ system.

1.1   Quantum versus classical

The structure of quantum mechanics seems to present a radical departure from that of classical mechanics. In classical mechanics the state of a system with 2 degrees of freedom is described by a point in 2 dimensional phase space with coordinates (q, p). The generalized coordinate q describes the configuration of the system in 1 dimensional configuration space and the coordinate p is the canonical conjugate momentum. The time evolution of this system is generated by the Hamiltonian $H(q, p)$. The system point (q, p) moves on the phase space along a particular trajectory according to Hamilton's equations of motion

$$\frac{dp}{dt} = \{p, H\}, \qquad \frac{dq}{dt} = \{q, H\} \ , \qquad (1.1)$$

where $\{f, g\}$ is the Poisson bracket of any two functions f and g. Moreover the classical phase space distribution ρ_{cl} evolves according to Liouville's equation

$$\frac{\partial}{\partial t}\rho_{cl} = -\{\rho_{cl}, H\} \ . \qquad (1.2)$$

By contrast, in quantum mechanics the state of a system is not represented by a point in the 2 dimensional phase space. For a pure state it is represented by a state vector $|\psi\rangle$ in a complex Hilbert space $\mathbb{H}$. The unitary time evolution of this state vector is generated by a hermitian Hamiltonian operator $\hat{H}$ acting in this space and the state vector evolves according to the Schrödinger equation:

$$i\hbar\frac{\partial}{\partial t}|\psi\rangle = \hat{H}|\psi\rangle. \tag{1.3}$$

These differences between Hilbert space formulation of quantum mechanics and classical mechanics have inspired a large amount of efforts since the early days of quantum mechanics to bridge the gap between the quantum and classical description of the world.

One notable effort in this direction is the formulation of quantum mechanics in phase space. The foundations of this remarkable formulation were laid out by H Weyl [2] and E Wigner [3]. In the phase space formulation every quantum observable $\hat{f}$ is mapped, using the so-called Wigner transform, to a real-valued function $W_f(q, p)$ in phase space. Conversely, one can go in the reverse direction using the so-called Weyl quantization: to every phase space function $W_f(q, p)$ one can associate a quantum observable $\hat{f}$ acting in the Hilbert space for the quantum system. The Wigner transform of the density operator $\hat{\rho} = |\psi\rangle\langle\psi|$ is called the Wigner quasi distribution function of the quantum system. All the predictions of quantum dynamics can be extracted from the Wigner function. Moreover since the Wigner function is defined on phase space we can easily compare its time evolution to that of the classical phase space distribution.

1.2 Phase space formulation: an overview

Let us introduce position eigenstates $\{|q\rangle, -\infty < q < \infty\}$ for which $\hat{q}|q\rangle = q|q\rangle$. This basis is complete so we may expand any ket $|\psi\rangle$ as

$$|\psi\rangle = \int dq\, |q\rangle\langle q|\,\psi\rangle \tag{1.4}$$

with $\langle q|\,\psi\rangle = \psi(q)$ the wave function of the system evaluated at position q. From a wave function $\psi(q)$ associated to the ket $|\psi\rangle$ one constructs the Wigner function W_ρ defined on phase space:

$$W_\rho(q, p) = 2\int_{-\infty}^{\infty} dz\, e^{2ipz/\hbar}\,\psi^*(q+z)\,\psi(q-z), \tag{1.5}$$

with $\hat{\rho}$ the density operator $|\psi\rangle\langle\psi|$. For later convenience we have introduced the Wigner function in Eq. (1.5) in such a way that is proportional to the function introduced by Wigner in a somewhat *ad hoc* manner. To find the position probability density we integrate the Wigner function over the momentum

$$|\psi(q)|^2 = \frac{1}{2\pi\hbar}\int_{-\infty}^{\infty} dp\, W_\rho(q, p), \tag{1.6}$$

and to find the momentum distribution we integrate over the position

$$|\psi(p)|^2 = \frac{1}{2\pi\hbar}\int_{-\infty}^{\infty} dq\, W_\rho(q, p). \tag{1.7}$$

A direct result of these two equations is that the Wigner distribution satisfies

$$\int_{-\infty}^{\infty}\int_{-\infty}^{\infty} dq dp\, W_\rho(q, p) = \frac{1}{2\pi\hbar}. \tag{1.8}$$

Fig. 1.1: Wigner function of the number state $|1\rangle$. Left: calculated. Right: as obtained experimentally by Wineland *et. al.*[4].

The Wigner function is thus a probability distribution in phase space. However, even though it is real, it is not everywhere non negative, so it is not a true probability density. For instance the Wigner function of the harmonic oscillator number state $|1\rangle$ is found to be

$$W_{|1\rangle}(q,p) = 2\left(\frac{2p^2}{\hbar m\omega} + \frac{2q^2 m\omega}{\hbar} - 1\right)\exp\left(-\frac{q^2 m\omega}{\hbar} - \frac{p^2}{m\omega\hbar}\right) \tag{1.9}$$

and is plotted in Fig. 1.1. Although Wigner functions can acquire negative values one still obtains the correct marginal distribution if the function is integrated over the entire range of the complementary variable and multiplied by $2\pi\hbar$. Thus, we usually refer to the Wigner function as a quasi probability distribution.

To prove that the Wigner function cannot be everywhere positive consider two orthogonal states $|\psi_1\rangle$ and $|\psi_2\rangle$: $\langle\psi_1|\psi_2\rangle = 0$. For the density operators $\hat{\rho}_1 = |\psi_1\rangle\langle\psi_1|$ and $\hat{\rho}_2 = |\psi_2\rangle\langle\psi_2|$ one can show

$$|\langle\psi_1|\psi_2\rangle|^2 = \text{Tr}(\hat{\rho}_1\hat{\rho}_2) = \frac{1}{2\pi\hbar}\int_{-\infty}^{\infty}\int_{-\infty}^{\infty}dq\,dp\,W_{\rho_1}(q,p)\,W_{\rho_2}(q,p) = 0. \tag{1.10}$$

Thus $W_{\rho_1}(q,p)$ and $W_{\rho_2}(q,p)$ cannot both be positive everywhere.

Now let us have a look at the time evolution of the Wigner function. The Wigner function inherits its time dependence through the time dependence of the wave function as governed by the Schrödinger equation:

$$i\hbar\frac{\partial}{\partial t}\psi(q,t) = -\frac{\hbar^2}{2m}\frac{\partial^2}{\partial q^2}\psi(q,t) + V(q)\psi(q,t). \tag{1.11}$$

This can be substituted into

$$\frac{\partial W_\rho(q,p,t)}{\partial t} = 2\int_{-\infty}^{\infty}dz\left[\psi(q-z,t)\frac{\partial\psi^*(q+z,t)}{\partial t} + \psi^*(q+z,t)\frac{\partial\psi(q-z,t)}{\partial t}\right]e^{2ipz/\hbar}, \tag{1.12}$$

to get, after straightforward but tedious manipulations, the so-called quantum Liouville equation

$$\frac{\partial W_\rho(q,p,t)}{\partial t} = -\{W_\rho, W_H\} - \frac{\hbar^2}{24}\frac{\partial^3 V}{\partial q^3}\frac{\partial^3 W_\rho(q,p,t)}{\partial p^3} + \dots. \tag{1.13}$$
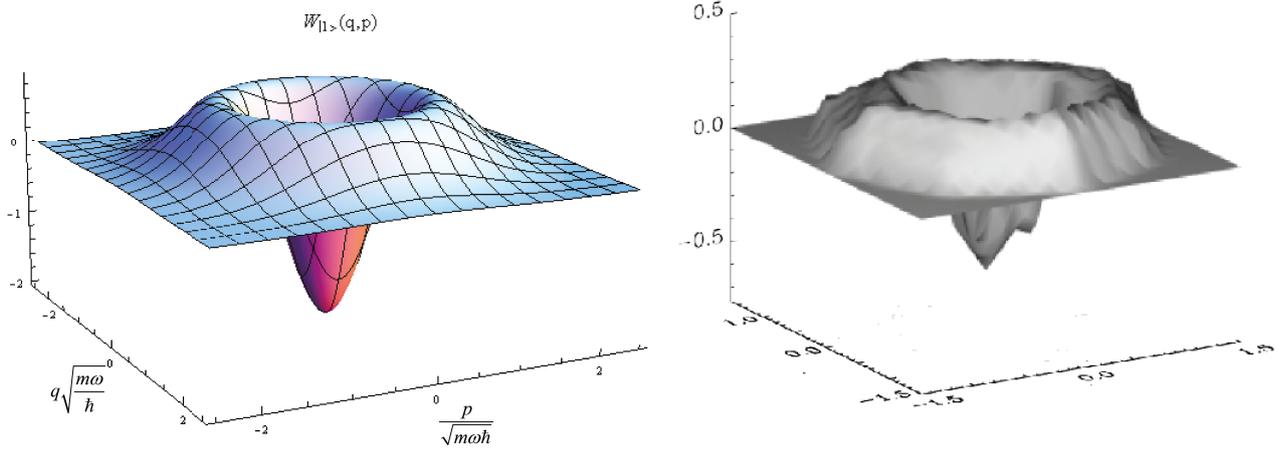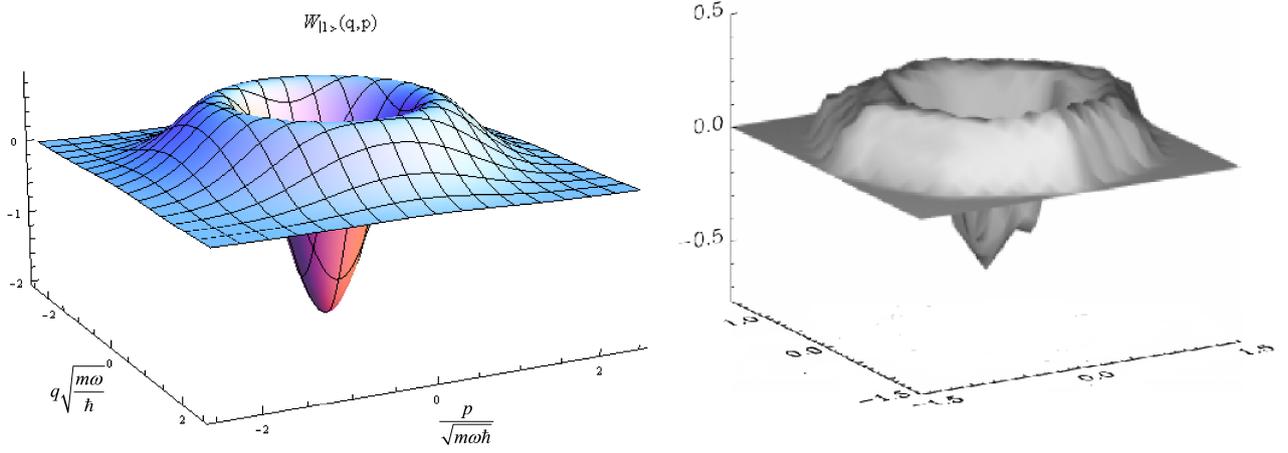
Fig. 1.1: Wigner function of the number state $|1\rangle$. Left: calculated. Right: as obtained experimentally by Wineland *et. al.*[4].

The Wigner function is thus a probability distribution in phase space. However, even though it is real, it is not everywhere non negative, so it is not a true probability density. For instance the Wigner function of the harmonic oscillator number state $|1\rangle$ is found to be

$$W_{|1\rangle}(q,p) = 2\left(\frac{2p^2}{\hbar m\omega} + \frac{2q^2 m\omega}{\hbar} - 1\right)\exp\left(-\frac{q^2 m\omega}{\hbar} - \frac{p^2}{m\omega\hbar}\right) \tag{1.9}$$

and is plotted in Fig. 1.1. Although Wigner functions can acquire negative values one still obtains the correct marginal distribution if the function is integrated over the entire range of the complementary variable and multiplied by $2\pi\hbar$. Thus, we usually refer to the Wigner function as a quasi probability distribution.

To prove that the Wigner function cannot be everywhere positive consider two orthogonal states $|\psi_1\rangle$ and $|\psi_2\rangle$: $\langle\psi_1|\psi_2\rangle = 0$. For the density operators $\hat{\rho}_1 = |\psi_1\rangle\langle\psi_1|$ and $\hat{\rho}_2 = |\psi_2\rangle\langle\psi_2|$ one can show

$$|\langle\psi_1|\psi_2\rangle|^2 = \text{Tr}(\hat{\rho}_1\hat{\rho}_2) = \frac{1}{2\pi\hbar}\int_{-\infty}^{\infty}\int_{-\infty}^{\infty}dqdp\, W_{\rho_1}(q,p)\,W_{\rho_2}(q,p) = 0\,. \tag{1.10}$$

Thus $W_{\rho_1}(q,p)$ and $W_{\rho_2}(q,p)$ cannot both be positive everywhere.

Now let us have a look at the time evolution of the Wigner function. The Wigner function inherits its time dependence through the time dependence of the wave function as governed by the Schrödinger equation:

$$i\hbar\frac{\partial}{\partial t}\psi(q,t) = -\frac{\hbar^2}{2m}\frac{\partial^2}{\partial q^2}\psi(q,t) + V(q)\psi(q,t)\,. \tag{1.11}$$

This can be substituted into

$$\frac{\partial W_\rho(q,p,t)}{\partial t} = 2\int_{-\infty}^{\infty}dz\left[\psi(q-z,t)\frac{\partial\psi^*(q+z,t)}{\partial t} + \psi^*(q+z,t)\frac{\partial\psi(q-z,t)}{\partial t}\right]e^{2ipz/\hbar}\,, \tag{1.12}$$

to get, after straightforward but tedious manipulations, the so-called quantum Liouville equation

$$\frac{\partial W_\rho(q,p,t)}{\partial t} = -\{W_\rho, W_H\} - \frac{\hbar^2}{24}\frac{\partial^3 V}{\partial q^3}\frac{\partial^3 W_\rho(q,p,t)}{\partial p^3} + \ldots\,. \tag{1.13}$$

The above equation is the classical Liouville equation (1.2) with the addition of extra correction terms that depend on powers of $\hbar$ and higher order derivatives of potential. Thus for systems with vanishing third and higher order derivatives of the potential, like the harmonic oscillator, the evolution of the system is classical. Moreover the quantum Liouville equation shows a quantum-classical correspondence: for $\hbar \to 0$ the higher order corrections vanish and we are left with the classical Liouville equation.

The Wigner function is only one of an infinite number of possible quasi probability distributions. A serious obstacle in associating a quantum observable $\hat{f}$ to the phase space function $W_f(q, p)$ is that, although the classical variables q and p commute, the quantum operators $\hat{q}$ and $\hat{p}$ do not commute:

$$[\hat{q}, \hat{p}] = \hat{q}\hat{p} - \hat{p}\hat{q} = i\hbar \, \mathbb{1} \,. \tag{1.14}$$

For instance for the classical phase space function $q^2 p^2$ we cannot simply replace q and p with the operators $\hat{q}$ and $\hat{p}$ since there are many possible ways to order the operators. For instance two of the possible quantized versions of $q^2 p^2$ are $\hat{q}\hat{p}^2\hat{q}$ and $\frac{1}{2}\left(\hat{q}^2\hat{p}^2 + \hat{p}^2\hat{q}^2\right)$ which are not equal.

In order to overcome this problem an ordering rule must be considered in any quantization scheme. In this thesis, we will work exclusively with the so-called Weyl ordering. According to the Weyl rule the quantized form of the polynomial $q^2 p^2$, is $\frac{1}{4}\left(\hat{q}^2\hat{p}^2 + 2\hat{q}\hat{p}^2\hat{q} + \hat{p}^2\hat{q}^2\right)$. This ordering produces the Wigner function given in Eq. (1.5). Other common orderings are the normal and anti-normal orderings, which correspond respectively to the Husimi Q-function and to the Glauber-Sudarshan P function.

In general, the phase space symbol $W_f(q, p)$ of a given symmetric-ordered operator $\hat{f}$ is most conveniently related to the trace of the operator by the so-called quantization kernel $\hat{w}(q, p)$:

$$W_f(p, q) = 2\mathrm{Tr}\left(\hat{w}(q, p)\hat{f}\right) \,. \tag{1.15}$$

The Wigner function of Eq.(1.5) is then written as

$$W_\rho(q, p) = 2\mathrm{Tr}\left(\hat{w}(q, p)\hat{\rho}\right) = 2\left\langle\psi\right|\hat{w}(q, p)\left|\psi\right\rangle \,. \tag{1.16}$$

The quantization kernel is different for different orderings, and different for different physical systems. For the symmetric ordering in position-momentum space, the kernel is conveniently given in the form [5]

$$\hat{w}(q, p) = \hat{D}(q, p)\,\hat{P}\,\hat{D}^\dagger(q, p) \,, \tag{1.17}$$

where

$$\hat{D}(q, p) = \exp\left[i\left(p\hat{q} - q\hat{p}\right)/\hbar\right] \tag{1.18}$$

is a unitary displacement operator and $\hat{P}$ is a parity operator

$$\hat{P} = \int dq \, \left|-q\right\rangle\left\langle q\right| = \int dp \, \left|-p\right\rangle\left\langle p\right| \,. \tag{1.19}$$

The quantization kernel also allows us to go from phase space to operators. In general, for a given function $W_f(q, p)$, the corresponding symmetric-ordered operator is given by the Weyl quantization as

$$\hat{f} = \frac{1}{\pi\hbar}\int dq\,dp\,\hat{w}(q, p)\,W_f(q, p) \,. \tag{1.20}$$

The Wigner transform of Eq. (1.15) and Weyl quantization are inverse of each other.

One can show

$$\hat{w}(q,p)\,|q'\rangle = e^{2ip(q-q')/\hbar}\,|2q-q'\rangle\,,\quad \hat{w}(q,p)\,|p'\rangle = e^{-2iq(p-p')/\hbar}\,|2p-p'\rangle\,. \tag{1.21}$$

Thus $\text{Tr}\,(\hat{w}(q,p)) = \frac{1}{2}$ and

$$\text{Tr}\,(\hat{w}(q,p)\,\hat{w}(q',p')) = \pi\hbar\delta(2q-2q')\,\delta(p-p')\,. \tag{1.22}$$

Therefore for an operator $\hat{f}$, one can write the trace as:

$$\text{Tr}\left(\hat{f}\right) = \int dq'\,\langle q'|\,\hat{f}\,|q'\rangle = \frac{1}{2\pi\hbar}\int dq\,dp\,W_f(q,p)\,. \tag{1.23}$$

This corresponds to integrating the corresponding function in phase space over the entire phase space. For $\hat{A} = \hat{f}\hat{g}$ one can show

$$\text{Tr}\left(\hat{A}\right) = \text{Tr}\left(\hat{f}\hat{g}\right) = \frac{1}{2\pi\hbar}\int dq\,dp\,W_f(q,p)\,W_g(q,p)\,. \tag{1.24}$$

Now let us show how the phase space formulation of quantum mechanics resembles the Hamiltonian formulation of classical mechanics. In quantum mechanics the expectation value of an operator $\hat{f}$ is calculated by

$$\langle\hat{f}\rangle = \text{Tr}\left(\hat{f}\hat{\rho}\right)\,. \tag{1.25}$$

Eq. (1.24) then gives

$$\langle\hat{f}\rangle = \frac{1}{2\pi\hbar}\int dq\,dp\,W_f(q,p)\,W_\rho(q,p)\,. \tag{1.26}$$

Therefore the expectation value of a quantum observable $\hat{f}$ can be expressed as the average of a classical function $W_f(q,p)$ over the phase space with Wigner quasi distribution function as the distribution function, and is similar to the calculation of expectation values in classical mechanics.

1.3   Harmonic oscillator coherent states

Coherent states are of central importance to quantum mechanics. The concept of what is now called coherent states was proposed by Schrödinger [6] in connection with the classical states of the quantum harmonic oscillator. It was Glauber [7] who first used the term coherent states for the eigenstates of the annihilation operator $\hat{a}$. He used the coherent states to study the electromagnetic correlation functions, which are of great importance in quantum optics.

For the harmonic oscillator coherent state $|\alpha\rangle$ we have

$$\hat{a}\,|\alpha\rangle = \alpha\,|\alpha\rangle\,, \tag{1.27}$$

where α is an arbitrary complex number. As always the annihilation and creation operators, $\hat{a}$ and $\hat{a}^\dagger$, have the property that

$$\hat{a}\,|n\rangle = \sqrt{n}\,|n-1\rangle\,,\qquad \hat{a}^\dagger\,|n\rangle = \sqrt{n+1}\,|n+1\rangle\,, \tag{1.28}$$

where $|n\rangle$ is the number state, that is, $\hat{a}^\dagger\hat{a}\,|n\rangle = n\,|n\rangle$. They satisfy the commutation relations

$$\left[\hat{a},\hat{a}^\dagger\right] = \mathbb{1}\,,\qquad \left[\hat{a}^\dagger,\hat{a}^\dagger\right] = [\hat{a},\hat{a}] = 0\,. \tag{1.29}$$
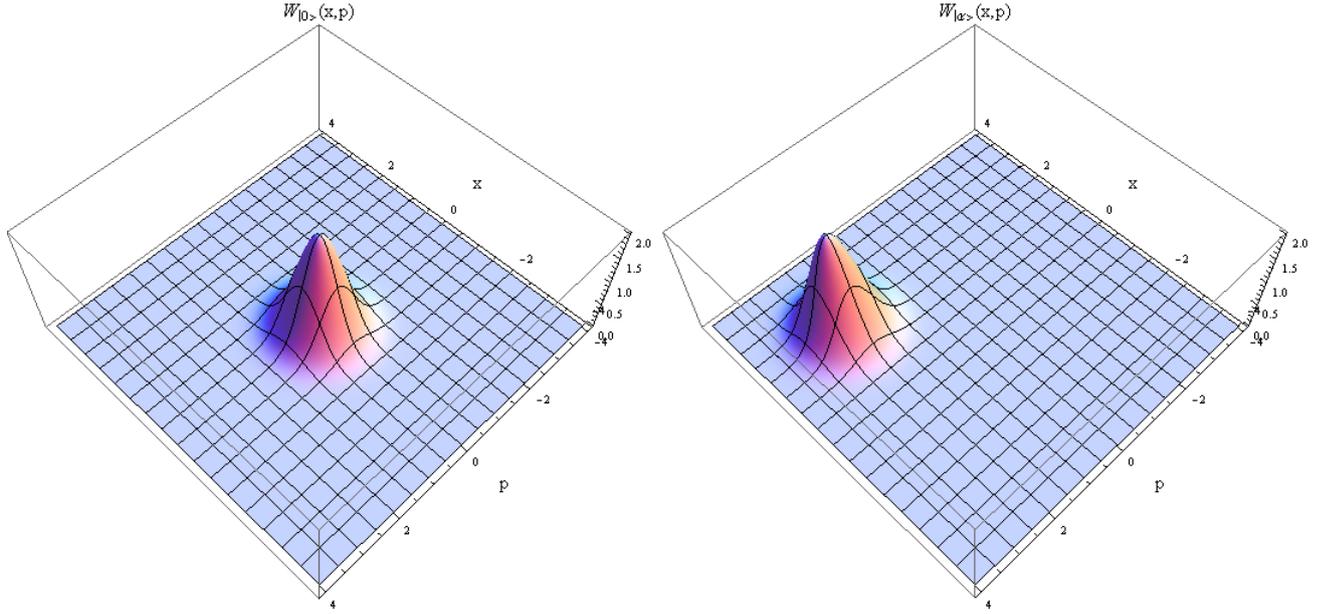
Fig. 1.2: Wigner function of the vacuum state $|0\rangle$ (left), and harmonic oscillator coherent state $|\alpha\rangle$ for $\bar{x} = \bar{p} = 2$

One other way to define the coherent state of the harmonic oscillator which is the one we will use and generalize, is as a displaced vacuum state *i.e.* as resulting from the action of the displacement operator $\hat{D}(\alpha)$ on the vacuum state $|0\rangle$,

$$|\alpha\rangle = \hat{D}(\alpha)|0\rangle, \quad \hat{D}(\alpha) = e^{\alpha \hat{a}^\dagger - \alpha^* \hat{a}}, \tag{1.30}$$

where $\hat{D}(\alpha)$ is a unitary transformation, $\hat{D}^{-1}(\alpha) = \hat{D}^\dagger(\alpha)$. When expressed in terms of p and q, $\hat{D}(\alpha)$ is exactly given in Eq. (1.18). Physically $\hat{D}(\alpha)$ is a translation operator: for $\hat{x}$ and $\hat{p}$ the dimensionless operators defined as

$$\hat{x} = \frac{1}{2}\left(\hat{a} + \hat{a}^\dagger\right), \quad \hat{p} = \frac{1}{2i}\left(\hat{a} - \hat{a}^\dagger\right), \tag{1.31}$$

we have

$$\begin{aligned}
\hat{D}^{-1}(\alpha)\,\hat{x}\hat{D}(\alpha) &= \hat{x} + \text{Re}(\alpha), \\
\hat{D}^{-1}(\alpha)\,\hat{p}\hat{D}(\alpha) &= \hat{p} + \text{Im}(\alpha).
\end{aligned} \tag{1.32}$$

As a result

$$\bar{x} = \langle\alpha|\,\hat{x}\,|\alpha\rangle = \text{Re}(\alpha), \quad \bar{p} = \langle\alpha|\,\hat{p}\,|\alpha\rangle = \text{Im}(\alpha). \tag{1.33}$$

One can obtain the Wigner function of the coherent state $|\alpha\rangle$ as

$$W_{|\alpha\rangle}(\alpha) = 2\exp\left(-2(x - \bar{x})^2 - 2(p - \bar{p})^2\right). \tag{1.34}$$

Comparing with the Wigner function of the vacuum state $|0\rangle$, given by

$$W_{|0\rangle}(\alpha) = 2\exp\left(-2x^2 - 2p^2\right), \tag{1.35}$$

it is clear that the coherent state is a displaced vacuum state, as illustrated in Fig. 1.2. This figure shows the Wigner functions of the vacuum state $|0\rangle$ and coherent state $|\alpha\rangle$. For both of these cases the Wigner function is positive.

1.4 Harmonic oscillator squeezed states

The uncertainty relation for the operators $\hat{x}$ and $\hat{p}$, with $[\hat{x}, \hat{p}] = \frac{i}{2}\,\mathbb{1}$, is

$$(\Delta\hat{x})^2(\Delta\hat{p})^2 \geq \frac{1}{16}\,. \tag{1.36}$$

For coherent states $|\alpha\rangle$ the variances of position and momentum are equal,

$$(\Delta\hat{x})^2 = (\Delta\hat{p})^2 = \frac{1}{4}\,. \tag{1.37}$$

However, there exists a set of states for which $(\Delta\hat{x})^2$ or $(\Delta\hat{p})^2$ is smaller than $\frac{1}{4}$. States for which this occurs will have less uncertainty in position or momentum than a coherent state. These states are called squeezed states. Of course, the fluctuations in the other variable must be enhanced so as to not violate the uncertainty relation.

Generally, squeezing occurs when the variance is less than $\frac{1}{4}$ along any direction in the $x - p$ plane. We now introduce the operator $\hat{x}_\theta$ in the $x - p$ plane [8]

$$\hat{x}_\theta = e^{i\theta\hat{a}^\dagger\hat{a}}\hat{x}e^{-i\theta\hat{a}^\dagger\hat{a}} = \hat{x}\cos\theta + \hat{p}\sin\theta\,, \tag{1.38}$$

where $0 \leq \theta \leq 2\pi$. Special cases are $\hat{x}_0 = \hat{x}$ and $\hat{x}_{\pi/2} = \hat{p}$. The squeezing parameter is then defined as

$$\xi = \min(\Delta\hat{x}_\theta)^2\,, \tag{1.39}$$

which is the minimum value of $(\Delta\hat{x}_\theta)^2$ with respect to θ. If $\xi < \frac{1}{4}$ the state for which the variance is calculated is squeezed.

One of the ways to generate a squeezed state is through the action of the so-called squeezing operator $\hat{S}(r)$ on the vacuum state $|0\rangle$,

$$|r\rangle = \hat{S}(r)|0\rangle\,, \qquad \hat{S}(r) = \exp\left[\frac{r}{2}\left(\hat{a}^2 - \hat{a}^{\dagger 2}\right)\right] \tag{1.40}$$

where r is a real parameter.

One can show

$$\hat{S}^\dagger(r)\hat{a}\hat{S}(r) = \hat{a}\cosh r - \hat{a}^\dagger\sinh r\,, \quad \hat{S}^\dagger(r)\hat{a}^\dagger\hat{S}(r) = \hat{a}^\dagger\cosh r - \hat{a}\sinh r\,. \tag{1.41}$$

This leads to

$$(\Delta\hat{x})^2 = \frac{1}{4}e^{-2r}, \quad (\Delta\hat{p})^2 = \frac{1}{4}e^{2r}\,. \tag{1.42}$$

Thus for $r > 0$ (resp. $r < 0$) the operator $\hat{x}$ (resp. $\hat{p}$) is squeezed.

The Wigner function of the squeezed vacuum state is calculated to be

$$W_{|r\rangle}(x, p) = 2\exp\left(-\frac{x^2}{2(\Delta x)^2} - \frac{p^2}{2(\Delta p)^2}\right), \tag{1.43}$$

and is plotted in Fig. 1.3(left) for $r = \frac{1}{2}$. It is a Gaussian, narrowed in the direction of squeezing and expanded in the orthogonal direction. Note that for the squeezed vacuum state the Wigner function is non negative.
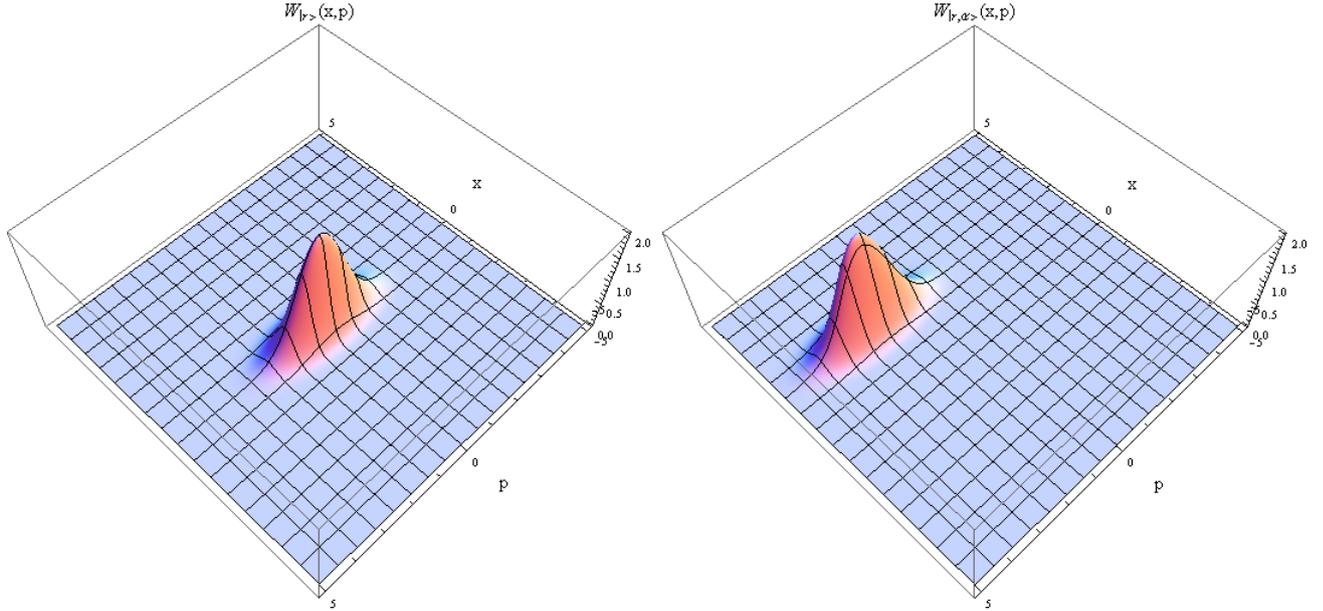
Fig. 1.3: Wigner function of the squeezed state $|r\rangle$ for $r = \frac{1}{2}$ (left) and the Wigner function of the displaced squeezed state $|r, \alpha\rangle$ for $r = \frac{1}{2}$ and $\bar{x} = \bar{p} = 2$ (right).

A more general squeezed state can be obtained by applying the displacement operator $\hat{D}(\alpha)$ on the vacuum squeezed state $|r\rangle$,

$$|\alpha, r\rangle = \hat{D}(\alpha)\,\hat{S}(r)\,|0\rangle \ . \tag{1.44}$$

This is called displaced squeezed state. The Wigner function of the x-squeezed state displaced by $\bar{x} = \bar{p} = 2$ is plotted in Fig. 1.3 (right).

As we have already mentioned squeezing can occur in any direction in the $x - p$ plane. Fig. 1.4 shows the Wigner function of the rotated squeezed state

$$|r, \alpha; \varphi\rangle = \hat{T}(\varphi)\,|r, \alpha\rangle, \quad \hat{T}(\varphi) = e^{i\varphi\hat{a}^\dagger\hat{a}}, \tag{1.45}$$

for $r = \frac{1}{2}$, $\varphi = \frac{1}{4}\pi$ and $\bar{x} = \bar{p} = 0$ for the plot on the left and $\bar{x} = \bar{p} = 2$ for the right plot. The Wigner function for this state is

$$W_{|r,\alpha;\varphi\rangle}(x, p) = 2\exp\left(-\frac{\left(x_\varphi - \bar{x}\right)^2}{2(\Delta x)^2} - \frac{\left(p_\varphi - \bar{p}\right)^2}{2(\Delta p)^2}\right) \tag{1.46}$$

where

$$x_\varphi = x\cos\varphi + p\sin\varphi, \qquad p_\varphi = p\cos\varphi - x\sin\varphi\,. \tag{1.47}$$

Squeezing can also be produced experimentally using a nonlinear transformation, for instance generated by the so-called Kerr Hamiltonian [9]

$$\hat{H} = \kappa\hat{a}^{\dagger 2}\hat{a}^2\,. \tag{1.48}$$

This Hamiltonian is not of the form of squeezing operator given in Eq. (1.40) but still produces squeezing.

Fig. 1.4: Wigner function of the rotated squeezed state $|r, \alpha; \varphi\rangle$ for $r = \frac{1}{2}, \varphi = \frac{1}{4}\pi$ and $\bar{x} = \bar{p} = 0$ (left) and $\bar{x} = \bar{p} = 2$ (right)

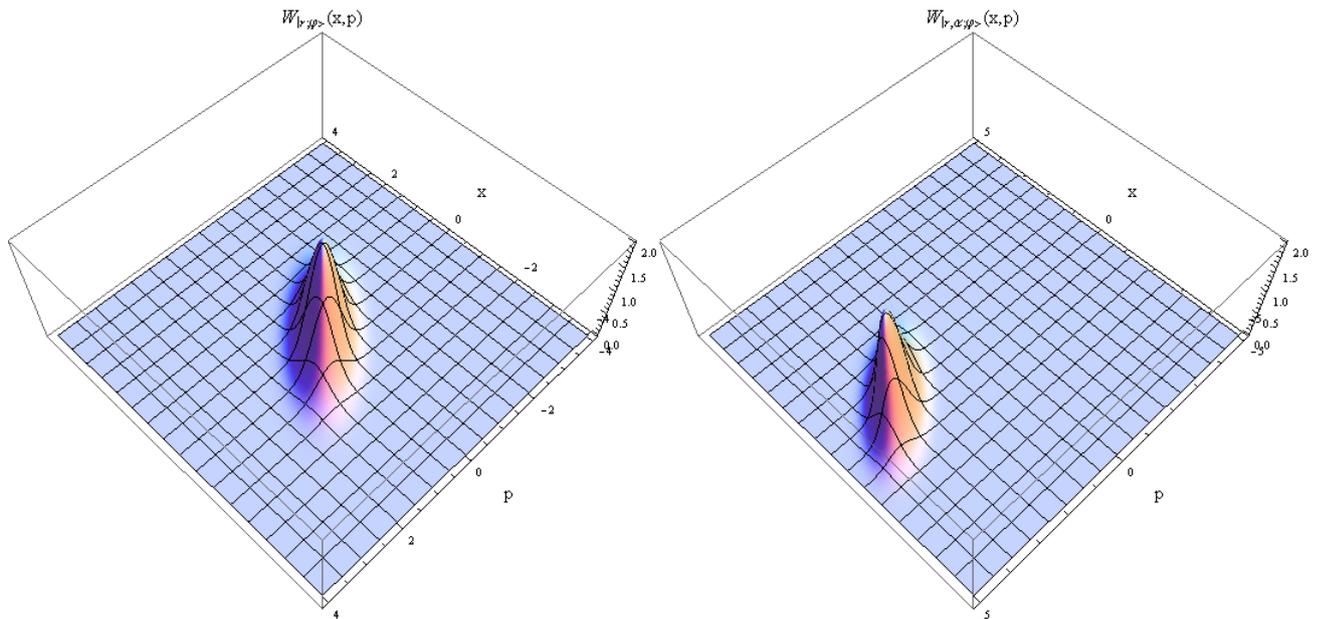Squeezed states of light have lots of applications; aside from its intrinsic usefulness in carrying out fundamental experiments in optical physics, there are a number of general areas in which the use of squeezed light are advantageous. These include spectroscopy [10], interferometry [11], precision measurement [12], optical communications [13] and enhancement the sensitivity of gravity-wave detectors [14]. The LIGO gravitational wave detector uses interferometry and squeezed states and is sufficiently sensitive to detect movements as small as $10^{-18}m$, *i.e.*, one thousandth the diameter of a proton.

1.5 Motivation and organization of the thesis

The original work of [2] and [3] has been expanded well beyond semiclassical dynamics to include quantum optics [15], [16], [17], [18], quantum chemistry [19], classical optics [20], [21], signal analysis [22], [23], speech analysis [24],[25], data analysis [26]and other areas: there is now a huge literature on Wigner function that uses Eq. (1.5) as a starting point. Various types of Wigner functions have been derived, each suited to the particular need of a problem [27], [28]. Some applications to quantum mechanics in phase space are reviewed in [29], [30], [31]. A collection of original papers can be found in [32]. This list of reference is by no means exhaustive: more than 4800 papers can be found on Web of Science on this topic in the last 20 years.

In this thesis we use phase space methods in the semiclassical limit to describe squeezing in $SU(2)$ and $SU(3)$ systems. The semiclassical calculations for the evolution of $SU(3)$ Wigner functions under a non-linear $su(3)$ Hamiltonian were published in [33] and represent the first calculations of this kind in $SU(3)$ systems.

The $SU(3)$ evolution depends on a Poisson bracket obtained by Medendorp and de Guise shortly before I arrived. I have verified their expression, starting from scratch and by verifying that the bracket of two symbols of generators is proportional to the symbol of the commutator.

The symbols are obtained from a quantization kernel, found in [34]. These were published in [33] but are otherwise original.

The time evolutions that we consider result in a deformed Wigner function (deformed in a sense to be explained later). The original results included in this thesis also include the evaluation of a squeezing parameter as a function of time. One example of this kind of calculation was included in [33]. The thesis also includes an additional case that will be included in a forthcoming paper.

Many of the results on $SU(3)$ were strongly inspired by similar results obtained by Klimov and collaborators for spin (or $SU(2)$) systems. Going from $SU(2)$ to $SU(3)$ is an interesting technical challenge; the thesis is constructed by first presenting results for $SU(2)$ and then (sometimes in parallel with $SU(2)$) results for $SU(3)$. Presenting the material in this way often clarifies and motivates definitions initially suggested in the context of the harmonic oscillator or $SU(2)$ systems. Although the results on $SU(2)$ are not original, many of them were re-derived separately to gain experience in preparation for challenging $SU(3)$ calculations, to illustrate some basic ideas or to complement the work on $SU(3)$. Finally, harmonic oscillator and $SU(2)$ Wigner functions are easily plotted, which makes some of the more abstract concepts easier to grasp.

The remainder of the thesis is organized in two parts. In the first part, we obtain the Wigner functions and required phase space functions for each of $SU(2)$ and $SU(3)$ systems, and derive the Liouville-like equation for the appropriate Wigner functions in the semiclassical limit.

Much like mentioned for the general potential $V(q)$ in section 1.2, the equations of motion for the density matrix usually contain the Poisson bracket as leading term, plus some correction terms. For $SU(2)$ and $SU(3)$ systems, these correction terms are respectively inverse powers of j, the angular momentum of the $SU(2)$ system and of inverse powers of λ, the number of excitation in the 3 dimensional system. For sufficiently large j and λ the equations of motion truncated at the Poisson bracket are a good approximation to the exact evolution for short times.

In the second part we show that squeezing can be described in the semiclassical limit *i.e.* by ignoring quantum correction terms in the equation of motion of the Wigner function. For squeezing in $SU(2)$ systems several criteria has been defined so far. We choose a well known criterion suggested in [35], similar to the definition of squeezing we presented here in this chapter for harmonic oscillator systems. We define our squeezing criterion for $SU(3)$ systems in the similar manner.

2. A CLOSER LOOK AT THE GENERAL PHASE SPACE FORMULATION OF QUANTUM MECHANICS

In this chapter at first we use coherent states to define the phase space of the system. We then discuss general formulation of phase space functions and their properties via the Stratonovich-Weyl correspondence. To make the phase space formulation of quantum mechanics an autonomous formulation a new product called star product must be defined between the phase space functions which will be discussed in the last section of this chapter.

2.1 *Generalized coherent states and the definition of quantum phase space*

It was Perelomov [36] who proposed the most useful generalization of coherent states for arbitrary Lie groups. His approach preserves important features of harmonic oscillator coherent states but also allows generalization to finite dimensional Hilbert spaces and emphasizes the role of group transformations and associated geometry in the construction of coherent states. The basic theme of this development was to intimately connect the coherent states with the dynamical group for each physical problem.

For instance, the commutation relations of $\hat{a}, \hat{a}^\dagger$ and $\mathbb{1}$ define the Heisenberg-Weyl Lie algebra $hw(1)$. Transformations generated by exponentiation of these elements form Heisenberg-Weyl group, $HW(1)$. The next ingredient of Perelomov's construction is a special state, the vacuum state $|0\rangle$. The $HW(1)$ group transformation $D(\alpha)$, introduced in chapter 1, acts on $|0\rangle$ produces the coherent state.

This is generalized as follows for spin system. The algebra is the $su(2)$ algebra, with elements $\hat{S}_x, \hat{S}_y$ and $\hat{S}_z$ satisfying the usual commutation relations

$$\left[\hat{S}_x, \hat{S}_y\right] = i\hat{S}_z, \quad \left[\hat{S}_y, \hat{S}_z\right] = i\hat{S}_x, \quad \left[\hat{S}_z, \hat{S}_x\right] = i\hat{S}_y. \tag{2.1}$$

The exponentiation of a general element of the algebra produces a group transformation. When this group transformation acts on the spin state $|j, j\rangle$, we obtain an $SU(2)$ coherent state. An $SU(2)$ transformation can always be written in the factored form $R_z(\varphi) R_y(\theta) R_z(\gamma)$ where $R_k(\varphi) = e^{-i\hat{S}_k \varphi}$ denotes a rotation about the k axis through the angle φ. Because $R_z(\gamma)|j, j\rangle$ is just $|j, j\rangle$ multiplied by a constant phase factor, we can eliminate this phase so that an $SU(2)$ coherent state depends on only two angles and can be written as:

$$|\varphi, \theta\rangle = R_z(\varphi) R_y(\theta) |j, j\rangle . \tag{2.2}$$

Thus, the role of the displacement operator $\hat{D}(\alpha)$ of the harmonic oscillator problem is played by the transformation $R_z(\varphi)R_y(\theta)$ in $SU(2)$ and the role of the vacuum state $|0\rangle$ is played by the angular momentum state $|j, j\rangle$.

As shown in [37], this definition of a coherent state can be extended to any group. The construction is straightforward. The coherent state is simply obtained by applying a unitary

transformation to an extremal state, a state which is killed by every raising or every lowering operator.

Now let us show how we can determine the phase space of a physical system using the concept of coherent states. The coherent state approach is not just a convenient mathematical tool, but it also helps to understand how physical properties of the system are reflected by the geometrical structure of the related phase space [38].

Imagine the Hamiltonian for a system is expressed as a polynomial in elements of an algebra $\mathfrak{g}$. As an example for $su(2)$ the algebra elements are $\hat{S}_x, \hat{S}_y$ and $\hat{S}_z$ so a possible Hamiltonian might be S_z^2 or some other polynomial. Then we say that $\mathfrak{g}$ is the dynamical algebra of the system and $\mathfrak{G}$ is the dynamical group of the system. Suppose now that $T(g)$ is a $k \times k$ matrix representing the element g in the abstract group. For simplicity, we suppose that it is not possible to make a change of basis in the k-dimensional space so that $T(g)$ becomes block diagonal, *i.e.* it is not possible to find a new basis where

$$T(g) = \begin{pmatrix} T_1(g) & 0 \\ 0 & T_2(g) \end{pmatrix}. \tag{2.3}$$

This is not a big assumption: if $T(g)$ can be written as block diagonal for every element g, then we work in $T_1(g)$ and $T_2(g)$ separately. When $T(g)$ cannot be brought to block diagonal form, it is said to be irreducible. A coherent state is then defined by picking an element g in the group and acting with its matrix representation $T(g)$ on a special state $|\psi_0\rangle$

$$|\psi_g\rangle = T(g) |\psi_0\rangle, \qquad g \in \mathfrak{G}. \tag{2.4}$$

The state $|\psi_0\rangle$ is chosen so it is killed either by every lowering operator or every raising operator. Thus, for the harmonic oscillator, one chooses $|\psi_0\rangle$ to be the vacuum state, killed by $\hat{a}$. For spin systems, one chooses $|\psi_0\rangle$ to be the $m = j$ state $|j, j\rangle$ which is killed by the raising operator $\hat{S}_+ = \hat{S}_x + i\hat{S}_y$.

In practice, Eq. (2.4) can be simplified. Within the set of group elements, there is a subset with the property that $T(h) |\psi_0\rangle$ returns $|\psi_0\rangle$ up to a phase:

$$T(h) |\psi_0\rangle = e^{i\phi(h)} |\psi_0\rangle. \tag{2.5}$$

This subset of elements forms a subgroup $\mathfrak{H}$ of the group $\mathfrak{G}$. For instance the subset of elements of the form $R_z(\gamma)$ form a subgroup of $SU(2)$; elements in the subset have the property that

$$R_z(\gamma) |j, j\rangle = e^{-i\hat{S}_z\gamma} |j, j\rangle = e^{-i\gamma j} |j, j\rangle. \tag{2.6}$$

As we mentioned before an element of $SU(2)$ can be factorized in the form $R_z(\varphi) R_y(\theta) R_z(\gamma)$. Since $R_z(\gamma) |j, j\rangle \propto |j, j\rangle$, we can eliminate this part in the factorization and see that a coherent state for $SU(2)$ can be written more simply as $R_z(\varphi) R_y(\theta) |j, j\rangle$. Thus, for $SU(2)$, $\mathfrak{H} = U(1)$ and $SU(2)$ coherent states are given by Eq. (2.2).

Every element $g \in \mathfrak{G}$ can be written as a product $g = \Omega \cdot h$ where h is in $\mathfrak{H}$ and Ω is the group element $g \cdot h^{-1}$ which is in the coset space $\mathfrak{M} = \mathfrak{G}/\mathfrak{H}$. Using this factorization of g, we see that two elements $g_1 = \Omega_1 \cdot h_1$ and $g_2 = \Omega_2 \cdot h_2$ will produce the same coherent state (up to a phase), if $\Omega_1 = \Omega_2$. Thus, distinct coherent states are really labeled by Ω's, not g's.

Using notions of geometry beyond the scope of this thesis, one can show that the cosets $\mathfrak{M}$ can be considered as a geometrical space (called the coset space) with properties of a classical phase space [38]. For the case of $SU(2)$ we have $g = R_z(\varphi)R_y(\theta)R_z(\gamma)$, $\Omega = R_z(\varphi) R_y(\theta)$ and

$h = R_z(\gamma)$. Thus the $SU(2)$ coherent states $|\varphi, \theta\rangle$ are determined by φ and θ in the coset $\mathfrak{M}$. The phase space of $SU(2)$ system is $SU(2)/U(1)$; one can show that this is geometrically identical to the 2-dimensional sphere [39], with θ the polar angle and φ the azymuthal angle on the sphere.

The two other examples that are given in this thesis are the harmonic oscillator coherent states, defined on the complex plane $\mathbb{C} = HW(1)/U(1)$, and the $SU(3)$ coherent states, defined on the 4-dimensional sphere $S^4 = SU(3)/U(2)$.

2.2 Stratonovich Weyl correspondence

According to the Stratonovich Weyl correspondence [40] an operator $\hat{f}$ in the Hilbert space $\mathbb{H}$ is mapped to a family of functions $W_f^{(s)}(\Omega)$, called phase space symbols, on the phase space $\mathfrak{M}$. The index s here is related to the ordering of the operators. In this thesis we always consider the symmetric ordering of the operators which for historical and convenience reasons is denoted by the index $s = 0$. With this blanket assumption we will no longer use the index s to lighten the notation.

It is desirable for the symbol $W_f(\Omega)$ to possess the following physically motivated properties [41]:

1. Linearity. The Hilbert space of a quantum mechanical system is linear. To preserve this the symbol for the sum of two operators should be the sum of the individual symbols:

$$W_{f+g}(\Omega) = W_f(\Omega) + W_g(\Omega) \,. \tag{2.7}$$

2. Reality. In order to guarantee that the symbol of an observable (*i.e.* a hermitian operator) be a real function, one requires

$$W_{f^\dagger}(\Omega) = \left(W_f(\Omega)\right)^* \,. \tag{2.8}$$

3. Normalization. This results in the constant function 1 as the symbol of the identity operator $\mathbb{1}$

$$\int d\mu(\Omega)\, W_f(\Omega) = \text{Tr}\left(\hat{f}\right) \tag{2.9}$$

where $d\mu(\Omega)$ is the invariant measure on the coset.

4. Covariance. This means that the phase space symbol of a transformed operator is the same as the symbol of the original operator but at the transformed point

$$W_{T(g)\hat{f}T(g)^\dagger}(\Omega) = W_f(g \cdot \Omega) \,. \tag{2.10}$$

This property has been used in chapter 1 to find the Wigner function of the rotated squeezed state.

5. Traciality. The tracing condition assures that the statistical average of the phase space symbol $W_f(\Omega)$ coincides with the quantum expectation value of the operator $\hat{f}$

$$\int d\mu(\Omega)\, W_f(\Omega)\, W_g(\Omega) = \text{Tr}\left(\hat{f}\hat{g}\right) \,. \tag{2.11}$$

The linearity is taken into account if we implement the map by

$$W_f(\Omega) = \text{Tr}\left(\hat{f}\hat{w}(\Omega)\right) \,, \tag{2.12}$$

where $\hat{w}(\Omega)$ is an operator-valued function on the phase space $\mathfrak{M}$ called quantization kernel. The traciality condition (2.11) is then taken in to account if

$$\hat{f} = \int d\mu(\Omega) W_f(\Omega) \hat{w}(\Omega) \tag{2.13}$$

and conditions (2.8) to (2.10) are satisfied by the following constraints on the quantization kernel

$$\hat{w}(\Omega) = (\hat{w}(\Omega))^\dagger, \tag{2.14}$$

$$\text{Tr}[\hat{w}(\Omega)] = 1, \tag{2.15}$$

$$T(g)\hat{w}(\Omega)T(g)^\dagger = \hat{w}\left(g^{-1} \cdot \Omega\right). \tag{2.16}$$

Substituting $\hat{f}$ and $\hat{g}$ from Eq. (2.13) into (2.11) we obtain the following condition on the quantization kernel,

$$\text{Tr}[\hat{w}(\Omega)\hat{w}(\Omega')] = \Delta(\Omega, \Omega') \tag{2.17}$$

where $\Delta(\Omega, \Omega')$ is called reproductive kernel and behaves like a δ function on $\mathfrak{M}$:

$$\hat{w}(\Omega') = \int d\mu(\Omega) \Delta(\Omega, \Omega') \hat{w}(\Omega). \tag{2.18}$$

Eq. (2.17) is the generalization of Eq. (1.22) in chapter 1. Within this framework, the quantization kernel for $SU(2)$ and $SU(3)$ systems were constructed in [34].

2.3 Star product and Moyal bracket

A final feature of the phase space formulation is the need to introduce a new kind of product rule, called the star product. In ordinary quantum mechanics, operators do not necessarily commute. On the other hand, operators are mapped to phase space functions of commuting variables. Thus, to preserve features related to the non-commutative nature of the operators, one must redefine the combination rules for the phase space functions. The star product of two symbols, $W_X(\Omega) \star W_Y(\Omega)$, is defined as

$$W_{XY}(\Omega) = W_X(\Omega) \star W_Y(\Omega) \tag{2.19}$$

The star product is associative,

$$W_X(\Omega) \star (W_Y(\Omega) \star W_Z(\Omega)) = (W_X(\Omega) \star W_Y(\Omega)) \star W_Z(\Omega), \tag{2.20}$$

but noncommutative,

$$W_X(\Omega) \star W_Y(\Omega) \neq W_Y(\Omega) \star W_X(\Omega). \tag{2.21}$$

The so-called Moyal bracket, defined as the symbol of the commutator, $W_{[\hat{X},\hat{Y}]}$, is written

$$\{W_X, W_Y\}_M \equiv W_{[\hat{X},\hat{Y}]} = W_X \star W_Y - W_Y \star W_X. \tag{2.22}$$

The von Neumann equation,

$$i\hbar \frac{\partial \hat{\rho}}{\partial t} = \left[\hat{H}, \hat{\rho}\right], \tag{2.23}$$

in which $\hat{H}$ is the Hamiltonian of the system and $\hat{\rho}$ is the density matrix, becomes a Liouville-like equation in the Moyal bracket for the Wigner quasi distribution function, the phase space symbol of the density operator,

$$i\hbar \frac{\partial}{\partial t} W_\rho(\Omega) = \left\{ W_H(\Omega), W_\rho(\Omega) \right\}_M = W_{[\hat{H}, \hat{\rho}]}. \tag{2.24}$$

In the next chapters, where the semiclassical dynamics of $SU(2)$ and $SU(3)$ systems will be discussed, this classical-like equation will be used. In particular, we will see that, under some assumptions that are reasonable for the physics of squeezing, the Moyal bracket can be approximated by the Poisson bracket, with correction terms going to zero in the "classical limit" of large representations, much like the correction terms of Eq.(1.13) go to zero in the limit where $\hbar$ goes to zero.

3. $SU(2)$ SEMICLASSICAL DYNAMICS

In this chapter we discuss dynamics of spin systems in the semiclassical regime. In spin systems the observables are spin operators $\hat{S}_x, \hat{S}_y, \hat{S}_z$ and their powers. The spin operators have the commutation relations of $su(2)$ algebra; hence the dynamical group of spin systems is the $SU(2)$ group. Systems of two level atoms and linear lossless passive device having two input ports and two output ports like beam splitters can be described by the group $SU(2)$. After giving some details on the $su(2)$ algebra, $SU(2)$ group and $SU(2)$ coherent states, the phase space symbol of $su(2)$ generators will be obtained. We write the quantum Liouville equation in terms of Poisson bracket and show that for large spin numbers j we can ignore quantum correction terms. Finally the semiclassical dynamics of spin systems under a linear and a nonlinear Hamiltonian will be discussed.

The results of this chapter are fully compatible with [42] in which discrete optical systems has been investigated using $SU(2)$ from a different perspective without using tensor operators on the group but functions. The fact that the two points of view are equivalent is discussed in [43].

3.1 su(2) algebra and $SU(2)$ group

The $su(2)$ algebra is spanned by 2×2 traceless hermitian matrices. The $su(2)$ algebra is constructed from spin operators $\hat{S}_x$, $\hat{S}_y$ and $\hat{S}_z$ with 2×2 matrix representation

$$\hat{S}_x = \frac{1}{2}\begin{pmatrix} 0 & 1 \\ 1 & 0 \end{pmatrix}, \quad \hat{S}_y = \frac{1}{2}\begin{pmatrix} 0 & -i \\ i & 0 \end{pmatrix}, \quad \hat{S}_z = \frac{1}{2}\begin{pmatrix} 1 & 0 \\ 0 & -1 \end{pmatrix}. \tag{3.1}$$

These operators and any real combination of them are called generators of the $su(2)$ algebra. The $su(2)$ operators in Eq. (3.1) have the following commutation relations

$$\left[\hat{S}_x, \hat{S}_y\right] = i\hat{S}_z, \quad \left[\hat{S}_y, \hat{S}_z\right] = i\hat{S}_x, \quad \left[\hat{S}_z, \hat{S}_x\right] = i\hat{S}_y. \tag{3.2}$$

The commutator of any two arbitrary generators is another linear generator. It is convenient to introduce $su(2)$ ladder operators

$$\hat{S}_{\pm} = \hat{S}_x \pm i\hat{S}_y, \tag{3.3}$$

which have the commutation relations:

$$\left[\hat{S}_z, \hat{S}_{\pm}\right] = \pm\hat{S}_{\pm}, \quad \left[\hat{S}_+, \hat{S}_-\right] = 2\hat{S}_z. \tag{3.4}$$

The action of the ladder operators $\hat{S}_{\pm}$ on the states $|j, m\rangle$ is as follows:

$$\hat{S}_{\pm} |j, m\rangle = \sqrt{(j \mp m)(j \pm m + 1)} |j, m \pm 1\rangle. \tag{3.5}$$

By exponentiating the generators of the $su(2)$ algebra we obtain the elements of the $SU(2)$ group. The set of 2×2 unitary matrices with determinant 1 forms the group $SU(2)$. The matrix multiplication is the group operation. In general any $SU(2)$ element can be written as

$$g = \begin{pmatrix} a & -b \\ b^* & a^* \end{pmatrix}, \quad |a|^2 + |b|^2 = 1 , \tag{3.6}$$

where a and b are complex numbers. In particular by writing

$$a = |a| e^{-i\xi_a}, \quad b = |b| e^{-i\xi_b} , \tag{3.7}$$

and defining,

$$|a| = \cos(\theta/2), \quad |b| = \sin(\theta/2) , \tag{3.8}$$

then

$$\begin{aligned} g &= \begin{pmatrix} \cos(\theta/2) e^{-i\xi_a} & -\sin(\theta/2) e^{-i\xi_b} \\ \sin(\theta/2) e^{i\xi_b} & \cos(\theta/2) e^{-i\xi_a} \end{pmatrix} \\ &= \begin{pmatrix} e^{-i\varphi/2} & 0 \\ 0 & e^{i\varphi/2} \end{pmatrix} \begin{pmatrix} \cos(\theta/2) & -\sin(\theta/2) \\ \sin(\theta/2) & \cos(\theta/2) \end{pmatrix} \begin{pmatrix} e^{-i\gamma/2} & 0 \\ 0 & e^{i\gamma/2} \end{pmatrix} , \end{aligned} \tag{3.9}$$

where $\xi_a = \frac{1}{2}(\varphi + \gamma)$, $\xi_b = \frac{1}{2}(\varphi - \gamma)$. From Eq. (3.1) one can verify that

$$\begin{pmatrix} e^{-i\varphi/2} & 0 \\ 0 & e^{i\varphi/2} \end{pmatrix} = e^{-i\varphi \hat{S}_z}, \qquad \begin{pmatrix} \cos(\theta/2) & -\sin(\theta/2) \\ \sin(\theta/2) & \cos(\theta/2) \end{pmatrix} = e^{-i\theta \hat{S}_y} . \tag{3.10}$$

Therefore a general element of the $SU(2)$ group can be written as

$$R(\varphi, \theta, \gamma) = R_z(\varphi) R_y(\theta) R_z(\gamma) , \tag{3.11}$$

with

$$R_z(\varphi) = e^{-i\varphi \hat{S}_z}, \qquad R_y(\theta) = e^{-i\theta \hat{S}_y} . \tag{3.12}$$

There exists a very interesting connection between the algebra of spin systems and the algebra of two dimensional harmonic oscillator [44]. Using creation and destruction operators $\hat{a}_1, \hat{a}_1^\dagger, \hat{a}_2$ and $\hat{a}_2^\dagger$ and the number operators $\hat{n}_1 = \hat{a}_1^\dagger \hat{a}_1$ and $\hat{n}_2 = \hat{a}_2^\dagger \hat{a}_2$ for the 2 dimensional harmonic oscillator we note the commutation relations in Eq. (3.4) are reproduced if one identifies

$$\hat{S}_+ \equiv \hat{a}_1^\dagger \hat{a}_2 , \tag{3.13}$$

$$\hat{S}_- \equiv \hat{a}_2^\dagger \hat{a}_1 , \tag{3.14}$$

$$\hat{S}_z \equiv \frac{1}{2}\left(\hat{a}_1^\dagger \hat{a}_1 - \hat{a}_2^\dagger \hat{a}_2\right) = \frac{1}{2}(\hat{n}_1 - \hat{n}_2) . \tag{3.15}$$

Using this harmonic oscillator realization the states $|j, m\rangle$ can be written as $|n_1, n_2\rangle$ with

$$\hat{S}_+ |n_1, n_2\rangle = \sqrt{(n_1 + 1) n_2} |n_1 + 1, n_2 - 1\rangle , \tag{3.16}$$

$$\hat{S}_- |n_1, n_2\rangle = \sqrt{n_1 (n_2 + 1)} |n_1 - 1, n_2 + 1\rangle , \tag{3.17}$$

$$\hat{S}_z |n_1, n_2\rangle = \frac{1}{2}(n_1 - n_2) |n_1, n_2\rangle . \tag{3.18}$$

The ladder operators $\hat{S}_\pm$ keep the total number $n = n_1 + n_2$ constant. From Eq. (3.18) it is clear that $m = \frac{1}{2}(n_1 - n_2)$. On the other hand we know that, for the state $|j, j\rangle$ (killed by the raising operator $\hat{S}_+$) we have $j = m$. In terms of harmonic oscillator kets, the state killed by $\hat{S}_+$ is $|n, 0\rangle$ with $n = n_1 + n_2$. For this state $\hat{S}_z |n, 0\rangle = \frac{1}{2}n |n, 0\rangle$ therefore $j = \frac{1}{2}(n_1 + n_2)$.

For a spin $\frac{1}{2}$ system, n_1 and n_2 specifies the number of particles with spin up or down, respectively. $\hat{S}_\pm$ destroys one unit of spin down(resp. up) and creates one unit of spin up(resp. down).

3.2   *S U(2) or spin coherent states*

S U(2) coherent states are constructed by the action of the rotation operator of Eq. (3.11) on the extremal state $|j, j\rangle$ [45]. Ignoring the phase factor that results from the action of $R_z(\gamma)$ on $|j, j\rangle$, the *S U*(2) coherent states can be written as

$$
\begin{aligned}
|\varphi, \theta\rangle &= R_z(\varphi) R_y(\theta) |j, j\rangle && (3.19) \\
&= \sum_{m=-j}^{j} |j, m\rangle \langle j, m| R_z(\varphi) R_y(\theta) |j, j\rangle \\
&= \sum_{m=-j}^{j} |j, m\rangle D_{m,j}^{j}(\varphi, \theta, 0), && (3.20)
\end{aligned}
$$

where $D_{m,j}^{j}(\varphi, \theta, \gamma)$ is the *S U*(2) Wigner *D* function [46] which is defined by

$$
\begin{aligned}
D_{m,j}^{j}(\varphi, \theta, \gamma) &\equiv \langle j, m| R_z(\varphi) R_y(\theta) R_z(\gamma) |j, j\rangle \\
&= e^{-i(m\varphi + j\gamma)} \sqrt{\frac{(2j)!}{(j+m)!\,(j-m)!}} \cos^{j+m}\left(\frac{\theta}{2}\right) \sin^{j-m}\left(\frac{\theta}{2}\right). && (3.21)
\end{aligned}
$$

The physical meaning of φ and θ angles is made clear by writing the spin coherent state of Eq. (3.19) as a product of $2j$ states $|\varphi, \theta\rangle_i$ which are superposition of states of a two level system like spin up and spin down for a spin $\frac{1}{2}$ particle,

$$
|\varphi, \theta\rangle \propto |\varphi, \theta\rangle_1 \otimes |\varphi, \theta\rangle_2 \otimes ... \otimes |\varphi, \theta\rangle_{2j}, \tag{3.22}
$$

$$
|\varphi, \theta\rangle_i \equiv e^{i\varphi/2} \cos\left(\tfrac{1}{2}\theta\right)\left|+\tfrac{1}{2}\right\rangle_i + e^{-i\varphi/2} \sin\left(\tfrac{1}{2}\theta\right)\left|-\tfrac{1}{2}\right\rangle_i. \tag{3.23}
$$

3.3   *Phase space symbols*

As mentioned in previous chapter the reference state $|j, j\rangle$ is invariant under the $U(1)$ subgroup generated by $e^{-i\gamma \hat{S}_z}$. The resulting phase space for spin systems is the 2-dimensional sphere $S^2 = S U(2)/U(1)$, also called Bloch sphere. In this section we obtain phase space symbols of *S U*(2) operators.

Following the prescription given in Chapter 2, the phase space symbol, W_X of an operator $\hat{X}$ is

$$
W_X(\varphi, \theta) = \mathrm{Tr}\left(\hat{X}\hat{w}(\varphi, \theta)\right). \tag{3.24}
$$

For *S U*(2), the quantization kernel can be written as

$$
\hat{w}(\varphi, \theta) = \Lambda(\varphi, \theta)\hat{P}\Lambda^\dagger(\varphi, \theta), \tag{3.25}
$$

where $\Lambda(\varphi, \theta) \equiv R_z(\varphi) R_y(\theta)$ and [34]

$$
\hat{P} = \int_0^{2\pi} d\omega\, e^{i\omega \hat{S}_z} f(\omega), \tag{3.26}
$$

where $f(\omega)$ is a scalar function and is constructed in such a way that the quantization kernel satisfies all the requirements we mentioned in chapter 2.

Notice how the general form of this kernel is similar to the kernel for the harmonic oscillator in Eq. (1.17): it is a diagonal operator $\hat{P}$ that has been "displaced" by the rotation $\Lambda(\theta, \varphi)$. The operator $\hat{P}$ commutes with $\hat{S}_z$ so the displacement can be limited to element of the form $R_z(\varphi)R_y(\theta)$.

Since $e^{i\omega\hat{S}_z}$ is a diagonal operator, $\hat{P}$ can be expanded as

$$\hat{P} = \sum_m c_{j,m} |j, m\rangle \langle j, m| , \tag{3.27}$$

where $c_{j,m}$ is a factor that must be determined. An alternative, more convenient form to obtain the result of the displacement of $\hat{P}$ is to write $\hat{P}$ in terms of tensor operators $\hat{T}^j_{L,M}$. These operators are defined as

$$\hat{T}^j_{L,M} = \sum_{m,m'=-j}^{j} |j, m\rangle \langle j, m'| C^{L,M}_{j,m;j,-m'}(-1)^{j-m} , \tag{3.28}$$

where $C^{L,M}_{j,m;j,-m'}$ is the Clebsch Gordan coefficient for $S U(2)$,

$$C^{L,M}_{j,m;j,-m'} = \langle j, m; j, -m' \mid L, M \rangle . \tag{3.29}$$

The tensors cleanly transform as

$$\Lambda(\varphi, \theta) \hat{T}^j_{L,M} \Lambda^{-1}(\varphi, \theta) = \sum_{M'=-L}^{L} \hat{T}^j_{L,M'} D^L_{M',M}(\varphi, \theta, 0) . \tag{3.30}$$

Technical manipulations eventually give

$$\hat{P} = \sum_{L=0}^{2j} \sqrt{\frac{2L+1}{2j+1}} \, \hat{T}^j_{L0} . \tag{3.31}$$

The displacement of $\hat{P}$ yields a useful form of the quantization kernel as

$$\hat{w}(\varphi, \theta) = \sum_{L=0}^{2j} \sqrt{\frac{2L+1}{2j+1}} \sum_{M=-L}^{L} D^L_{M0}(\varphi, \theta, 0)\hat{T}^j_{L,M} . \tag{3.32}$$

To obtain the phase space symbol of $su(2)$ generators one conveniently expresses the generators in terms of tensor operators:

$$\hat{S}_z = N \hat{T}_{10} , \tag{3.33}$$
$$\hat{S}_+ = -\sqrt{2} N \hat{T}_{1,1} , \tag{3.34}$$
$$\hat{S}_- = \sqrt{2} N \hat{T}_{1,-1} , \tag{3.35}$$

where $N = \sqrt{\frac{1}{3}j(j+1)(2j+1)}$. Using Eqs. (3.24), (3.28), (3.32) and using the orthogonality of tensors under trace:

$$\mathrm{Tr}\left(\hat{T}^j_{L,M}\hat{T}^{j'}_{L',M'}\right) = \delta_{j,j'}\delta_{L,L'}\delta_{M,M'} \tag{3.36}$$

one obtains

$$W_{S_k}(\varphi, \theta) = \sqrt{j(j+1)} n_k, \quad k = x, y, z , \tag{3.37}$$

where n_k are components of the unit vector

$$\vec{n} = (\sin\theta\cos\varphi, \sin\theta\sin\varphi, \cos\theta) \,. \tag{3.38}$$

A diagonal operator like $\hat{S}_z^2$ can be written as a sum of diagonal tensors:

$$\hat{S}_z^2 = c_0\hat{T}_{0,0} + c_2\hat{T}_{2,0} \,, \tag{3.39}$$

where

$$c_0 = \frac{1}{3}j(j+1)\sqrt{2j+1}, \quad c_2 = \frac{\sqrt{5}}{15}\sqrt{(2j+1)(2j-1)(2j+3)j(j+1)}. \tag{3.40}$$

From these and the quantization kernel we find:

$$W_{S_z^2}(\varphi,\theta) = \frac{j(j+1)}{3} + \frac{1}{2}\sqrt{(2j-1)(2j+3)j(j+1)}\left(\cos^2\theta - \frac{1}{3}\right). \tag{3.41}$$

It is clear that $W_{S_z^2}$ is not equal to $\left(W_{S_z}\right)^2$. For later use, we note that similar manipulations produce

$$W_{S_x^2}(\varphi,\theta) = \frac{j(j+1)}{3} + \frac{1}{2}\sqrt{(2j-1)(2j+3)j(j+1)}\left(\sin^2\theta\cos^2\varphi - \frac{1}{3}\right), \tag{3.42}$$

which again is not the square of W_{S_x}.

3.4 Semiclassical dynamics

In this section we discuss the dynamics of $S U(2)$ systems in phase space in the semiclassical approximation. We use Eq. (2.24) to expand the symbol of a commutator and express this to leading order as a Poisson bracket, ignoring quantum correction terms that occur in expansion. Thus we need to find the relation between the symbol of a commutator and the Poisson bracket of the symbols.

The Poisson bracket on the two-dimensional sphere S^2 can be deduced from the parametrization of $S U(2)$ coherent states. The final result for the bracket is [47]:

$$\{f,g\} = \frac{1}{\sin\theta}\left(\frac{\partial f}{\partial\varphi}\frac{\partial g}{\partial\theta} - \frac{\partial f}{\partial\theta}\frac{\partial g}{\partial\varphi}\right), \tag{3.43}$$

where f and g are two functions on S^2.

If f and g are the symbols of two generators, the Poisson bracket is proportional to the symbol of the commutator. For instance

$$\left\{W_{S_z}, W_{S_x}\right\} = i\sqrt{j(j+1)}\, W_{S_y} = \varepsilon W_{[S_z,S_x]} \,, \tag{3.44}$$

where the proportionality factor, $\varepsilon = i\sqrt{j(j+1)}$, is called the semiclassical parameter. Likewise, if f is a polynomial in the generators and g is a generator, the Poisson bracket of the symbols is proportional to the symbol of the commutator. For instance:

$$\left\{W_{S_z^2}, W_{S_x}\right\} = \varepsilon W_{[S_z^2,S_x]} \,, \tag{3.45}$$

where

$$W_{[\hat{S}_z^2,\hat{S}_y]} = \sqrt{(2j-1)(2j+3)\,j(j+1)}\,\cos\theta\sin\theta\sin\varphi\,.\tag{3.46}$$

However for two polynomials of degree 2 or greater in the generators, correction terms appear. For instance:

$$\left\{W_{S_z^2},W_{S_x^2}\right\} = \varepsilon W_{[\hat{S}_z^2,\hat{S}_x^2]} + O\left(\varepsilon^{-2}\right).\tag{3.47}$$

Operators and observables in this thesis will be expanded in terms of tensors, introduced for $su(2)$ in Eq. (3.28). It is thus convenient to reformulate the results of Eqs. (3.45) and (3.47) in terms of tensors. Constant terms are proportional to the tensor with $L = 0$. Generators are always proportional to tensors with $L = 1$, as illustrated explicitly in Eqs. (3.33)-(3.35). Powers of generators will usually contain tensors with $L > 1$. *Vice versa*, tensors with $L > 1$ are proportional to linear combinations of powers of generators. Thus, Eq. (3.45) expresses the general rule that the Poisson bracket of the symbols of a tensor with $L = 1$ and any other symbol is exactly the symbol of the commutator of the tensors, while Eq. (3.47) expresses the general rule that the Poisson bracket of the symbol of two tensors, both with $L > 1$, contains correction terms.

Therefore if the Hamiltonian is linear in generators and so proportional to a combination of $L = 1$ tensors, the equations of motion for the Wigner function is given exactly by the Poisson bracket ($\hbar = 1$):

$$i\frac{\partial W_\rho}{\partial t} = W_{[H,\rho]} = \varepsilon^{-1}\left\{W_H,W_\rho\right\}\,.\tag{3.48}$$

If, on the other hand, the Hamiltonian is non-linear in the generators, it will generally contain terms with $L > 1$. As the density operator is expected to also contain terms with $L > 1$, correction terms will appear in the evolution:

$$i\frac{\partial W_\rho}{\partial t} = \varepsilon^{-1}\left\{W_H,W_\rho\right\} + O\left(\varepsilon^{-3}\right),\tag{3.49}$$

where the second term is a quantum correction to the classical dynamics and is of the order of ε^{-3}. In the semiclassical limit, $\varepsilon^{-1} \to 0$ or $j \gg 1$; we can ignore the corrections beyond the Poisson bracket and obtain a truncated Liouville evolution.

3.4.1 Linear dynamics

Equipped with the necessary tools we first investigate the dynamics of the $SU(2)$ system for the simplest case: the evolution of the system under linear Hamiltonian.

As an initial state we consider the atomic coherent state located along the $\hat{x}$ direction, $|\varphi = 0, \theta = \pi/2 \rangle$. This choice of initial state will be justified on physical grounds when we later consider the evolution under a quadratic Hamiltonian. Using Eq. (3.19) we can write

$$|0,\frac{\pi}{2}\rangle = \frac{1}{2^j}\sum_{k=-j}^{j}\sqrt{\frac{(2j)!}{(j+k)!\,(j-k)!}}\,|j,k\rangle\,.\tag{3.50}$$

Using Eqs (3.24), (3.28) and (3.32) the Wigner function $W_\rho(\varphi,\theta)$ of the initial density operator,
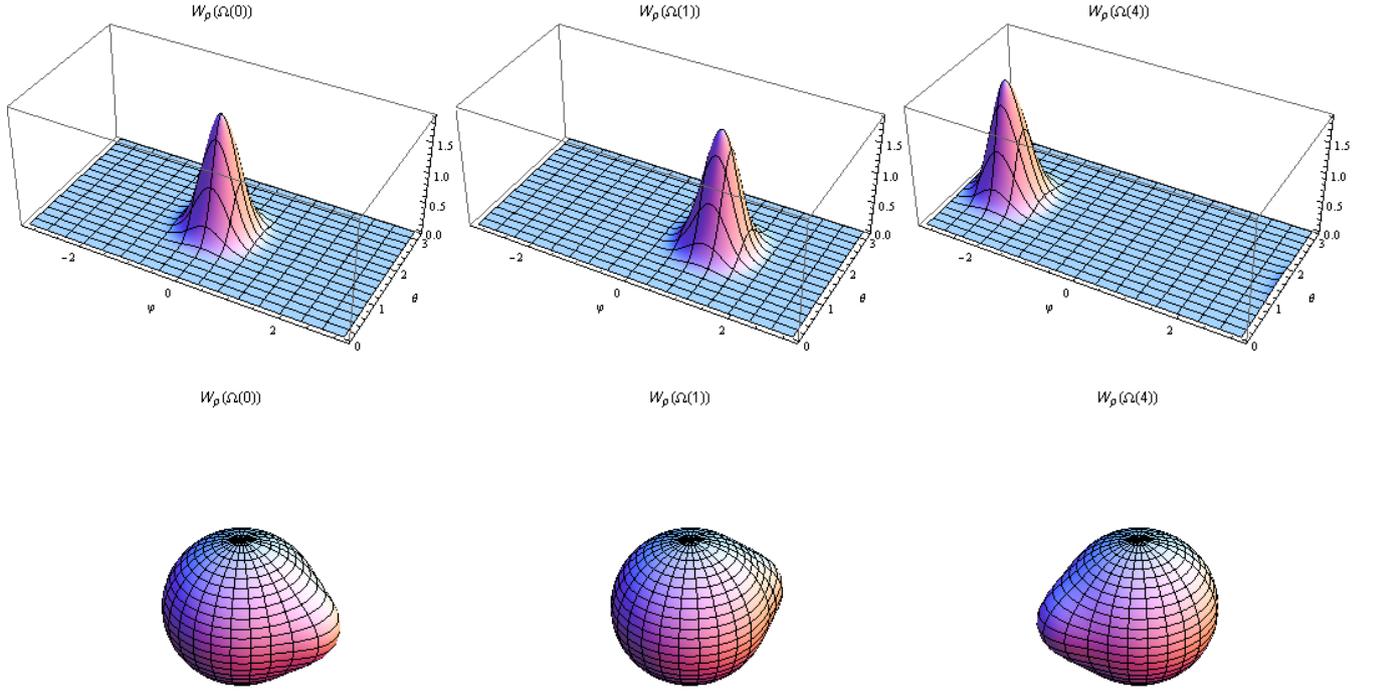
Fig. 3.1: Time evolved Wigner function in Eq. (3.51) under linear Hamiltonian $\hat{H} = \hat{S}_z$ at $t = 0, 1$ and $t = 4$ for $j = 5$.

$\rho = |0, \pi/2 \rangle \langle 0, \pi/2 |$, is obtained as

$$
\begin{aligned}
W_\rho(\varphi, \theta) &= \frac{(2j)!}{2^{2j}(2j+1)} \sum_{L=0}^{2j} (2L+1) \sum_{M=-L}^{L} D_{M,0}^L(\varphi, \theta, 0) \\
&\times \sum_{m,m'=-j}^{j} \frac{C_{j,m;L,M}^{j,m'}}{\sqrt{(j+m)!\,(j-m)!\,(j+m')!\,(j-m')!}} .
\end{aligned}
\tag{3.51}
$$

Now let us see how this Wigner function evolves under a general linear Hamiltonian

$$
\hat{H} = \omega_z \hat{S}_z + \omega_x \hat{S}_x + \omega_y \hat{S}_y .
\tag{3.52}
$$

This Hamiltonian can be reduced to a diagonal Hamiltonian by a transformation U,

$$
\hat{H}_d = U^\dagger \hat{H} U = \omega \hat{S}_z, \quad \omega = \sqrt{\omega_x^2 + \omega_y^2 + \omega_z^2} .
\tag{3.53}
$$

Here we work with H_d and set $\omega = 1$.

Using Eq. (3.48) we obtain

$$
\partial_t W_\rho(\theta, \varphi) = \varepsilon^{-1} \left\{ W_H, W_\rho \right\} = -\frac{\partial}{\partial \varphi} W_\rho(\theta, \varphi) .
\tag{3.54}
$$

By the method of characteristics this partial differential equation is transformed into an ordinary differential equation along the appropriate curve, *i.e.*, something of the form

$$
\frac{d}{ds} W_\rho(\varphi(s), t(s)) = F\left(W_\rho, \varphi(s), t(s)\right) ,
\tag{3.55}
$$

where $(\varphi(s), t(s))$ is the characteristic. By the chain rule we have

$$\frac{dW_\rho}{ds} = \frac{\partial W_\rho}{\partial \varphi}\frac{d\varphi}{ds} + \frac{\partial W_\rho}{\partial t}\frac{dt}{ds}. \tag{3.56}$$

Now if we set $dt/ds = 1, d\varphi/ds = 1$ we obtain $\partial W_\rho/\partial t + \partial W_\rho/\partial \varphi$ which, according to Eq. (3.54), equals to zero. Thus, along the characteristic the original partial differential equation becomes the ordinary differential equation $dW_\rho/ds = F\left(W_\rho, \varphi(s), t(s)\right) = 0$. That is to say: along the characteristics, the solution is constant. Therefore if we set $t(0) = 0$ we have $t = s$ and $\varphi(t) = t + \varphi(0)$. This means that if $W_\rho(0) = f(\varphi(0))$ then $W_\rho(\varphi(t), t) = f(\varphi - t)$. In other words the evolved Wigner function is obtained by replacing φ with $\varphi - t$. This corresponds to a rotation of Wigner function around $\hat{z}$ axis as illustrated in Fig. 3.1.

To check the validity of our solution one can compare, for example, the variance (as a function of time) of the observable $\hat{S}_x$,

$$(\Delta S_x)^2 = \langle S_x^2 \rangle - \langle S_x \rangle^2, \tag{3.57}$$

calculated using the usual quantum mechanical evolution

$$\langle \hat{S}_x \rangle = \langle 0, \frac{\pi}{2} | e^{i\hat{H}t} \hat{S}_x e^{-i\hat{H}t} | 0, \frac{\pi}{2} \rangle, \tag{3.58}$$

and calculated using the phase space formulation,

$$\langle \hat{S}_x \rangle = \frac{2j+1}{4\pi} \int_0^\pi \sin\theta d\theta \int_0^{2\pi} d\varphi W_{S_x}(\varphi, \theta) W_\rho(\varphi - t, \theta). \tag{3.59}$$

This is done on the left of Fig. 3.2. Since the classical evolution in phase space is exact for linear Hamiltonians, both semiclassical and quantum mechanical evolutions give the same result: the two curves on the left of Fig. 3.2 cannot be distinguished.
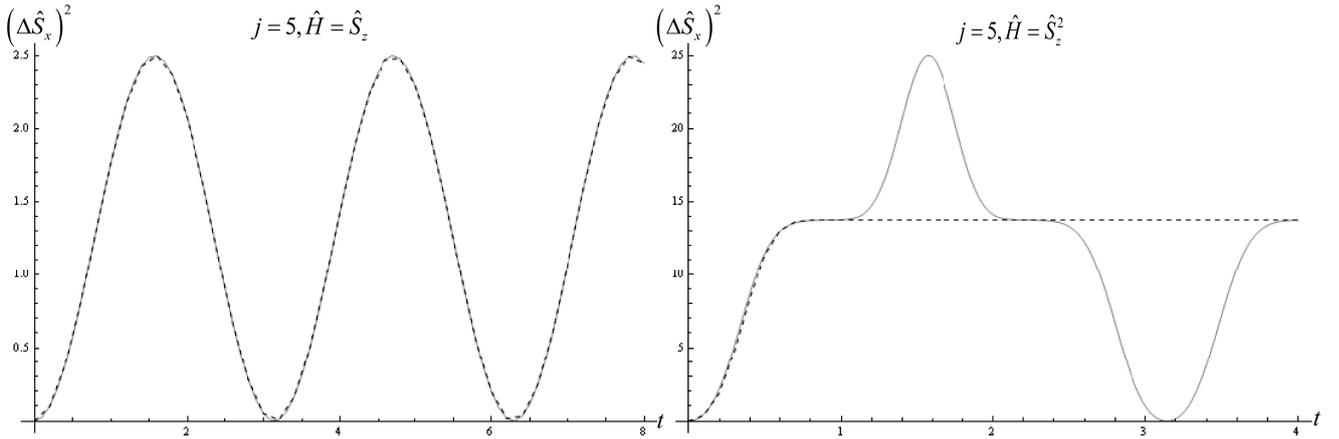

Fig. 3.2: Time evolution of the variance of $\hat{S}_x$, $\left(\Delta \hat{S}_x\right)^2$, calculated semiclassically using Eq. (3.59) (dashed line) and quantum mechanically using Eq. (3.58) (solid line) for $j = 5$. Left plot is the time evolution under linear Hamiltonian $\hat{H} = \hat{S}_z$ and right plot is the time evolution under nonlinear Hamiltonian $\hat{H} = \hat{S}_z^2$

3.4.2 Nonlinear dynamics

Now let us consider the simplest nonlinear Hamiltonian

$$\hat{H} = \hat{S}_z^2 , \tag{3.60}$$

which, in spite of its simplicity, leads to a number of interesting features such as generation of atomic squeezed states (see chapter 5) and atomic Schrödinger cats [48], [49]. This is also the simplest Hamiltonian for which quantum dynamics differs from semiclassical dynamics.

The semiclassical approximation is expected to work well for localized states located near the classical minimum (in phase space) of the Hamiltonian. The symbol for $W_{S_z^2}$ is given in Eq. (3.41); its minimum is located at $\theta = \frac{1}{2}\pi$ and $\varphi = 0$. One can show that for this choice of initial states the influence of quantum corrections to the classical evolution is small [50].

For nonlinear Hamiltonians in the semiclassical limit, $j \gg 1$, we ignore quantum correction terms in the equation of motion of the Wigner function, (3.49), and write

$$\frac{\partial W_\rho(\varphi, \theta)}{\partial t} \approx \varepsilon^{-1} \left\{ W_H, W_\rho \right\} = -\sqrt{(2j+3)(2j-1)} \cos\theta \frac{\partial W_\rho}{\partial \varphi} . \tag{3.61}$$

Using the method of characteristics the time-evolved Wigner function will be obtained as

$$W_\rho(\Omega(t)) = W_\rho\left(\varphi - \sqrt{(2j+3)(2j-1)} \cos(\theta) t, \theta\right) , \tag{3.62}$$

which basically means that the spherical angles evolve along classical trajectories.

The interpretation of this solution is that points located at different positions rotate about the $\hat{z}$ axis of the sphere at velocities which depend on $\cos\theta$. This leads to deformation of initial distribution and eventually to spin squeezing as shown in Fig. 3.4. This will be discussed at greater length in chapter 5. In Fig. 3.3 the exact quantum mechanical evolution of the Wigner function has been plotted. The details of the calculations of the exact quantum mechanical evolution of the Wigner function is given in appendix C.1. As can be seen from Figs. 3.4 and 3.3 at $t = 0.1$ the agreement between semiclassical approximation and exact quantum mechanical is good. For larger values of t, the phase spread exceeds 2π and the front of the distribution interferes with its tail [49]. This self-interference is a quantum effect and cannot be described by the semiclassical approximation. As it can be seen from Fig. 3.3 at $t = 0.3$ several dips and peaks appear which cannot be reproduced by the semiclassical approximation; the later dips and peaks are due to self interference.

On the right of Fig. 3.2, the variance $\left(\Delta\hat{S}_x\right)^2$ computed using the semiclassical evolution and using the exact quantum evolution are plotted. The semiclassical approximation describes the evolution of the variance to a good proportion; for larger values of j the agreement between the semiclassical and quantum evolution increases. The peak in the quantum mechanical curve is the result of the appearance of Schrödinger's cat states which cannot be obtained by the semiclassical method. The semiclassical curve is able to catch the quantum mechanical curve up to some time but after that it remains constant. It is remained constant because the evolution of the Wigner function in the semiclassical approximation remains uniform.

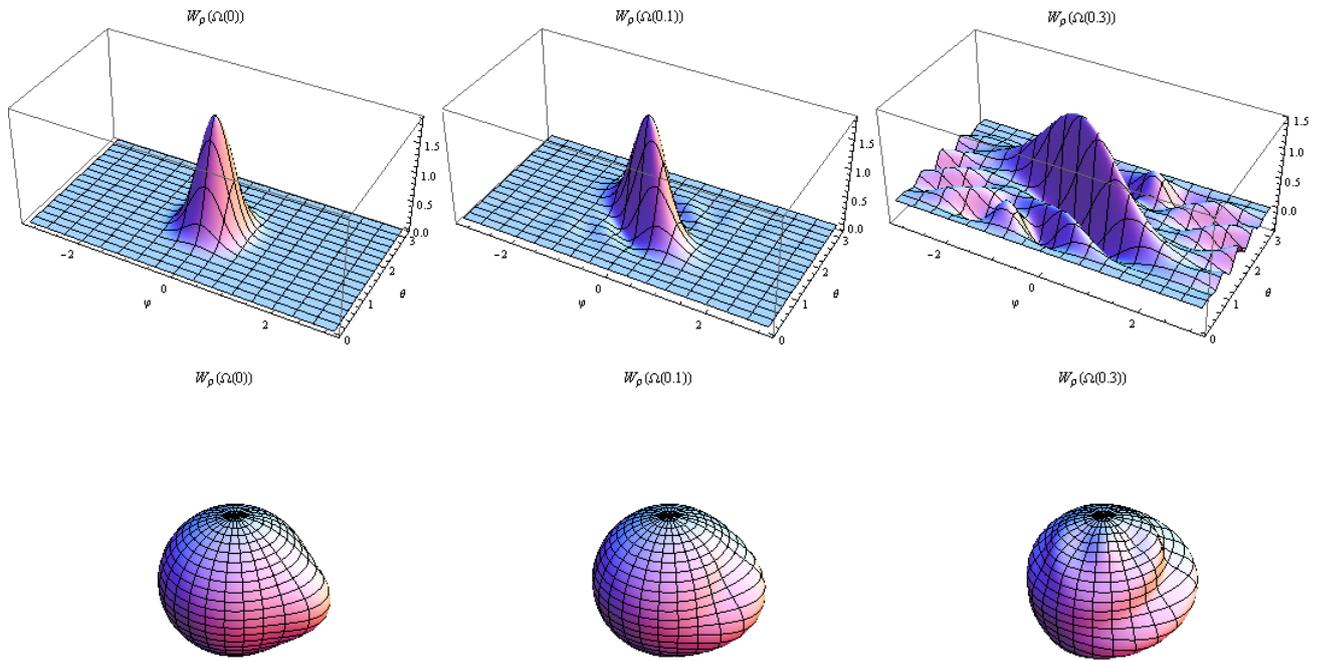*Fig. 3.3:* Exact quantum mechanical evolution of the Wigner function of the initial state in Eq.(3.19) with $\varphi = 0$, $\theta = \frac{\pi}{2}$ under nonlinear Hamiltonian $\hat{H} = \hat{S}_z^2$ at $t = 0$, 0.1 and $t = 0.3$ for $j = 5$.
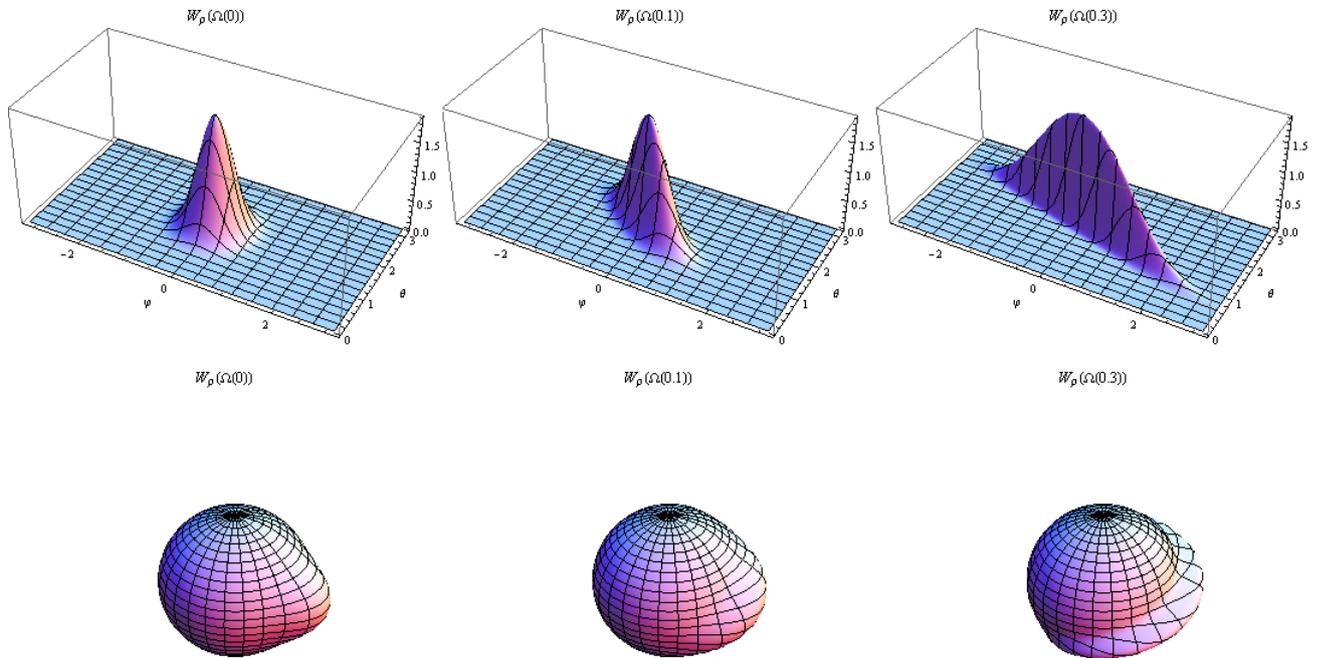

Fig. 3.4: Semiclassical evolution of the Wigner function in Eq.(3.51) under nonlinear Hamiltonian $\hat{H} = \hat{S}_z^2$ at $t = 0$, 0.1 and $t = 0.3$ for $j = 5$.

4. $SU(3)$ SEMICLASSICAL DYNAMICS

In this chapter we investigate dynamics of $SU(3)$ systems under the evolution of a linear and a nonlinear Hamiltonian in the semiclassical regime. As examples of $SU(3)$ systems one can consider systems of three-level atoms or three-well Bose Einstein condensate systems. The approach is a generalization of the procedure given for $SU(2)$ in the previous chapter. The possible dynamics of $SU(3)$ systems is considerably richer than the corresponding $SU(2)$ dynamics: for instance in three-level atoms transitions between levels 1-2, 2-3 and 1-3 are possible, may or may not be simultaneously resonant, may be restricted to pairs of levels or occur simultaneously. The mathematical structure of $SU(3)$ is more complicated than $SU(2)$: $SU(3)$ transformations need to model the richness of the underlying possible physical processes such as those given above.

After giving some details about the $su(3)$ algebra, the $SU(3)$ group and $SU(3)$ coherent states we use the Liouville equation written in terms of Poisson bracket to investigate the dynamics of the system.

4.1 $SU(3)$ group and $su(3)$ algebra

$SU(3)$ like $SU(2)$, is a group. Its elements can be represented as 3×3 unitary matrices with determinant 1. The group elements are constructed by exponentiating a set of 8 generators of $su(3)$ algebra.

4.1.1 The algebra $su(3)$ and its generators

In the defining form the generators of $su(3)$ algebra are 3×3 traceless hermitian matrices

$$T_1 = \begin{pmatrix} 1 & 0 & 0 \\ 0 & -1 & 0 \\ 0 & 0 & 0 \end{pmatrix}, \quad T_2 = \begin{pmatrix} 0 & 0 & 0 \\ 0 & 1 & 0 \\ 0 & 0 & -1 \end{pmatrix},$$

$$T_3 = \begin{pmatrix} 0 & 1 & 0 \\ 1 & 0 & 0 \\ 0 & 0 & 0 \end{pmatrix}, \quad T_4 = \begin{pmatrix} 0 & -i & 0 \\ i & 0 & 0 \\ 0 & 0 & 0 \end{pmatrix}, \quad T_5 = \begin{pmatrix} 0 & 0 & 1 \\ 0 & 0 & 0 \\ 1 & 0 & 0 \end{pmatrix},$$

$$T_6 = \begin{pmatrix} 0 & 0 & -i \\ 0 & 0 & 0 \\ i & 0 & 0 \end{pmatrix}, \quad T_7 = \begin{pmatrix} 0 & 0 & 0 \\ 0 & 0 & 1 \\ 0 & 1 & 0 \end{pmatrix}, \quad T_8 = \begin{pmatrix} 0 & 0 & 0 \\ 0 & 0 & -i \\ 0 & i & 0 \end{pmatrix}. \tag{4.1}$$

To better understand the structure of the operators it is convenient to define, much like what was done for the operators $\hat{S}_\pm$ of $su(2)$, complex linear combinations of $su(3)$ generators that

function as ladder operators:

$$E_{(2,-1)} = \frac{1}{2}(T_3 + iT_4), \quad E_{(-2,1)} = \frac{1}{2}(T_3 - iT_4),$$

$$E_{(1,1)} = \frac{1}{2}(T_5 + iT_6), \quad E_{(-1,-1)} = \frac{1}{2}(T_5 - iT_6),$$

$$E_{(-1,2)} = \frac{1}{2}(T_7 + iT_8), \quad E_{(1,-2)} = \frac{1}{2}(T_7 - iT_8). \tag{4.2}$$

Here, the indices α_1 and α_2 in $E_{(\alpha_1,\alpha_2)}$ are specified from the commutation relations of $E_{(\alpha_1,\alpha_2)}$ with T_1 and T_2 respectively:

$$[T_i, E_{(\alpha_1,\alpha_2)}] = \alpha_i E_{(\alpha_1,\alpha_2)}, \quad i = 1, 2. \tag{4.3}$$

The remaining commutation relations are

$$[T_1, T_2] = 0, \quad [E_\alpha, E_\beta] = N_{\alpha,\beta} E_{\alpha+\beta}. \tag{4.4}$$

The pair $(\alpha_1, \alpha_2) \equiv \alpha$ is called the root vector; the constant $N_{\alpha,\beta}$ is zero if $\alpha + \beta$ is not a root vector.

Using the creation and destruction operators of the three-dimensional harmonic oscillator, $\hat{a}_i$ and $\hat{a}_i^\dagger$ with $i = 1, 2, 3$, the abstract commutation relations of $su(3)$ algebra can be implemented by defining

$$\begin{aligned}
\hat{C}_{ij} &= \hat{a}_i^\dagger \hat{a}_j, & i, j = 1, 2, 3, \quad i \neq j, \\
\hat{T}_1 &= \hat{a}_1^\dagger \hat{a}_1 - \hat{a}_2^\dagger \hat{a}_2, & \hat{T}_2 = \hat{a}_2^\dagger \hat{a}_2 - \hat{a}_3^\dagger \hat{a}_3.
\end{aligned} \tag{4.5}$$

Using the usual commutation relation for harmonic oscillator creation and destruction operators, we find

$$[\hat{C}_{ij}, \hat{C}_{kl}] = \hat{C}_{il}\delta_{jk} - \hat{C}_{kj}\delta_{il}. \tag{4.6}$$

The root vectors of $\hat{C}_{ij}$ operators are then obtained by the commutation relation of these operators with the $\hat{T}_1$ and $\hat{T}_2$ operators.

From Eq. (4.5), we see that the abstract $su(3)$ operators are closely related to the action of creation and destruction operators acting on the states $|n_1, n_2, n_3\rangle$ of a three dimensional harmonic oscillator. We see that the operator $\hat{C}_{ij}$ transfers one quantum from level j to level i, *i.e.* it generates transition between levels j and i. For example, with reference to Fig. 4.1, we see that $\hat{C}_{12}|110\rangle$ is proportional to $|200\rangle$. It is obvious that the ladder operators $\hat{C}_{ij}$ keep the total number $N = n_1 + n_2 + n_3$ constant.

The formal correspondence between the abstract $E_{(\alpha_1,\alpha_2)}$ and $\hat{C}_{ij}$ operators is given in the following table. For convenience, we call raising operators the set $\hat{C}_{12}, \hat{C}_{13}, \hat{C}_{23}$. The state $|\lambda 00\rangle$ cannot be raised any more (it is killed by all raising operators) and is thus called the highest weight state.

root vector	$E_{(2,-1)}$	$E_{(1,1)}$	$E_{(-1,2)}$	$E_{(-2,1)}$	$E_{(-1,-1)}$	$E_{(1,-2)}$
$\hat{C}_{ij}$	$\hat{C}_{12}$	$\hat{C}_{13}$	$\hat{C}_{23}$	$\hat{C}_{21}$	$\hat{C}_{31}$	$\hat{C}_{32}$
action	raising	raising	raising	lowering	lowering	lowering

The root diagram in terms of $\hat{C}_{ij}$ operators is shown on the left of Fig. 4.1. The operator associated with a specific root vector is indicated next to the root vector. The circled dot at the center indicates that two operators, $\hat{T}_1$ and $\hat{T}_2$, should be considered as lying at the center of the root diagram. Anticipating future discussion, we note that the subset of operators $\hat{C}_{23}, \hat{C}_{32}$ and $\hat{h}_2 \equiv \frac{1}{2}\hat{T}_2$ have the commutation relations of *su*(2) thus make an *su*(2) subalgebra of *su*(3). We denote this subalgebra by $su(2)_{23}$.
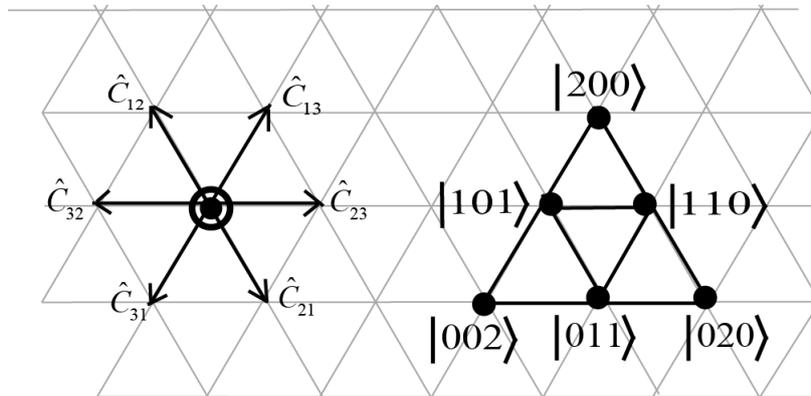

Fig. 4.1: The *su*(3) root diagram (left) and the weight diagram of $(2,0)$ irrep (right). The geometry of $(\lambda, 0)$ irreps is a triangular lattice.

4.1.2   Representations of su(3)

The realization of abstract *su*(3) operators in terms of creation and destruction operators acting on states of a three dimensional harmonic oscillator is a direct generalization of a similar realization of *su*(2), described in the previous chapter. Recall that the two-dimensional harmonic oscillator states $|n_1, n_2\rangle$ is equivalent to $|j, m\rangle$ where $j = \frac{1}{2}(n_1 + n_2)$ specifies the representation and *m* which is called the weight of the state is $\frac{1}{2}(n_1 - n_2)$.

In *su*(3) things are more complicated. There are two diagonal operators $\hat{T}_1$ and $\hat{T}_2$, so states are labeled by the eigenvalues of these diagonal operators called weights. These weights are related to the harmonic oscillator excitation numbers by $w_1 = n_1 - n_2$, $w_2 = n_2 - n_3$. In *su*(2), the representation label *j* is the eigenvalue of the diagonal operator $\hat{S}_z$ for the state killed by $\hat{S}_+$. In *su*(3), the representation labels are the eigenvalues of the diagonal operators $\hat{T}_1$ and $\hat{T}_2$ acting on the highest weight state, the state killed by all the raising operators. For the representation with $|\lambda, 0, 0\rangle$ as the highest weight state, the representation label is thus $(\lambda, 0)$.

Irreps of the type $(\lambda, 0)$

As an example, we consider the irreducible representation (irrep) $(1, 0)$. The highest weight state is $|1, 0, 0\rangle$. The other states are obtained by the action of lowering operators on the highest weight state; they are $|0, 1, 0\rangle = \hat{C}_{21}|1, 0, 0\rangle$ and $|0, 0, 1\rangle = \hat{C}_{32}|1, 0, 0\rangle$. As another example consider the $(2, 0)$ irrep. The highest weight state for this irrep is $|2, 0, 0\rangle$ and the other states are shown on the right of Fig. 4.1.

<center>*Irreps of the type* $(0, \mu)$</center>

Representations of $su(3)$ are not limited to those of the $(\lambda, 0)$ type. The simplest illustration of this comes from looking at the possible states obtained by considering two copies of the $(1, 0)$ representation of $su(3)$. The nine resulting states are of the form $|n_{1+}, n_{2+}, n_{3+}\rangle_+ |n_{1-}, n_{2-}, n_{3-}\rangle_-$, where the indices $+$ and $-$ are introduced to distinguish the copies and later convenience. Defining

$$\hat{C}_{ij} = \hat{C}_{ij+} + \hat{C}_{ij-} = \hat{a}^\dagger_{i+}\hat{a}_{j+} + \hat{a}^\dagger_{i-}\hat{a}_{j-}, \tag{4.7}$$

with the "+" operators commuting with the "-" operators, we see that the resulting commutation relations for the total operators $\hat{C}_{ij}$ are still those of $su(3)$. Moreover, the state $|100\rangle_+ |100\rangle_-$ has weight $(2, 0)$ and is killed by all raising operators. It is therefore the highest weight for the representation $(2, 0)$. Other states in $(2, 0)$ are obtained by acting on this highest weight with the lowering operators. As an example consider

$$\hat{C}_{21}|1, 0, 0\rangle_+ |1, 0, 0\rangle_- = |0, 1, 0\rangle_+ |1, 0, 0\rangle_- + |1, 0, 0\rangle_+ |0, 1, 0\rangle_- . \tag{4.8}$$

All the states in $(2, 0)$ are symmetric under interchange of the + and - index and there are 6 such states.

In addition to the six symmetric states, one also observes that the combination $|100\rangle_+ |010\rangle_- - |010\rangle_+ |100\rangle_-$ has weight $(0, 1)$ and is killed by all raising operators. It is thus the highest weight for the irrep $(0, 1)$. This state can be constructed by the creation operators $\hat{a}^\dagger_{i+}$ and $\hat{a}^\dagger_{i-}$ with $i = 1, 2$ as follows:

$$|\psi\rangle = \begin{vmatrix} \hat{a}^\dagger_{2+} & \hat{a}^\dagger_{1+} \\ \hat{a}^\dagger_{2-} & \hat{a}^\dagger_{1-} \end{vmatrix} |0\rangle = \left(\hat{a}^\dagger_{2+}\hat{a}^\dagger_{1-} - \hat{a}^\dagger_{2-}\hat{a}^\dagger_{1+} \right) |0\rangle$$
$$= |0, 1, 0\rangle_+ |1, 0, 0\rangle_- - |1, 0, 0\rangle_+ |0, 1, 0\rangle_- . \tag{4.9}$$

There are two other states that can be reached from the above state by acting the lowering operators:

$$\hat{C}_{32} |\psi\rangle = |0, 0, 1\rangle_+ |1, 0, 0\rangle_- - |1, 0, 0\rangle_+ |0, 0, 1\rangle_- , \tag{4.10}$$

$$\hat{C}_{31} |\psi\rangle = |0, 1, 0\rangle_+ |0, 0, 1\rangle_- - |0, 0, 1\rangle_+ |0, 1, 0\rangle_- . \tag{4.11}$$

The three states in $(0, 1)$ are antisymmetric under interchange of the + and - index. Note that although there are three states in $(0, 1)$ irrep just like there are three states in $(1, 0)$ irrep, the $(0, 1)$ is really a representation distinct from $(1, 0)$. The set of weights for the $(0, 1)$ irrep are $(0, 1), (-1, 0)$ and $(1, -1)$ while the weights of states in $(1, 0)$ irrep are $(1, 0), (0, -1)$ and $(-1, 1)$. Since the weights are eigenvalues of the diagonal operators $\hat{T}_1$ and $\hat{T}_2$, and because eigenvalues do not depend on the choice of basis, we see there cannot be a choice of basis that will transform the states of $(0, 1)$ into the states of $(1, 0)$.

<center>*Irreps of* (λ, μ) *type*</center>

Finally, there is a third type of $su(3)$ irreps. Consider the coupling of two irreps $(1, 0)$ and $(0, 1)$ which is denoted by $(1, 0) \otimes (0, 1)$. The highest weight of the coupling can be written as

$$|\psi\rangle = a^\dagger_{1+} \begin{vmatrix} \hat{a}^\dagger_{2+} & \hat{a}^\dagger_{1+} \\ \hat{a}^\dagger_{2-} & \hat{a}^\dagger_{1-} \end{vmatrix} |0\rangle = a^\dagger_{1+} \left(\hat{a}^\dagger_{2+}\hat{a}^\dagger_{1-} - \hat{a}^\dagger_{2-}\hat{a}^\dagger_{1+} \right) |0\rangle$$
$$= |(11)_1 (10)_2 (00)_3\rangle - |(20)_1 (01)_2 (00)_3\rangle \tag{4.12}$$

where the states are denoted by $|(n_{1+}n_{1-})_1, (n_{2+}n_{2-})_2, (n_{3+}n_{3-})_3\rangle$. This state is killed by all raising operators and its weight is $(1, 1)$. Thus it is the highest weight of the irrep $(1, 1)$. All the other states can be obtained by using the lowering operators of Eq. (4.7).
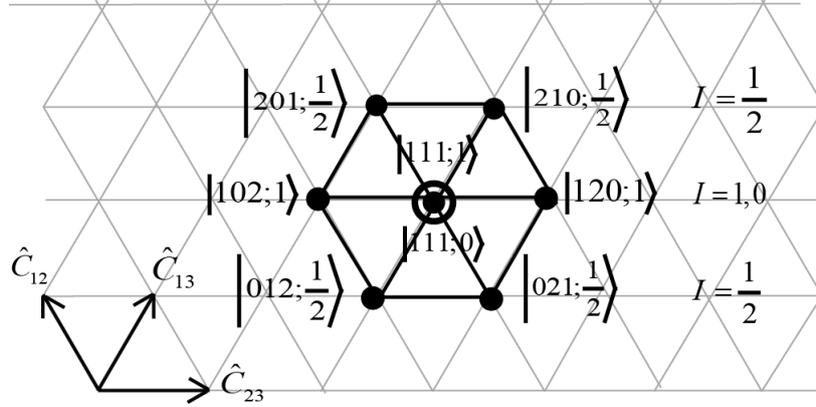

Fig. 4.2: Weight diagram for $(1, 1)$ irrep of $su(3)$. The weights are labeled by the corresponding states. There are two different states at the center with the same weight. These states are specified by the I label. The one that is killed by $\hat{C}_{23}$ has $I = 0$ and the other one that is obtained by the action of $\hat{C}_{32}$ on the $|120; 1\rangle$ has $I = 1$. The geometry of (σ, σ) irreps is a hexagonal lattice.

For the irrep $(1, 1)$ there is a feature that does not occur for $(1, 0)$ and $(0, 1)$. If we crank down using $\hat{C}_{31}$ from the highest weight state $|\psi\rangle$ in Eq. (4.12), and crank down from $|\psi\rangle$ separately using $\hat{C}_{32}\hat{C}_{21}$ we find that $\hat{C}_{31}|\psi\rangle$ is not proportional to $\hat{C}_{32}\hat{C}_{21}|\psi\rangle$ although both states have identical weight $(0, 0)$. The two states are not orthogonal either.

This is where we need another label to distinguish the states; we call it I (this label is called the isospin in particle physics). This label is determined by the eigenvalue of $\hat{h}_2$ of the highest weight state of the $su(2)_{23}$ subalgebra and is the same for all the states in that $su(2)_{23}$ subalgebra. The highest weight state of $su(2)_{23}$ subalgebra is the state that is killed by $\hat{C}_{23}$ operator.

Thus we can label the states in $(1, 1)$ irrep as $|n_1, n_2, n_3; I\rangle$ in which $n_i = n_{i+} + n_{i-}$. In this notation the highest weight state of $(1, 1)$ is $\left|210; \frac{1}{2}\right\rangle$. One can also verify that $\hat{C}_{21}\left|210; \frac{1}{2}\right\rangle$ is killed by $\hat{C}_{23}$ and has $h_2 = 1$ thus it is proportional to a state with $I = 1$. We label this state by $|120; 1\rangle$; the state $\hat{C}_{32}|120; 1\rangle$ must have the same value for I. Its normalized version is thus $|111; 1\rangle$.

On the other hand the state $\hat{C}_{31}\left|210; \frac{1}{2}\right\rangle$ is not orthogonal to $|111; 1\rangle$; it can be written as a linear combination of $|111; 1\rangle$ and another state, $|111; 0\rangle$, which is killed by $\hat{C}_{23}$ has eigenvalue $h_2 = 0$ and is orthogonal to $|111; 1\rangle$. In terms of two coupled harmonic oscillator states, we have

$$|111; 1\rangle = \sqrt{\frac{2}{3}}|(01)_1(10)_2(10)_3\rangle - \frac{1}{\sqrt{6}}|(10)_1(10)_2(01)_3\rangle - \frac{1}{\sqrt{6}}|(10)_1(01)_2(10)_3\rangle \quad (4.13)$$

$$|111; 0\rangle = -\frac{1}{\sqrt{2}}|(10)_1(10)_2(01)_3\rangle + \frac{1}{\sqrt{2}}|(10)_1(01)_2(10)_3\rangle. \quad (4.14)$$

In general an $su(3)$ representation is of the form of (λ, μ) in which λ and μ are determined by the highest weight state. We denote $su(3)$ states by $|(\lambda, \mu) n_1 n_2 n_3, I\rangle$ where $n_1 + n_2 + n_3 = \lambda + 2\mu$. Unless we have to, we will not indicate the representation labels λ and μ, as those will usually be clear from the context. In irreps $(\lambda, 0)$ or $(0, \mu)$ the I label is redundant because the eigenvalues

are enough to identify the states; thus the label I is not indicated. In terms of coupled harmonic oscillator states the general state $|n_1 n_2 n_3, I\rangle$ can be written as [51]

$$|n_1 n_2 n_3, I\rangle = \sum_{M_1, M_2, M_3} C^{I,N}_{\frac{1}{2}\nu_3, M_3; \frac{1}{2}\nu_2, M_2} C^{\frac{1}{2}\lambda, \frac{1}{2}\lambda}_{I,N; \frac{1}{2}\nu_1, M_1} |(n_{1+}n_{1-})_1, (n_{2+}n_{2-})_2, (n_{3+}n_{3-})_3\rangle, \qquad (4.15)$$

where $C^{J,M}_{j_1, m_1; j_2, m_2}$ is an $S U(2)$ Clebsch Gordan coefficient, $\nu_i = n_{i+} + n_{i-}$ and $M_i = \frac{1}{2}(n_{i+} - n_{i-})$ and $N = n_1 + n_2 + n_3$. For the highest weight state this turns out to be

$$\left|\lambda + \mu, \mu, 0, \tfrac{1}{2}\mu\right\rangle = \sum_{M_1, M_2} C^{\frac{1}{2}\lambda, \frac{1}{2}\lambda}_{\frac{1}{2}\mu, M_2; \frac{1}{2}\nu_1, M_1} |(n_{1+}n_{1-})_1, (n_{2+}n_{2-})_2, (n_{3+}n_{3-})_3\rangle. \qquad (4.16)$$

4.1.3 The group $S U(3)$ and the coherent states for $(\lambda, 0)$ irreps

One can show that any $S U(3)$ transformation $R(\Omega')$ can be parameterized as [52]

$$R(\Omega') = R_{23}(\alpha_1', \beta_1', -\alpha_1') R_{12}(\alpha_2', \beta_2', -\alpha_2') R_{23}(\alpha_3', \beta_3', -\alpha_3') e^{-i\gamma_1' \hat{h}_1} e^{-i\gamma_2' \hat{h}_2}, \qquad (4.17)$$

where $\hat{h}_1 \equiv 2\hat{T}_1 + \hat{T}_2 = 2\hat{C}_{11} - \hat{C}_{22} - \hat{C}_{33}$, $\hat{h}_2 \equiv \frac{1}{2}\hat{T}_2 = \frac{1}{2}(\hat{C}_{22} - \hat{C}_{33})$ and R_{ij} transformations are block $S U(2)$ transformations *i.e.*

$$R_{ij}(\alpha', \beta', -\alpha') = R_z^{ij}(\alpha') R_y^{ij}(\beta') R_z^{ij}(-\alpha'). \qquad (4.18)$$

$S U(3)$ coherent states are, as always, defined as the unitary transformation of the highest weight state. For $(\lambda, 0)$ irrep, with highest weight $|\lambda, 0, 0\rangle$, we therefore have

$$|\Omega'\rangle = R(\Omega')|\lambda, 0, 0\rangle. \qquad (4.19)$$

In Eq. (4.19) we have

$$R_{23}(\alpha_3', \beta_3', -\alpha_3') e^{-i\gamma_1' \hat{h}_1} e^{-i\gamma_2' \hat{h}_2} |\lambda, 0, 0\rangle = e^{-2i\gamma_1' \lambda} |\lambda, 0, 0\rangle. \qquad (4.20)$$

Ignoring the above phase factor, and using the completeness relation

$$\sum_{n_1=0,\, n_2=0}^{\lambda,\ \lambda-n_1} |n_1, n_2, n_3\rangle \langle n_1, n_2, n_3| = 1, \qquad n_3 = \lambda - n_1 - n_2, \qquad (4.21)$$

the $S U(3)$ coherent states can be written as

$$\begin{aligned} |\Omega'\rangle &= R_{23}(\alpha_1', \beta_1', -\alpha_1') R_{12}(\alpha_2', \beta_2', -\alpha_2')|\lambda, 0, 0\rangle \\ &= \sum_{n_2=0}^{\lambda} \sum_{n_3=0}^{n_2} |\lambda - n_2, n_2 - n_3, n_3\rangle D^{\frac{1}{2}\lambda}_{\frac{1}{2}\lambda - n_2, \frac{1}{2}\lambda}(\alpha_2', \beta_2', -\alpha_2') D^{\frac{1}{2}n_2}_{\frac{1}{2}n_2 - n_3, \frac{1}{2}n_2}(\alpha_1', \beta_1', -\alpha_1'), \end{aligned}$$
$$(4.22)$$

where $D^j_{m,m'}$ functions are $S U(2)$ Wigner D functions given in Eq. (3.21).

The $S U(3)$ coherent states of Eq. (4.22) can be written as the product of λ states $|\Omega'\rangle_i$ which are the superposition of states of a three level system;

$$|\Omega'\rangle \propto |\Omega'\rangle_1 \otimes |\Omega'\rangle_2 \otimes ... \otimes |\Omega'\rangle_\lambda, \qquad (4.23)$$
$$|\Omega'\rangle_i \equiv \cos\left(\tfrac{1}{2}\beta_2'\right)|100\rangle_i + e^{i\alpha_2'} \cos\left(\tfrac{1}{2}\beta_1'\right) \sin\left(\tfrac{1}{2}\beta_2'\right)|010\rangle_i + e^{i(\alpha_1' + \alpha_2')} \sin\left(\tfrac{1}{2}\beta_1'\right) \sin\left(\tfrac{1}{2}\beta_2'\right)|001\rangle_i. \qquad (4.24)$$

4.2   Phase space symbols

The highest weight state for $(\lambda, 0)$ irreps of $SU(3)$, $|\lambda, 0, 0\rangle$, is invariant under transformation of the subgroup $\mathfrak{H} = U_{23}(2)$. Following the discussion in chapter 2, the phase space of $(\lambda, 0)$ irreps is thus $\mathfrak{M} = SU(3)/U_{23}(2) \sim S^4$ which is a four dimensional sphere [39]. The location of points on this sphere is specified by the angles α_1, β_1, α_2 and β_2.

In this section we obtain the phase space symbol of $su(3)$ generators and some other operators needed to investigate the semiclassical dynamics later. As was done in chapter 2, the Wigner symbol, W_X, of an $su(3)$ operator $\hat{X}$, is constructed as

$$W_X(\Omega) = \mathrm{Tr}\left(\hat{X}\hat{w}(\Omega)\right), \tag{4.25}$$

where $\hat{w}(\Omega)$ is the quantization kernel. The construction of this kernel starts with a diagonal operator $\hat{P}$, given by

$$\hat{P} = \int_0^{2\pi} d\omega e^{-i\omega\hat{h}_1} f'(\omega), \tag{4.26}$$

where $f'(\omega)$ is a scalar function which, like the function $f(\omega)$ in the $SU(2)$ kernel, is constructed in such a way that the quantization kernel satisfies all the required conditions listed in chapter 2. Since $\hat{h}_1$ is diagonal and commutes with elements in $U_{23}(2)$, the full $SU(3)$ transformation can be reduced to $\Lambda(\Omega) = R_{23}(\alpha_1, \beta_1, -\alpha_1) R_{12}(\alpha_2, \beta_2, -\alpha_2)$ so the translation of the operator $\hat{P}$ can be ultimately written as

$$\hat{w}(\Omega) = \Lambda(\Omega)\hat{P}\Lambda^\dagger(\Omega), \quad \Omega \in SU(3)/U_{23}(2). \tag{4.27}$$

A more practical expression is obtained by first expanding the operator $\hat{P}$ in terms of $su(3)$ tensor operators, as was done for $su(2)$. These are defined in a manner analogous to the $su(2)$ tensors of Eq. (3.28). Explicitly, an $su(3)$ tensor labeled by $(n_1, n_2, n_3); I$ in the irrep (σ, σ) can be written in terms of kets and bras in $(\lambda, 0)$ irrep as

$$\hat{T}^\lambda_{(\sigma,\sigma);(\nu_1,\nu_2,\nu_3),I_\nu} = \sum_{n_1,n_2,m_1,m_2} |n_1, n_2, n_3\rangle \langle m_1, m_2, m_3| \, \tilde{C}^{\lambda(\sigma,\sigma)(\nu_1,\nu_2,\nu_3)I_\nu}_{n_1n_2n_3;m_1m_2m_3}, \tag{4.28}$$

where $\tilde{C}^{\lambda(\sigma,\sigma)(\nu_1,\nu_2,\nu_3)I_\nu}_{n_1n_2n_3;m_1m_2m_3}$ is a coefficient related to the $su(3)$ Clebsch Gordan coefficient occurring in the decomposition of $(\lambda, 0) \otimes (0, \lambda)$ into (σ, σ) [53],

$$(\lambda, 0) \otimes (0, \lambda) = (0,0) \oplus (1,1) \oplus \dots \oplus (\lambda, \lambda) = \sum_{\sigma=0}^\lambda (\sigma, \sigma). \tag{4.29}$$

The operator $\hat{P}$ is diagonal, and it commutes with $\hat{h}_1$ and $\hat{h}_2$. Thus, $\hat{P}$ as an operator has weight $(0,0)$ and also $I = 0$. The expansion of $\hat{P}$ in terms of weight $(0,0)$, $I = 0$ tensors is shown to be [34]:

$$\hat{P} = \sum_{\sigma=0}^\lambda \sqrt{\frac{\dim(\sigma,\sigma)}{\dim(\lambda,0)}} \, \hat{T}^\lambda_{(\sigma,\sigma);(\sigma,\sigma,\sigma),0}, \tag{4.30}$$

where $\dim(\lambda, 0) = \frac{1}{2}(\lambda + 1)(\lambda + 2)$ and $\dim(\sigma, \sigma) = (\sigma + 1)^3$ are the dimension of the irreps $(\lambda, 0)$ and (σ, σ) respectively.

After translations by $\Lambda(\Omega)$, the kernel takes the more convenient form

$$\hat{w}(\Omega) = \sum_{\sigma=0}^{\lambda} \sqrt{\frac{\dim(\sigma,\sigma)}{\dim(\lambda,0)}} \sum_{\nu_1,\nu_2} D^{(\sigma,\sigma)}_{(\nu_1,\nu_2,\nu_3),I_\nu;(\sigma,\sigma,\sigma),0}(\Omega)\hat{T}^{\lambda}_{(\sigma,\sigma);(\nu_1,\nu_2,\nu_3),I_\nu}, \tag{4.31}$$

in which $D^{(\sigma,\sigma)}_{(\nu_1,\nu_2,\nu_3),I_\nu;(\sigma,\sigma,\sigma),0}(\Omega)$ is $S U(3)$ Wigner D-function defined as the overlap of the $S U(3)$ transformation $\Lambda(\Omega)$ between the $S U(3)$ states $|(\nu_1,\nu_2,\nu_3),I_\nu\rangle$ and $|(\sigma,\sigma,\sigma),0\rangle$ of the irrep (σ,σ):

$$D^{(\sigma,\sigma)}_{(\nu_1,\nu_2,\nu_3),I_\nu;(\sigma,\sigma,\sigma),0}(\Omega) \equiv \langle(\nu_1,\nu_2,\nu_3),I_\nu| R_{23}(\alpha_1,\beta_1,-\alpha_1) R_{12}(\alpha_2,\beta_2,-\alpha_2) |(\sigma,\sigma,\sigma),0\rangle. \tag{4.32}$$

To obtain phase space symbols of $su(3)$ generators we express the generators as tensor operators. One can find

$$\hat{C}_{12} = \sum_{n_1=0}^{\lambda}\sum_{n_2=0}^{\lambda-n_1} \sqrt{(n_1+1)n_2}\,|n_1+1,n_2-1,n_3\rangle\langle n_1,n_2,n_3| = -\frac{N}{2\sqrt{6}}\hat{T}^{\lambda}_{(1,1);(2,0,1),\frac{1}{2}}, \tag{4.33}$$

$$\hat{C}_{13} = \sum_{n_1=0}^{\lambda}\sum_{n_2=0}^{\lambda-n_1} \sqrt{(n_1+1)n_3}\,|n_1+1,n_2,n_3-1\rangle\langle n_1,n_2,n_3| = \frac{N}{2\sqrt{6}}\hat{T}^{\lambda}_{(1,1);(2,1,0),\frac{1}{2}}, \tag{4.34}$$

$$\hat{C}_{23} = \sum_{n_1=0}^{\lambda}\sum_{n_2=0}^{\lambda-n_1} \sqrt{(n_2+1)n_3}\,|n_1,n_2+1,n_3-1\rangle\langle n_1,n_2,n_3| = \frac{N}{2\sqrt{6}}\hat{T}^{\lambda}_{(1,1);(1,2,0),1} \tag{4.35}$$

$$\hat{h}_1 = \sum_{n_1=0}^{\lambda}\sum_{n_2=0}^{\lambda-n_1} (2n_1-n_2-n_3)\,|n_1,n_2,n_3\rangle\langle n_1,n_2,n_3| = \frac{N}{2}\hat{T}^{\lambda}_{(1,1);(1,1,1),0}, \tag{4.36}$$

$$\hat{h}_2 = \sum_{n_1=0}^{\lambda}\sum_{n_2=0}^{\lambda-n_1} \frac{1}{2}(n_2-n_3)\,|n_1,n_2,n_3\rangle\langle n_1,n_2,n_3| = -\frac{N}{4\sqrt{3}}\hat{T}^{\lambda}_{(1,1);(1,1,1),1}, \tag{4.37}$$

with $N = \sqrt{\lambda(\lambda+1)(\lambda+2)(\lambda+3)}$. Using the trace orthogonality of tensors,

$$\text{Tr}\left(\left(\hat{T}^{\lambda}_{(\sigma,\sigma);(\nu_1,\nu_2,\nu_3),I_\nu}\right)^{\dagger} \hat{T}^{\lambda'}_{(\sigma',\sigma');(\nu_1',\nu_2',\nu_3'),I_{\nu'}}\right) = \delta_{\lambda,\lambda'}\delta_{\sigma,\sigma'}\delta_{\nu_1,\nu_1'}\delta_{\nu_2,\nu_2'}\delta_{\nu_3,\nu_3'}\delta_{I_\nu,I_{\nu'}} \tag{4.38}$$

and Eqs. (4.25) and (4.31) we obtain

$$W_{C_{12}} = \frac{1}{2}\sqrt{\lambda(\lambda+3)}e^{-i\alpha_2}\cos\left(\frac{\beta_1}{2}\right)\sin(\beta_2), \tag{4.39}$$

$$W_{C_{13}} = \frac{1}{2}\sqrt{\lambda(\lambda+3)}e^{-i(\alpha_1+\alpha_2)}\sin\left(\frac{\beta_1}{2}\right)\sin(\beta_2), \tag{4.40}$$

$$W_{C_{23}} = \frac{1}{2}\sqrt{\lambda(\lambda+3)}e^{-i\alpha_1}\sin(\beta_1)\sin^2\left(\frac{\beta_2}{2}\right), \tag{4.41}$$

$$W_{h_1} = \frac{1}{2}\sqrt{\lambda(\lambda+3)}(1+3\cos(\beta_2)), \tag{4.42}$$

$$W_{h_2} = \frac{1}{2}\sqrt{\lambda(\lambda+3)}\cos(\beta_1)\sin^2\left(\frac{\beta_2}{2}\right). \tag{4.43}$$

Since $\hat{C}_{ij} = \hat{C}_{ji}^{\dagger}$ and for an operator $\hat{X}$ we have $W_{X^{\dagger}} = (W_X)^*$, the phase space symbol of other $su(3)$ generators can be obtained easily.

For later purposes we give the phase space symbols of the operators $\hat{h}_1^2$ and $\hat{h}_2^2$. In terms of tensors they can be written as

$$
\begin{aligned}
\hat{h}_1^2 &= \sum_{n_1=0}^{\lambda} \sum_{n_2=0}^{\lambda-n_1} (2n_1 - n_2 - n_3)^2 |n_1, n_2, n_3\rangle \langle n_1, n_2, n_3| \\
&= \alpha_0 \hat{T}_{(0,0);(0,0,0),0}^{\lambda} + \alpha_1 \hat{T}_{(1,1);(1,1,1),0}^{\lambda} + \alpha_2 \hat{T}_{(2,2);(2,2,2),0}^{\lambda}, \quad (4.44) \\
\hat{h}_2^2 &= \sum_{n_1=0}^{\lambda} \sum_{n_2=0}^{\lambda-n_1} \frac{1}{4}(n_2 - n_3)^2 |n_1, n_2, n_3\rangle \langle n_1, n_2, n_3| \\
&= \beta_0 \hat{T}_{(0,0);(0,0,0),0}^{\lambda} + \beta_1 \hat{T}_{(1,1);(1,1,1),0}^{\lambda} + \beta_{20} \hat{T}_{(2,2);(2,2,2),0}^{\lambda} + \beta_{22} \hat{T}_{(2,2);(2,2,2),2}^{\lambda}. \quad (4.45)
\end{aligned}
$$

Using the explicit forms of tensors $\hat{T}_{(2,2);(2,2,2),I}^{\lambda}$ for $I = 0, 1, 2$ given in appendix B, we obtain

$$
\begin{aligned}
\alpha_0 &= \frac{\lambda(\lambda+3)}{2\sqrt{2}} \sqrt{(\lambda+1)(\lambda+2)}, \\
\alpha_1 &= \frac{2\lambda+3}{10} \sqrt{\lambda(\lambda+1)(\lambda+2)(\lambda+3)}, \\
\alpha_2 &= \frac{3}{10\sqrt{2}} \sqrt{3(\lambda-1)\lambda(\lambda+1)(\lambda+2)(\lambda+3)(\lambda+4)}, \quad (4.46)
\end{aligned}
$$

and

$$
\begin{aligned}
\beta_0 &= \frac{1}{6\sqrt{2}} \lambda(\lambda+3) \sqrt{(\lambda+1)(\lambda+2)}, \\
\beta_1 &= \frac{-1}{30}(2\lambda+3) \sqrt{\lambda(\lambda+1)(\lambda+2)(\lambda+3)}, \\
\beta_{20} &= \frac{1}{30\sqrt{6}} \sqrt{(\lambda-1)\lambda(\lambda+1)(\lambda+2)(\lambda+3)(\lambda+4)}, \\
\beta_{22} &= \frac{1}{3}\sqrt{\frac{2}{15}} \sqrt{(\lambda-1)\lambda(\lambda+1)(\lambda+2)(\lambda+3)(\lambda+4)}. \quad (4.47)
\end{aligned}
$$

The symbols are then given by

$$
\begin{aligned}
W_{h_1^2} &= \frac{1}{2}\lambda(\lambda+3) + \frac{1}{10}\sqrt{\lambda(\lambda+3)}(2\lambda+3)(1+3\cos(\beta_2)) \\
&\quad + \frac{9}{40}\sqrt{(\lambda-1)\lambda(\lambda+3)(\lambda+4)}(3+4\cos(\beta_2)+5\cos(2\beta_2)), \quad (4.48) \\
W_{h_2^2} &= \frac{1}{24}\lambda(\lambda+3) - \frac{1}{120}\sqrt{\lambda(\lambda+3)}(2\lambda+3)(1+3\cos(\beta_2)) \\
&\quad + \frac{1}{24}\sqrt{(\lambda-1)\lambda(\lambda+3)(\lambda+4)}\left[\frac{1}{20}(3+4\cos(\beta_2)+5\cos(2\beta_2)) + (1+3\cos(2\beta_1))\sin^4\left(\frac{\beta_2}{2}\right)\right].
\end{aligned}
$$

$$(4.49)$$

4.3   Semiclassical dynamics

In this section, we first find the relation between the Poisson bracket of the symbol of $su(3)$ observables and the symbol of the commutator of observables. We then investigate the dynamics of $su(3)$ systems in the semiclassical limit for a linear and a nonlinear Hamiltonian.

Using the $SU(3)$ coherent states of Eq. A.1, and the calculations given in appendix A, we find the Poisson bracket for $SU(3)$ systems of the type $(\lambda, 0)$ in terms of the coordinates on the 4-dimensional sphere to be

$$\{f, g\} = \frac{4}{\sin \beta_1 \sin^2\left(\frac{\beta_2}{2}\right)} \left(\frac{\partial f}{\partial \alpha_1} \frac{\partial g}{\partial \beta_1} - \frac{\partial f}{\partial \beta_1} \frac{\partial g}{\partial \alpha_1} \right) + \frac{2 \tan\left(\frac{\beta_1}{2}\right)}{\sin^2\left(\frac{\beta_2}{2}\right)} \left(\frac{\partial f}{\partial \beta_1} \frac{\partial g}{\partial \alpha_2} - \frac{\partial f}{\partial \alpha_2} \frac{\partial g}{\partial \beta_1} \right)$$
$$+ \frac{4}{\sin \beta_2} \left(\frac{\partial f}{\partial \alpha_2} \frac{\partial g}{\partial \beta_2} - \frac{\partial f}{\partial \beta_2} \frac{\partial g}{\partial \alpha_2} \right), \tag{4.50}$$

where f and g are two functions on S^4.

Now let us first find the semiclassical parameter for $SU(3)$ systems. For two $su(3)$ generators such as $\hat{h}_1$ and $\hat{C}_{13}$ the Poisson bracket is

$$\{W_{h_1}, W_{C_{13}}\} = -\frac{4}{\sin \beta_2} \frac{\partial W_{h_1}}{\partial \beta_2} \frac{\partial W_{C_{13}}}{\partial \alpha_2} = -6i \sqrt{\lambda (\lambda + 3)} W_{C_{13}}. \tag{4.51}$$

Since $\left[\hat{h}_1, \hat{C}_{13} \right] = 3\hat{C}_{13}$ we have

$$\{W_{h_1}, W_{C_{13}}\} = \varepsilon W_{[\hat{h}_1, \hat{C}_{13}]}, \qquad \varepsilon = -2i \sqrt{\lambda (\lambda + 3)}, \tag{4.52}$$

where ε is the semiclassical parameter.

Similar to the $SU(2)$ case, for a polynomial in the generators and an $su(3)$ generator, the Poisson bracket of the symbols is proportional to the symbol of the commutator. For instance, we find that for $\hat{h}_1^2$ and $\hat{C}_{13}$, we have $[\hat{h}_1^2, \hat{C}_{13}] = 3 \left(\hat{C}_{13} \hat{h}_1 + \hat{h}_1 \hat{C}_{13} \right)$ and therefore $W_{[\hat{h}_1^2, \hat{C}_{13}]} = 3 \left(W_{\hat{C}_{13} \hat{h}_1} + W_{\hat{h}_1 \hat{C}_{13}} \right)$. Since $\hat{C}_{13} \hat{h}_1 = \left[\hat{C}_{13}, \hat{h}_1 \right] + \hat{h}_1 \hat{C}_{13}$ and $\left[\hat{C}_{13}, \hat{h}_1 \right] = -3\hat{C}_{13}$, we have $W_{\hat{C}_{13} \hat{h}_1} = -3W_{C_{13}} + W_{\hat{h}_1 \hat{C}_{13}}$. Thus we just need to find the symbol of $\hat{h}_1 \hat{C}_{13}$. In terms of tensors it can be written as

$$\hat{h}_1 \hat{C}_{13} = \eta_1 \hat{T}^{\lambda}_{(1,1);(2,1,0),\frac{1}{2}} + \eta_2 \hat{T}^{\lambda}_{(2,2);(3,2,1),\frac{1}{2}}, \tag{4.53}$$

with

$$\eta_1 = \frac{1}{10 \sqrt{6}} \sqrt{\lambda (\lambda + 1)(\lambda + 2)(\lambda + 3)} (\lambda + 9),$$
$$\eta_2 = \frac{1}{10 \sqrt{2}} \sqrt{3 (\lambda - 1) \lambda (\lambda + 1)(\lambda + 2)(\lambda + 3)(\lambda + 4)}. \tag{4.54}$$

This gives

$$W_{\hat{h}_1 \hat{C}_{13}} = \frac{1}{10} \sqrt{\lambda (\lambda + 3)} (\lambda + 9) e^{-i(\alpha_1 + \alpha_2)} \sin\left(\frac{\beta_1}{2}\right) \sin (\beta_2)$$
$$+ \frac{3}{20} \sqrt{(\lambda - 1) \lambda (\lambda + 3)(\lambda + 4)} e^{-i(\alpha_1 + \alpha_2)} (1 + 5 \cos \beta_2) \sin\left(\frac{\beta_1}{2}\right) \sin (\beta_2). \tag{4.55}$$

One can then verify, using Eq. (4.50), that

$$\left\{ W_{h_1^2}, W_{C_{13}} \right\} = \varepsilon W_{[\hat{h}_1^2, \hat{C}_{13}]}, \tag{4.56}$$

where ε is given in Eq. (4.52).

Finally, we find once again that for two polynomials of degree 2 or greater in the generators of $su(3)$ like $\hat{h}_1^2$ and $\hat{C}_{13}^2$ we have correction terms:

$$\left\{ W_{h_1^2}, W_{C_{13}^2} \right\} = \varepsilon W_{[\hat{h}_1^2, \hat{C}_{13}^2]} + O\left(\varepsilon^{-2} \right) . \tag{4.57}$$

Thus for a Hamiltonian linear in the generators of $su(3)$ the equation of motion of the Wigner function, (2.24), turns out to be ($\hbar = 1$)

$$i \frac{\partial W_\rho}{\partial t} = W_{[H,\rho]} = \varepsilon^{-1} \left\{ W_H, W_\rho \right\} . \tag{4.58}$$

For a nonlinear Hamiltonian since the density matrix is written as an expansion of tensors of the type (σ, σ) with $\sigma > 2$, the evolution is thus

$$i \frac{\partial W_\rho}{\partial t} = \varepsilon^{-1} \left\{ W_H, W_\rho \right\} + O\left(\varepsilon^{-3} \right) , \tag{4.59}$$

where the second term on the right is a quantum correction to the classical dynamics and is of the order of ε^{-3}. In the semiclassical limit, $\lambda \gg 1$ thus $\varepsilon^{-1} \to 0$, we will ignore the correction terms to work with the truncated Liouville equation.

As we can now write the time evolution of Wigner function in terms of Poisson bracket we investigate the dynamics of an $S U(3)$ system under a linear and a simple nonlinear Hamiltonian. Our initial state will be an $S U(3)$ coherent state. We will obtain time-evolved Wigner function and use it to calculate the evolution of the fluctuations of an observable. We then compare this with the quantum mechanical calculation.

4.3.1   Linear dynamics

For the linear case we consider the Hamiltonian $\hat{H} = \hat{h}_1$. As an initial state we choose an $S U(3)$ coherent state located on S^4 at the minimum of W_{h_1} *i.e.*

$$|\psi(0)\rangle = \Lambda\left(\Omega'\right) |\lambda, 0, 0\rangle = R_{23}\left(\alpha_1', \beta_1', -\alpha_1'\right) R_{12}\left(\alpha_2', \beta_2', -\alpha_2'\right) |\lambda, 0, 0\rangle , \tag{4.60}$$

where $\alpha_1' = \alpha_2' = \beta_1' = 0$ and $\beta_2' = \frac{1}{2}\pi$. Now let us obtain the initial Wigner function for the density operator $\hat{\rho} = \Lambda\left(\Omega'\right) |\lambda, 0, 0\rangle \langle \lambda, 0, 0| \Lambda^\dagger\left(\Omega'\right)$. We can write

$$
\begin{aligned}
W_\rho\left(\Omega\right) &= \mathrm{Tr}\left(\hat{\rho}\Lambda\left(\Omega\right)\hat{P}\Lambda^\dagger\left(\Omega\right)\right) \\
&= \langle \lambda, 0, 0| \Lambda^\dagger\left(\Omega'\right) R_{23}\left(\alpha_1, \beta_1, -\alpha_1\right) R_{12}\left(\alpha_2, \beta_2, -\alpha_2\right) \hat{P} \\
&\quad \times (R_{23}\left(\alpha_1, \beta_1, -\alpha_1\right) R_{12}\left(\alpha_2, \beta_2, -\alpha_2\right))^\dagger \Lambda\left(\Omega'\right) |\lambda, 0, 0\rangle \\
&= W_{|\lambda,0,0\rangle\langle\lambda,0,0|}\left(\Omega'^{-1} \cdot \Omega\right) = W_{|\lambda,0,0\rangle\langle\lambda,0,0|}\left(\tilde{\Omega}\right) , \tag{4.61}
\end{aligned}
$$

where

$$\Lambda^\dagger\left(\Omega'\right) R_{23}\left(\alpha_1, \beta_1, -\alpha_1\right) R_{12}\left(\alpha_2, \beta_2, -\alpha_2\right) \equiv R\left(\tilde{\Omega}\right) = R\left(\tilde{\alpha}_1, \tilde{\beta}_1, \tilde{\alpha}_2, \tilde{\beta}_2, \tilde{\alpha}_3, \tilde{\beta}_3, \tilde{\gamma}_1, \tilde{\gamma}_2\right) . \tag{4.62}$$

In fact to obtain the tilde angles in terms of the initial parameters α_i', β_i', $i = 1, 2$, and the original coordinates on the sphere α_i, β_i we multiply the corresponding 3×3 matrices, $\Lambda^\dagger\left(\Omega'\right)$ and $\Lambda\left(\Omega\right)$, and decompose the result following the algorithm in [52]. Since $\hat{P}$ commutes with $R_{23}\left(\tilde{\alpha}_3, \tilde{\beta}_3, -\tilde{\alpha}_3\right) e^{i\tilde{\gamma}_1 h_1} e^{i\tilde{\gamma}_2 h_2}$ Eq. (4.61) can then be written as

$$
\begin{aligned}
W_{|\lambda,0,0\rangle\langle\lambda,0,0|}\left(\tilde{\Omega}\right) &= \langle \lambda, 0, 0| R_{23}\left(\tilde{\alpha}_1, \tilde{\beta}_1, -\tilde{\alpha}_1\right) R_{12}\left(\tilde{\alpha}_2, \tilde{\beta}_2, -\tilde{\alpha}_2\right) \hat{P} \\
&\quad \times \left(R_{23}\left(\tilde{\alpha}_1, \tilde{\beta}_1, -\tilde{\alpha}_1\right) R_{12}\left(\tilde{\alpha}_2, \tilde{\beta}_2, -\tilde{\alpha}_2\right)\right)^\dagger |\lambda, 0, 0\rangle . \tag{4.63}
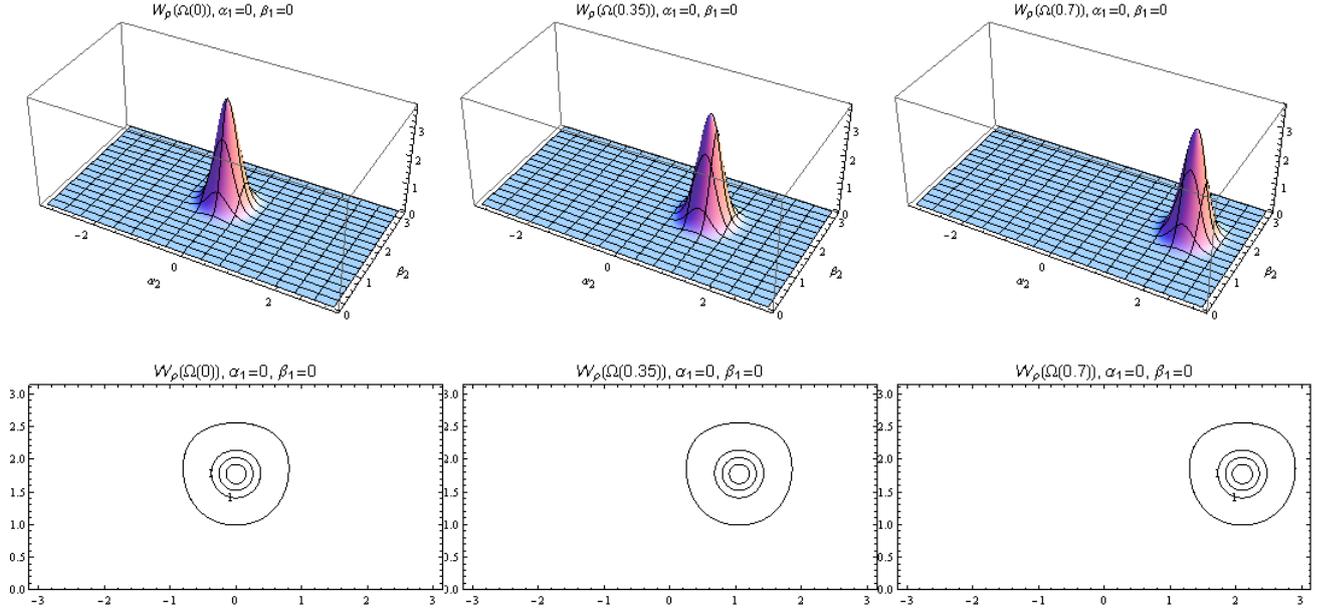\end{aligned}
$$

Fig. 4.3: Time evolution of the slices of the Wigner function of the initial state, Eq. (4.66), under the linear Hamiltonian $\hat{H} = \hat{h}_1$ for $\lambda = 20$ at $t = 0, 0.35, 0.7$. The slices are taken at $\alpha_1 = 0$ and $\beta_1 = 0$.

Thus from Eqs. (4.25),(4.28) and (4.31) we obtain

$$W_{|\lambda,0,0\rangle\langle\lambda,0,0|}\left(\tilde{\Omega}\right) = \sum_{\sigma=0}^{\lambda} \sqrt{\frac{2(\sigma+1)}{(\lambda+1)(\lambda+2)}} \tilde{C}^{\lambda(\sigma\sigma)(\sigma\sigma\sigma)0}_{\lambda00;\lambda00} D^{(\sigma,\sigma)}_{(\sigma,\sigma,\sigma),0;(\sigma,\sigma,\sigma),0}\left(\tilde{\Omega}\right). \tag{4.64}$$

The $SU(3)$ Wigner D-function turns out to depend only on the angle, $\tilde{\beta}_2$. The explicit expression given in [52] for this D-function collapses to a sum of Legendre polynomials as

$$D^{(\sigma,\sigma)}_{(\sigma,\sigma,\sigma),0;(\sigma,\sigma,\sigma),0}\left(\tilde{\alpha}_1,\tilde{\beta}_1,\tilde{\alpha}_2,\tilde{\beta}_2,0,0,0,0\right) = \frac{1}{\left(\cos\tilde{\beta}_2-1\right)(\sigma+1)}\left(P_{\sigma+1}\left(\cos\tilde{\beta}_2\right) - P_\sigma\left(\cos\tilde{\beta}_2\right)\right),$$
$$\tag{4.65}$$

in which $P_k(x)$ is the kth Legendre polynomial. Therefore we have

$$
\begin{aligned}
W_{|\lambda,0,0\rangle\langle\lambda,0,0|}\left(\tilde{\Omega}\right) &= \sum_{\sigma=0}^{\lambda} \tilde{C}^{\lambda(\sigma\sigma)(\sigma\sigma\sigma)0}_{\lambda00;\lambda00}\sqrt{\frac{2(\sigma+1)}{(\lambda+1)(\lambda+2)}}\left(\frac{P_{\sigma+1}\left(\cos\tilde{\beta}_2\right) - P_\sigma\left(\cos\tilde{\beta}_2\right)}{\cos\tilde{\beta}_2-1}\right)\\
&\equiv W_{|\lambda,0,0\rangle\langle\lambda,0,0|}\left(\tilde{\beta}_2\right), \tag{4.66}
\end{aligned}
$$

For our choice of initial state, we find $\tilde{\beta}_2$ as

$$\cos\tilde{\beta}_2 = \sin\beta_2\cos\alpha_2\cos\left(\frac{\beta_1}{2}\right) - \sin^2\left(\frac{\beta_1}{2}\right)\sin^2\left(\frac{\beta_2}{2}\right). \tag{4.67}$$

The time-evolved Wigner function is given exactly by

$$\partial_t W_\rho = \varepsilon^{-1}\left\{W_{h_1}, W_\rho\right\} = -\frac{1}{2\sqrt{\lambda(\lambda+3)}}\frac{4}{\sin\beta_2}\frac{\partial W_{h_1}}{\partial\beta_2}\frac{\partial W_\rho}{\partial\alpha_2} = 3\frac{\partial W_\rho}{\partial\alpha_2} \tag{4.68}$$
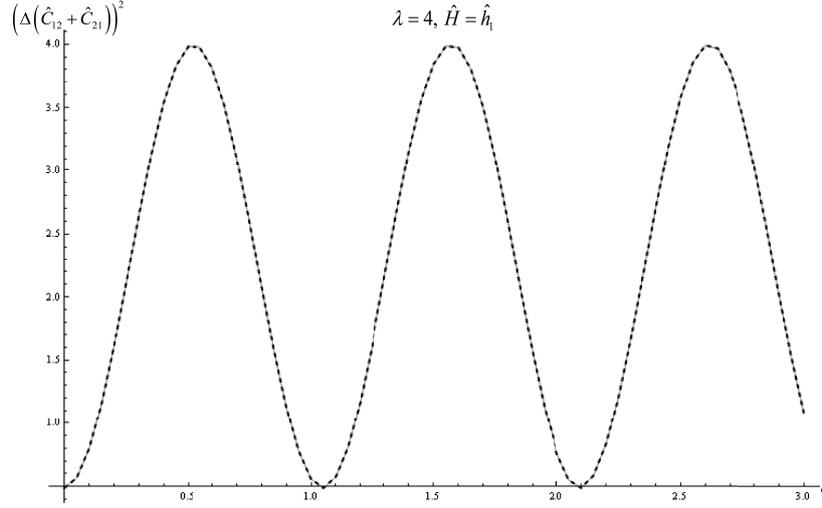
Fig. 4.4: The time evolution of the variance of $\hat{C}_{12} + \hat{C}_{21}$ calculated using phase space method, Eq. (4.69) (dashed line) and Hilbert space quantum mechanical method, (4.71) (solid line) for $\lambda = 4$. Since we haven't used any approximation in the phase space calculations both methods give the same result.

and is obtained by substituting α_2 with $\alpha_2(t) = \alpha_2 - 3t$ in Eq. (4.67).

In Fig 4.3 slices of the Wigner function are plotted for $\lambda = 20$ at $t = 0$, $t = 0.35$ and $t = 0.7$. The figure shows the projection of the Wigner functions in the (α_2, β_2) plane, with slices taken at $(\alpha_1 = 0, \beta_1 = 0)$. It is clear from figure that Wigner function is just translated without any deformation.

Knowing the time-evolution of the Wigner function, we can calculate the time evolution of the expectation value of an operator $\hat{X}$ by

$$\langle \hat{X}(t) \rangle = \frac{(\lambda+1)(\lambda+2)}{8\pi^2} \int d\Omega W_X(\Omega) W_\rho(\Omega(t)) , \qquad (4.69)$$

where

$$\int d\Omega = \int_0^{2\pi} d\alpha_1 \int_0^{2\pi} d\alpha_2 \int_0^\pi d\beta_1 \sin\beta_1 \int_0^\pi d\beta_2 \sin\beta_2 \left(\frac{1 - \cos\beta_2}{4} \right) . \qquad (4.70)$$

This will be compared to the expectation value computed from the quantum mechanical evolution:

$$\langle \hat{X}(t) \rangle = \langle \lambda, 0, 0 | \Lambda^\dagger(\Omega') e^{i\hat{H}t} \hat{X} e^{-i\hat{H}t} \Lambda(\Omega') | \lambda, 0, 0 \rangle . \qquad (4.71)$$

Fig. 4.4 shows the variance of $\hat{X}$, $\left(\Delta\hat{X} \right)^2 = \langle \hat{X}^2 \rangle - \langle \hat{X} \rangle^2$, for $\hat{X} = \hat{C}_{12} + \hat{C}_{21}$. The dashed line has been plotted using Eq. (4.69) and the solid line has been plotted using Eq. (4.71); as expected both methods give the same result. For calculating the variance by using Eq. (4.69) we need the phase space symbol of $\hat{C}_{12} + \hat{C}_{21}$ which is Eq. (4.39) plus its complex conjugate. We also need the symbol of $\left(\hat{C}_{12} + \hat{C}_{21} \right)^2$ given in Eqs. (B.8) to (B.11).

4.3.2 Nonlinear dynamics

Now let us consider the evolution generated by a simple non-linear Hamiltonian like $\hat{h}_1^2$. From Eq. (4.44), we see that $\hat{h}_1^2$ decomposes into a sum of tensors, including a tensor in the $(1, 1)$ representation, and a constant term in the $(0, 0)$ representation. The constant term can be safely
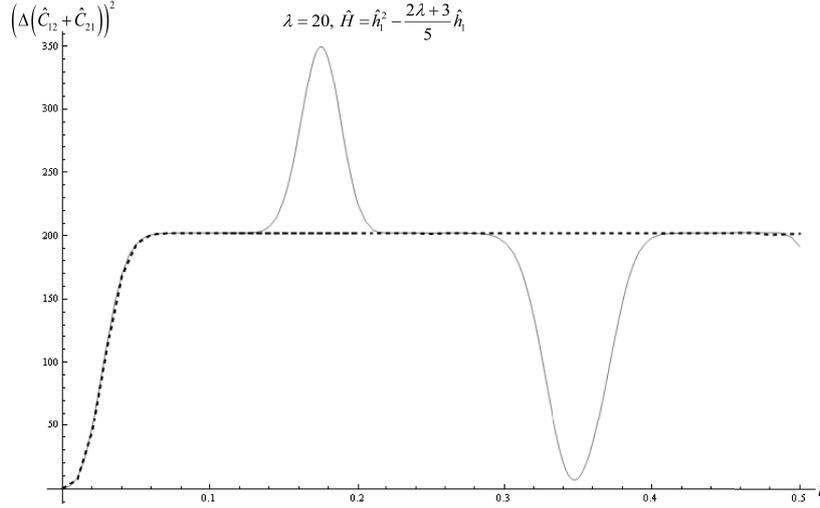
Fig. 4.5: Time evolution of the variance of $\hat{C}_{12} + \hat{C}_{21}$ under the Hamiltonian $H = \hat{h}_1^2 - \frac{2\lambda+3}{5}\hat{h}_1$ plotted using semiclassical method using Eq. (4.69) (dashed line) and quantum mechanical method using (4.71) (solid line) for $\lambda = 20$.

ignored as it plays no role in the evolution (its bracket with any other function is zero). The part proportional to $(1, 1)$ is in fact a multiple of the generator $\hat{h}_1$. As we have just seen, the evolution generated by $\hat{h}_1$ simply produces a rigid displacement of the Wigner function. The new effects arise out of the $(2, 2)$ term in $\hat{h}_1^2$. We can highlight this by removing the linear terms and look instead at the Hamitonian $\hat{H} = \hat{h}_1^2 - \frac{2\lambda+3}{5}\hat{h}_1$, which produces no rigid displacement of the distribution but will generate the same deformation as $\hat{h}_1^2$. The symbol for this Hamiltonian is

$$W_H = \frac{1}{2}\lambda(\lambda+3) + \frac{9}{40}\sqrt{(\lambda-1)\lambda(\lambda+3)(\lambda+4)}\,(3 + 4\cos(\beta_2) + 5\cos(2\beta_2)) . \qquad (4.72)$$

Using Eq. (4.59) and ignoring the quantum correction term we obtain

$$\partial_t W_\rho = \frac{1}{2\sqrt{\lambda(\lambda+3)}}\{W_H, W_\rho\} = \frac{9}{5}\sqrt{(\lambda-1)(\lambda+4)}\,(1 + 5\cos(\beta_2))\frac{\partial W_\rho}{\partial \alpha_2}, \qquad (4.73)$$

with solution

$$\alpha_2(t) = \alpha_2 - \frac{9}{5}\sqrt{(\lambda-1)(\lambda+4)}\,(1 + 5\cos(\beta_2))\,t. \qquad (4.74)$$

Here again we choose our initial state to be a coherent state located above the minimum of the symbol of the Hamiltonian. W_H is minimized by $\alpha_1' = \alpha_2' = \beta_1' = 0$ and $\beta_2' = \arccos(-1/5)$. This set of angles leads to an expression for $\cos(\tilde{\beta}_2)$ given by

$$\begin{aligned}
\cos(\tilde{\beta}_2) &= -1 + 2\cos^2\left(\tfrac{1}{2}\beta_2'\right)\cos^2\left(\tfrac{1}{2}\beta_2\right) + 2\cos^2\left(\tfrac{1}{2}\beta_1\right)\sin^2\left(\tfrac{1}{2}\beta_2\right)\sin^2\left(\tfrac{1}{2}\beta_2'\right) \\
&\quad + \cos(\alpha_2)\cos\left(\tfrac{1}{2}\beta_1\right)\sin(\beta_2)\sin(\beta_2') .
\end{aligned} \qquad (4.75)$$

By substituting this into Eq. (4.66) we get the initial Wigner function and by replacing α_2 with $\alpha_2(t)$ given in Eq. (4.74), we obtain the time-evolved Wigner function.

We can now compare the quantum mechanical evolution and the truncated semiclassical evolution of the variance of an observable as a function of time. The variance of $\hat{C}_{12} + \hat{C}_{21}$
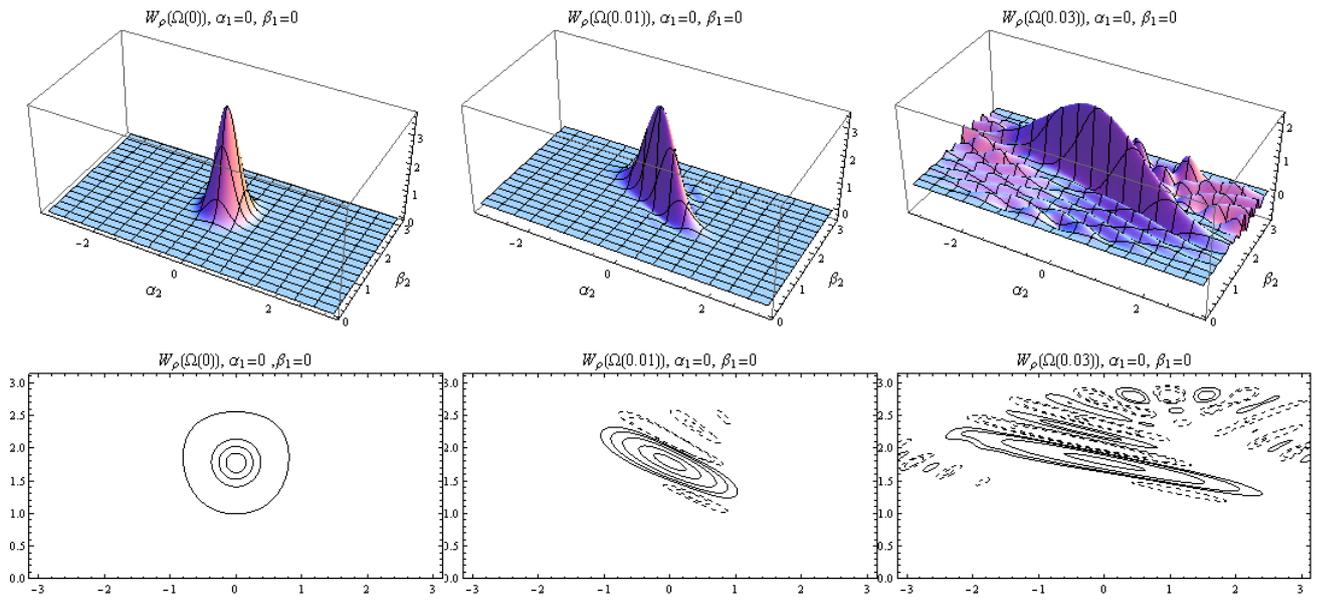
Fig. 4.6: Slices of the full quantum mechanical time evolution of the Wigner function of the initial state given in Eq. (4.60) at $\alpha_1' = \alpha_2' = \beta_1' = 0$ and $\beta_2' = \arccos(-1/5)$ for $\lambda = 20$ at $t = 0, 0.01, 0.03$. The slices are taken at $\alpha_1 = \beta_1 = 0$.
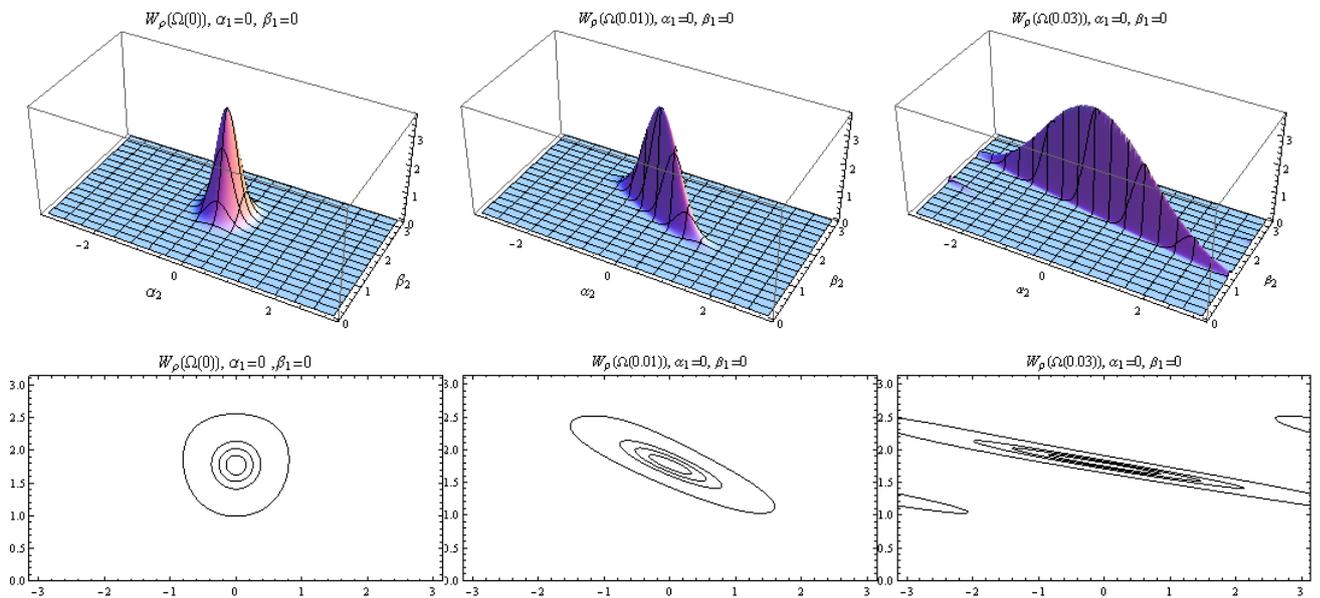

Fig. 4.7: Slices of the semiclassically evolved Wigner function in Eq. (4.66) with $\cos(\tilde{\beta}_2)$ given in Eq. (4.75) for $\lambda = 20$ at $t = 0, 0.01, 0.03$. The slices are taken at $\alpha_1 = \beta_1 = 0$.

has been plotted in Fig. 4.5 calculated both semiclassically, using Eq. (4.69) and the required symbols, and quantum mechanically, using Eq. (4.71).

As it can be seen from the Fig. 4.5 the semiclassical calculation predicts the evolution of the system for a good proportion. Similar to the $SU(2)$ case peaks and dips are not reproducible by the semiclassical method. It must be noted that by increasing λ the difference between the quantum and semiclassical calculation decreases but the time over which the two calculations remain close does not change very much. The explanation of the behavior of the curves is similar to the $SU(2)$ case given in section 3.4.2.

Fig. 4.6 shows 3D plots and contour plots of the Wigner function for the initial state (4.66), time-evolved using the full quantum mechanical evolution equation. The details of the calculations is given in appendix C.2. The slices are taken at $\alpha_1 = \beta_1 = 0$ and at specific values of $t = 0, 0.01$ and $t = 0.03$. One observes that the initial coherent state is rapidly deformed from its nearly Gaussian shape in S^4. In particular, small negative regions are generated rapidly in the vicinity of the main peak.

Fig. 4.7 illustrates the 3D and contour plots of slices of the Wigner function time-evolved using this time, semiclassical evolution of the initial state. Although we cannot observe negative regions in Fig. 4.7 at $t = 0.01$, the agreement between semiclassical evolution and full quantum mechanical evolution is good. For longer times, for instance $t = 0.03$, as can be seen from Fig. 4.6, several other dips and peaks appear in the exact quantum mechanical evolution of the Wigner function which is the result of self-interference effect. Fig. 4.7 shows that this cannot be predicted by the semiclassical method.

5. SQUEEZING VIA SEMICLASSICAL EVOLUTION

We talked about squeezed states of harmonic oscillator in chapter 1. The notion of squeezing has propagated to other systems and has attracted significant attention in atomic systems with spin $\frac{1}{2}$ and higher.

Squeezing in atomic systems would allow standard quantum noise limits in atomic clocks and magnetometers to be overcome, and could also have their uses for the teleportation of atomic systems and for memory stores in quantum communication and quantum computing [54].

Moreover squeezing intrinsically reflects the existence of some particular correlations between basis states in the Hilbert space of a quantum system. This entails successful application of squeezing criteria to detect quantum entanglement [55].

In this chapter we investigate squeezing in $SU(2)$ and $SU(3)$ systems using phase space method in the semiclassical approximation and compare the generation and time evolution of squeezing predicted by this approximation with the exact quantum calculation.

5.1 $SU(2)$ squeezing

In spin-like systems several approaches have been used to define the squeezing parameter [8]. Squeezing parameters can be defined as fluctuations of a suitably chosen observable compared to a threshold given by fluctuations in the coherent states of the corresponding quantum system. Following the approach of [35] we define the $SU(2)$ squeezing parameter similar to the squeezing parameter ξ for harmonic oscillator systems defined in Eq. (1.39).

We first define the observable $\hat{S}(\delta)$:

$$\hat{S}(\delta) \equiv T(\delta)\hat{S}_x T^{-1}(\delta) = \hat{S}_x \cos\delta + \hat{S}_y \sin\delta, \qquad (5.1)$$

where $T(\delta) = e^{-i\delta\hat{S}_z}$ is an element of the subgroup of transformations that leaves the highest weight state invariant. Geometrically the operator $\hat{S}(\delta)$ is located on a plane tangent to the sphere, perpendicular to the $\hat{z}$ axis; this plane is shown on the left of Fig. 5.2.

The variance of $\hat{S}(\delta)$ for the highest weight state $|j, j\rangle$ is

$$\left(\Delta\hat{S}(\delta)\right)^2 = \langle j, j|\hat{S}(\delta)^2|j, j\rangle - \langle j, j|\hat{S}(\delta)|j, j\rangle^2 = \frac{1}{2}j, \qquad (5.2)$$

and is independent of the angle δ. This feature is also clear from Fig. 5.2: the Wigner function of the density operator $\hat{\rho} = |j, j\rangle\langle j, j|$ has a Gaussian shape so the projection of W_ρ on the tangent plane is invariant under rotation about $\hat{z}$ axis. As a result the variance of $\hat{S}(\delta)$ is independent of the angle δ.

As we mentioned in chapter 3, the $SU(2)$ coherent states $|\varphi', \theta'\rangle$, are defined by rotating the reference state $|j, j\rangle$, i.e. $\Lambda(\varphi', \theta')|j, j\rangle = R_z(\varphi')R_y(\theta')|j, j\rangle$. If we similarly rotate the
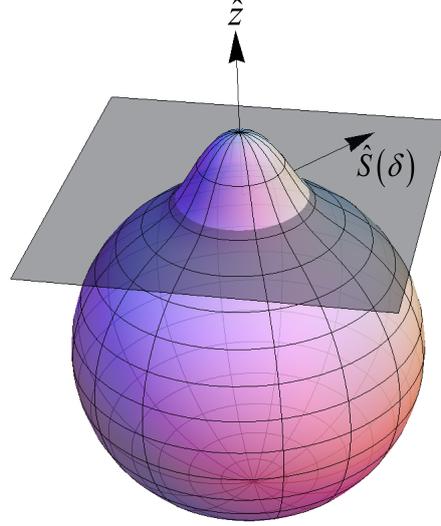
Fig. 5.1: Wigner function of the highest weight state, $|j, j\rangle$ and the tangent plane to the sphere. The operator $\hat{S}(\delta)$ is located on the tangent plane.

observable $\hat{S}(\delta)$ of (5.1) we obtain

$$
\begin{aligned}
\hat{S}_\perp(\varphi', \theta', \delta) &\equiv \Lambda(\varphi', \theta') \hat{S}(\delta) \Lambda^{-1}(\varphi', \theta') \\
&= \Lambda(\varphi', \theta') T(\delta) \hat{S}_x T^{-1}(\delta) \Lambda^{-1}(\varphi', \theta') ,
\end{aligned} \tag{5.3}
$$

located on the tangent plane to the sphere, perpendicular to the direction $\vec{n} = (n_x, n_y, n_z)$ defined by the coherent state $|\varphi', \theta'\rangle$ via

$$
\begin{aligned}
n_x &= \sin\theta' \cos\varphi' = \langle\varphi', \theta'|\hat{S}_x|\varphi', \theta'\rangle / j , \\
n_y &= \sin\theta' \sin\varphi' = \langle\varphi', \theta'|\hat{S}_y|\varphi', \theta'\rangle / j , \\
n_z &= \cos\theta' = \langle\varphi', \theta'|\hat{S}_z|\varphi', \theta'\rangle / j .
\end{aligned} \tag{5.4}
$$

By construction, the fluctuations of $\hat{S}_\perp(\varphi', \theta', \delta)$, when evaluated in the coherent state $|\varphi', \theta'\rangle$, are again independent of the angles φ', θ' and δ. Explicitly, one can verify that for the coherent state $|\varphi', \theta'\rangle$

$$
\left(\Delta\hat{S}_\perp(\varphi', \theta', \delta)\right)^2 = \frac{1}{2}j. \tag{5.5}
$$

We will use the condition (5.5) to define spin squeezing. A state of angular momentum j is squeezed if there is an operator $\hat{S}_\perp(\varphi', \theta', \delta^*)$ in the tangent plane, for which

$$
\left(\Delta\hat{S}_\perp(\varphi', \theta', \delta^*)\right)^2 < \frac{1}{2}j, \tag{5.6}
$$

5.1.1 Semiclassical squeezing

Spin-squeezed states, like position-squeezed or momentum-squeezed states for the harmonic oscillator, can be obtained from the evolution generated by a nonlinear Hamiltonian. The unitary transformation $U(t) = \exp\left(-i\hat{H}t\right)$ generated by the nonlinear Hamiltonian $\hat{H}$ deforms the initial coherent state to a squeezed state. A simple non-linear Hamiltonian, inspired by the Kerr Hamiltonian in Eq. (1.48), is $\hat{H} = \hat{S}_z^2$.
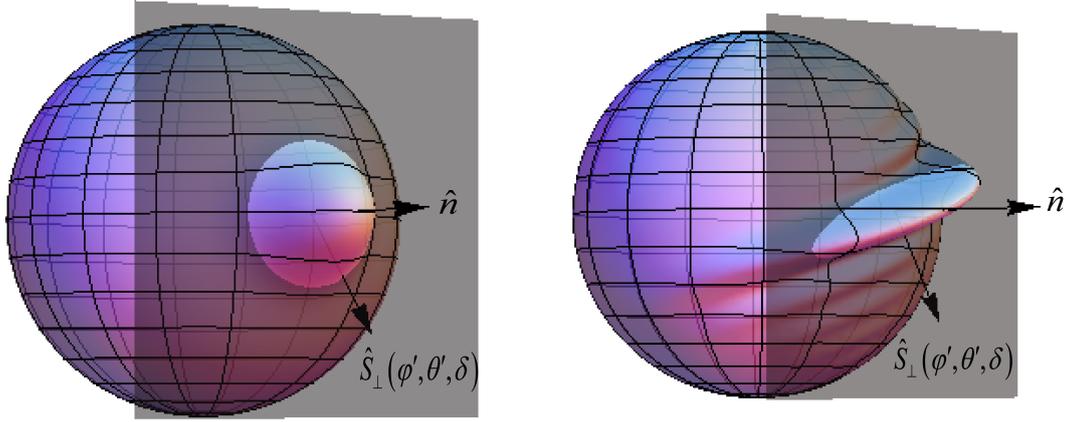
Fig. 5.2: Wigner function of the coherent state $|\varphi', \theta'\rangle$ (left), Wigner function of a squeezed state (right) and the tangent plane to the sphere perpendicular to the direction $\hat{n}$. The operator $\hat{S}_\perp (\varphi', \theta', \delta)$ is located on the tangent plane

The semiclassical squeezing of $SU(2)$ systems has been investigated in [56]. We discussed the semiclassical evolution generated by $\hat{H} = \hat{S}_z^2$ in chapter 3. As initial state we consider the coherent state $|\varphi' = 0, \theta' = \pi/2\rangle$. The Wigner function for this state at time t is given by Eqs. (3.51) and (3.62). This Wigner function can be approximated by

$$W_\rho (\varphi, \theta) \approx (\sin \theta \cos \varphi(t))^{2j-1} (1 + \sin \theta \cos \varphi(t)) , \tag{5.7}$$

where

$$\varphi(t) = \varphi - \sqrt{(2j-1)(2j+3)} \cos(\theta) t . \tag{5.8}$$

This approximation is very useful in calculations especially for large values of j when numerical calculations take a very long time. Using this approximate form of the Wigner function one can calculate the variance of $\hat{S}_\perp (\varphi', \theta', \delta)$ analytically.

For angles $\varphi' = 0$ and $\theta' = \pi/2$ the operator $\hat{S}_\perp (\varphi', \theta', \delta)$ in Eq. (5.3) turns out to be

$$\hat{S}_\perp (\varphi', \theta', \delta) = \hat{S}_y \sin \delta - \hat{S}_z \cos \delta . \tag{5.9}$$

The resulting variance depends on the angle δ. We calculated the minimization of this variance with respect to the angle δ semiclassically using the approximate Wigner function in Eq. (5.7) and the phase space symbols of the required $su(2)$ operators from chapter 3.

In Fig. 5.3 we present plots of the minimum of $(\Delta \hat{S}_\perp (\varphi', \theta', \delta))^2$ with respect to δ as a function of time, calculated quantum mechanically and semiclassically for $j = 30$. The agreement between semiclassical (dashed line) and quantum mechanical calculations (solid line) is very good for the values of t of order 1. This agreement gets better for larger values of j. However for longer times there are other dips in the quantum mechanical graph which cannot be reproduced by the semiclassical method. In fact the semiclassical approximation is just able to reproduce the first dip and after that it remains constant. This can also be seen from the Wigner function graphs in Figs. 3.4 and 3.3. For longer times the Wigner function in the semiclassical approximation is no longer reliable. Moreover for longer times, the very oscillatory behavior of the integrals that appear in the semiclassical calculations, leads to numerical issues; as a result we have decided to plot the graphs in a region where quantum mechanical and semiclassical methods are in agreement.
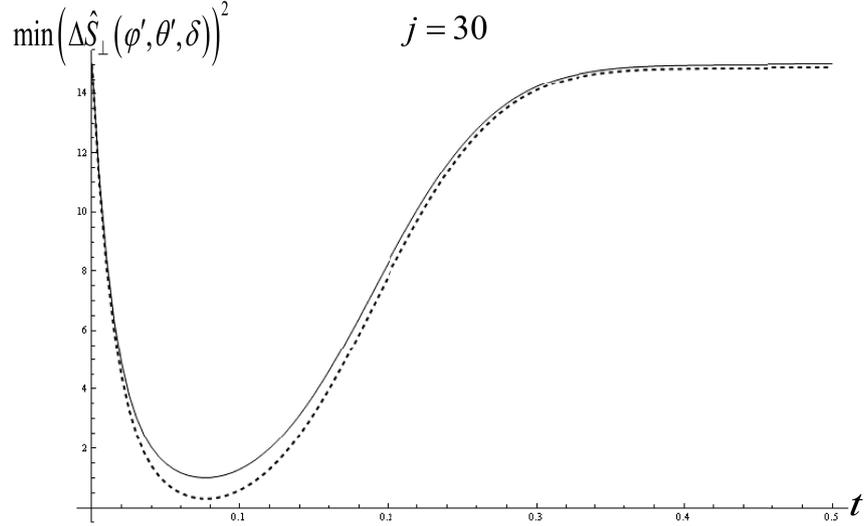
Fig. 5.3: The time evolution of the minimum of $(\Delta \hat{S}_\perp (\varphi', \theta', \delta))^2$ at $\varphi' = 0$ and $\theta' = \pi/2$ for $j = 30$. The solid line is plotted using quantum mechanical calculations and the dashed line is plotted using the approximate form of the Wigner function in Eq. (5.7).

The log-log graph on the left side of Fig. (5.4) shows that the time location of the minimum of $(\Delta \hat{S}_\perp (\varphi' = 0, \theta' = \pi/2, \delta))^2$ scales as $t_{min} \approx j^{-0.65}$ and the log-log graph on the right side of the Fig. (5.4) shows that the minimum of $(\Delta \hat{S}_\perp (\varphi' = 0, \theta' = \pi/2, \delta))^2$ scales like $j^{+0.35}$. This scaling behavior will be compared with the similar behaviors in $SU(3)$ case.

Fig. 5.4: log-log plots of the time location of the minimum of the $SU(2)$ squeezing versus j (left) and the minimum versus j

5.1.2 Experimental implementation

An example of a spin squeezing experiment using condensates of ^{87}Rb atoms has been reported in [57]. The hyperfine states $|+\rangle \equiv |f = 2, m_f = 1\rangle$ and $|-\rangle \equiv |f = 1, m_f = -1\rangle$ of ^{87}Rb form a two level system. The Hamiltonian of the interaction of these levels with a microwave radiation can be expressed in terms of spin operators as

$$\hat{H} = \omega_0 \hat{S}_z + \Omega \hat{S}(\delta) + \chi \hat{S}_z^2 \tag{5.10}$$

where $\hat{S}_z = (N_+ - N_-)/2$ is half the atom number difference between the states and directly measurable. The first term in the above equation describes spin precession around z at the detuning ω_0. The second term describes spin rotations around an axis $\hat{S}(\delta) = \hat{S}_x \cos \delta + \hat{S}_y \sin \delta$ with frequency Ω. The third, nonlinear term of strength χ arises from elastic collisional interactions in the Bose Einstein Condensate. It deforms the state on the Bloch sphere which results in spin squeezing.

The initial state of this experiment is all individual atoms in $|-\rangle$. This is just the highest weight state $|j, j\rangle$ with $j = N/2$, $N = N_+ + N_-$. A $\pi/2$ pulse rotates this state and prepares a spin coherent state along x axis and isotropic quantum noise in the $y - z$ plane, $(\Delta \hat{S}_y)^2 = (\Delta \hat{S}_z)^2 = N/4$. Subsequent nonlinear evolution with χS_z^2 for the time of best squeezing deforms the noise circle into an ellipse, creating a spin squeezed state with reduced noise at an angle δ_{min}. The observable $\hat{S}_\perp(\delta) = \hat{S}_y \sin \delta - \hat{S}_z \cos \delta$ is measured by rotating the state around x axis by a variable angle δ, before detecting $\hat{S}_z$. The normalized variance $(\Delta_n \hat{S}_\perp(\delta))^2 = 4(\Delta \hat{S}_\perp(\delta))^2 / \langle N \rangle$ has been measured. For the squeezed state the spin noise falls significantly below the standard quantum limit, $(\Delta_n \hat{S}_\perp(\delta))^2 = 0$dB, reaching a minimum of $(\Delta_n \hat{S}_\perp(\delta))^2 = -3.7 \pm 0.4$dB at $\delta_{min} = 6°$. For more details see [57].

5.2 $SU(3)$ squeezing

There is renewed interest in squeezing in systems of higher symmetry, spin-1 [58]-[60] and also arbitrary spin particles [61].

In this section we define a new criterion for squeezing in $SU(3)$ systems [33]. We define the squeezing criterion in a manner similar to $SU(2)$ criterion of Eq. (5.6). The main idea consists in defining the family of collective operators $\hat{K}$ (which in practice are some linear combinations of generators of the $su(3)$ algebra) for which the fluctuations evaluated using $SU(3)$ coherent states are invariant under the same group transformation

$$T(\alpha_3, \beta_3, \gamma_1, \gamma_2) \equiv R_{23}(\alpha_3, \beta_3, -\alpha_3) e^{-i\gamma_1 \hat{h}_1} e^{-i\gamma_2 \hat{h}_2} \tag{5.11}$$

that leaves invariant the reference state used to construct the set of coherent states.

We define the family of operators $\hat{K}(\alpha_3, \beta_3, \chi)$ as

$$\hat{K}(\alpha_3, \beta_3, \chi) = T(\alpha_3, \beta_3, \gamma_1, \gamma_2)\left(\hat{C}_{13} + \hat{C}_{31}\right) T^{-1}(\alpha_3, \beta_3, \gamma_1, \gamma_2), \tag{5.12}$$

where $\chi = 6\gamma_1 + \gamma_2$. The explicit expansion of $\hat{K}(\alpha_3, \beta_3, \chi)$ in terms of generators is obtained by multiplying the 3×3 matrices for T and $\left(\hat{C}_{13} + \hat{C}_{31}\right)$, and expanding the results in terms of the 3×3 matrices for the generators. Because the transformation is linear, the expansion coefficients do not depend on the size of the matrices. The final result can therefore be written for any representation as:

$$
\begin{aligned}
\hat{K}(\alpha_3, \beta_3, \chi) = \\
-\left(\hat{C}_{12} + \hat{C}_{21}\right) \sin\left(\tfrac{1}{2}\beta_3\right) \cos\left(\alpha_3 - \tfrac{1}{2}\chi\right) - i\left(\hat{C}_{12} - \hat{C}_{21}\right) \sin\left(\tfrac{1}{2}\beta_3\right) \sin\left(\alpha_3 - \tfrac{1}{2}\chi\right) \\
+\left(\hat{C}_{13} + \hat{C}_{31}\right) \cos\left(\tfrac{1}{2}\beta_3\right) \cos\left(\tfrac{1}{2}\chi\right) - i\left(\hat{C}_{13} - \hat{C}_{31}\right) \cos\left(\tfrac{1}{2}\beta_3\right) \sin\left(\tfrac{1}{2}\chi\right).
\end{aligned}
\tag{5.13}
$$

It is easy to verify that the variance $\left(\Delta \hat{K}(\alpha_3, \beta_3, \chi)\right)^2$ when evaluated using the highest weight state $|\lambda, 0, 0\rangle$ is λ and independent of the angles α_3, β_3, χ. Hence, the variance of

$$\hat{K}_\perp(\omega'; \alpha_3, \beta_3, \chi) = D(\omega') \hat{K}(\alpha_3, \beta_3, \chi) D^{-1}(\omega'), \tag{5.14}$$

when evaluated using the coherent state $|\omega'\rangle$,

$$|\omega'\rangle = D(\omega')|\lambda, 0, 0\rangle = R_{23}(\alpha_1', \beta_1', -\alpha_1') R_{12}(\alpha_2', \beta_2', -\alpha_2')|\lambda, 0, 0\rangle, \qquad (5.15)$$

is also independent of the direction $(\alpha_3, \beta_3, \chi)$ in the tangent hyperplane perpendicular to $\vec{n}$, and equals to λ. Here $\vec{n}$ is the mean vector with complex components

$$\vec{n} = \left(\langle\hat{C}_{23}\rangle, \langle\hat{C}_{32}\rangle, \langle\hat{C}_{12}\rangle, \langle\hat{C}_{21}\rangle, \langle\hat{C}_{13}\rangle, \langle\hat{C}_{31}\rangle, \langle\hat{h}_1\rangle, \langle\hat{h}_2\rangle\right). \qquad (5.16)$$

Thus, we will use $(\Delta\hat{K}_\perp(\omega'; \alpha_3, \beta_3, \chi))^2 = \lambda$ as our squeezing threshold and define an $SU(3)$ state $|\psi\rangle$ as squeezed if there is an observable of the form $\hat{K}_\perp\left(\omega'; \alpha_3^*, \beta_3^*, \chi^*\right)$ for which

$$\left(\Delta\hat{K}_\perp(\omega'; \alpha_3^*, \beta_3^*, \chi^*)\right)^2 < \lambda, \qquad (5.17)$$

when evaluated in $|\psi\rangle$.

In a very recent experiment [62] squeezing in an $SU(3)$ system which consists of spin-1 atomic Bose-Einstein condensates have been realized using the $f = 1$ hyperfine manifold of ^{87}Rb. This system can be described in terms of creation and destruction operators of three Zeeman states $m_f = -1, 0, 1$, $\hat{a}_{m_f}$ and $\hat{a}_{m_f}^\dagger$, in the single-mode approximation. These destruction and creation operators correspond to the ones that we used in chapter 4 to construct ladder operators $\hat{C}_{ij}$. In the experiment they prepared condensate of $N = 45,000$, ^{87}Rb atoms in the $|f = 1, m_f = 0\rangle$ hyperfine state in a $2G$ magnetic field. The Hamiltonian describing the collisionally induced spin dynamics of the condensate and the effects of an applied magnetic field B along z axis is a nonlinear Hamiltonian contains terms $\hat{H}_{sq} = 2\lambda\left(\hat{a}_0^{\dagger 2}\hat{a}_1\hat{a}_{-1} + \hat{a}_1^\dagger\hat{a}_{-1}^\dagger\hat{a}_0^2\right)$ which generates squeezing. λ characterize the inter-spin energy. They used a squeezing parameter which is different from what we defined here and they observed squeezing of $-8.3^{+0.6}_{-0.7}$dB. For more details see [62].

5.2.1   Semiclassical squeezing

Squeezing reflects correlations between components of a basis. As mentioned before, group transformations generated by exponentiating linear combinations of elements of the $su(3)$ algebra, produce rigid displacements of the basis states. Correlations between basis states cannot as a matter of definition be induced by such group transformations. Rather, correlations are obtained as a result of non-linear (in terms of the algebra of observables) transformations, usually from non-linear Hamiltonian evolution. Here we consider the following simple non-linear Hamiltonians that lead to squeezing,

$$\hat{H}_1 = \hat{h}_1^2 - \frac{2\lambda + 3}{5}\hat{h}_1, \qquad \hat{H}_2 = \hat{h}_2^2 + \frac{2\lambda + 3}{60}\hat{h}_1. \qquad (5.18)$$

We remind the reader that the decomposition of $\hat{h}_1^2$ and $\hat{h}_2^2$ in terms of tensor operators contains terms that transform by representations $(2, 2)$, $(1, 1)$ and $(0, 0)$. The $(1, 1)$ terms are proportional to generators and so produce rigid displacements. We remove displacements by adding a term proportional to $\hat{h}_1$ which transform by $(1, 1)$.

Squeezing generated by $\hat{H}_1$

We discussed the semiclassical evolution of $SU(3)$ systems under $\hat{H}_1$ Hamiltonian in chapter 4. For semiclassical squeezing we have to find the phase space symbol of the observables $\hat{K}_\perp$ and $\hat{K}_\perp^2$.

We write the explicit expansion of $\hat{K}_\perp$ in terms of generators by multiplying the 3×3 matrices for $D(\omega')$ and $\hat{K}$ and expanding the result in terms of the 3×3 matrices for the generators. The final result, which is true for any representation, is:

$$
\begin{aligned}
\hat{K}_\perp \left(\omega; \alpha_3, \beta_3, \chi\right) = & \\
& + \left(\hat{C}_{13} + \hat{C}_{31}\right) \cos\left(\tfrac{1}{2}\chi\right) \cos\left(\tfrac{1}{2}\beta_3\right) \cos\left(\tfrac{1}{2}\beta_2'\right) + i\left(\hat{C}_{31} - \hat{C}_{13}\right) \cos\left(\tfrac{1}{2}\beta_3\right) \cos\left(\tfrac{1}{2}\beta_2'\right) \sin\left(\tfrac{1}{2}\chi\right) \\
& + \left(\hat{C}_{32} + \hat{C}_{23}\right) \cos\left(\tfrac{1}{2}\chi\right) \cos\left(\tfrac{1}{2}\beta_3\right) \sin\left(\tfrac{1}{2}\beta_2'\right) + i\left(\hat{C}_{32} - \hat{C}_{23}\right) \sin\left(\tfrac{1}{2}\chi\right) \cos\left(\tfrac{1}{2}\beta_3\right) \sin\left(\tfrac{1}{2}\beta_2'\right) \\
& - \left(\hat{C}_{12} + \hat{C}_{21}\right) \cos\left(\alpha_3 - \tfrac{1}{2}\chi\right) \cos\left(\beta_2'\right) \sin\left(\tfrac{1}{2}\beta_3\right) + i\left(\hat{C}_{21} - \hat{C}_{12}\right) \sin\left(\alpha_3 - \tfrac{1}{2}\chi\right) \sin\left(\tfrac{1}{2}\beta_3\right) \\
& + \tfrac{1}{2}\left(\hat{h}_1 - \hat{h}_2\right) \cos\left(\alpha_3 - \tfrac{1}{2}\chi\right) \sin\left(\beta_2'\right) \sin\left(\tfrac{1}{2}\beta_3\right) ,
\end{aligned} \tag{5.19}
$$

Using the phase space symbol of $su(3)$ generators from chapter 4, $W_{K_\perp}$ can be written easily.

We also need the symbol for $(\hat{C}_{13} + \hat{C}_{31})^2$ to obtain the variance of $\hat{K}_\perp\left(\omega'; \alpha_3, \beta_3, \chi\right)$ using the semiclassical evolution. The expression is complicated but can be written as:

$$
\begin{aligned}
\left(\hat{C}_{13} + \hat{C}_{31}\right)^2 &= \hat{C}_{13}^2 + \hat{C}_{31}^2 + \hat{C}_{31}\hat{C}_{13} + \hat{C}_{13}\hat{C}_{31} \\
&= \sum_{\sigma=0}^{2} \sum_{\mu_1,\mu_2,I_\mu} g^\sigma_{\mu I_\mu} T^\lambda_{(\sigma,\sigma);(\mu_1,\mu_2,\mu_3),I_\mu} ,
\end{aligned} \tag{5.20}
$$

where coefficients $g^\sigma_{\mu I_\mu}$ are given in Eqs.(B.1) and (B.7). Transforming Eq. (5.20) gives

$$
\begin{aligned}
\hat{K}_\perp^2 &= D(\omega') T(\alpha_3, \beta_3, \gamma_1, \gamma_2) \left(\hat{C}_{13} + \hat{C}_{31}\right)^2 T^{-1}(\alpha_3, \beta_3, \gamma_1, \gamma_2) D^{-1}(\omega') \\
&= \sum_{\sigma=0}^{2} \sum_{\mu_1,\mu_2,I_\mu} \sum_{\nu_1,\nu_2,I_\nu} g^\sigma_{\mu I_\mu} T^\lambda_{(\sigma,\sigma);(\mu_1,\mu_2,\mu_3),I_\mu} D^{(\sigma,\sigma)}_{(\nu_1,\nu_2,\nu_3)I_\nu,(\mu_1,\mu_2,\mu_3)I_\mu}\left(\alpha_1', \beta_1', \alpha_2', \beta_2', \alpha_3, \beta_3, \gamma_1, \gamma_2\right),
\end{aligned}
$$
$$\tag{5.21}$$

where

$$
D^{(\sigma,\sigma)}_{(\nu_1,\nu_2,\nu_3)I_\nu,(\mu_1,\mu_2,\mu_3)I_\mu}(\Omega) = \left\langle (\nu_1, \nu_2, \nu_3) I_\nu \right| R(\Omega) \left| (\mu_1, \mu_2, \mu_3) I_\mu \right\rangle \tag{5.22}
$$

with $R(\Omega)$ given in Eq. (4.17). The symbol for $\hat{K}_\perp^2$ of Eq. (5.21) is found to be

$$
W_{K_\perp^2} = \sum_{\sigma\mu_1\mu_2 I_\mu \nu_1\nu_2 I_\nu} g^\sigma_{\mu I_\mu} D^{(\sigma,\sigma)}_{(\nu_1,\nu_2,\nu_3)I_\nu,(\mu_1,\mu_2,\mu_3)I_\mu}\left(\alpha_1', \beta_1', \alpha_2', \beta_2', \alpha_3, \beta_3, \gamma_1, \gamma_2\right) W_{T^{(\sigma,\sigma)}_{(\mu_1,\mu_2,\mu_3)I}}(\Omega) , \tag{5.23}
$$

where $W_{T^{(\sigma,\sigma)}_{(\mu_1,\mu_2,\mu_3)I}}$, the phase space symbol of $T^{(\sigma,\sigma)}_{(\mu_1,\mu_2,\mu_3)I}$, can be obtained from Eq. (4.25):

$$
W_{T^{(\sigma,\sigma)}_{(\mu_1,\mu_2,\mu_3)I}}(\Omega) = \sqrt{\frac{2(\sigma+1)^3}{(\lambda+1)(\lambda+2)}} D^{(\sigma,\sigma)}_{(\mu_1,\mu_2,\mu_3)I;(\sigma,\sigma)0}(\Omega) . \tag{5.24}
$$

We choose once again the initial state as a coherent state that sits above the minimum of W_{H_1}. This minimum is located at $\alpha_1' = \beta_1' = \alpha_2' = 0$, $\beta_2' = \arccos(-1/5)$. The time-evolved Wigner function, neglecting correction terms of order ε^{-3}, is given by Eqs. (4.66), (4.74) and (4.75).

For $\lambda \gg 1$ we have found, with much similarity to the $SU(2)$ case, that $W_{|\lambda,0,0\rangle\langle\lambda,0,0|}(\beta_2)$ is well approximated by

$$
W_{|\lambda,0,0\rangle\langle\lambda,0,0|}(\beta_2) \approx A e^{\lambda(\cos\beta_2 - 1)}, \quad A = \frac{4\lambda^2}{(\lambda+1)(\lambda+2)}, \tag{5.25}
$$

$$\min\left(\Delta\hat{K}_\perp\left(\omega';\alpha_3,\beta_3,\chi\right)\right)^2 \qquad \lambda=20, \ \hat{H}_1 = \hat{h}_1^2 - \frac{2\lambda+3}{5}\hat{h}_1$$
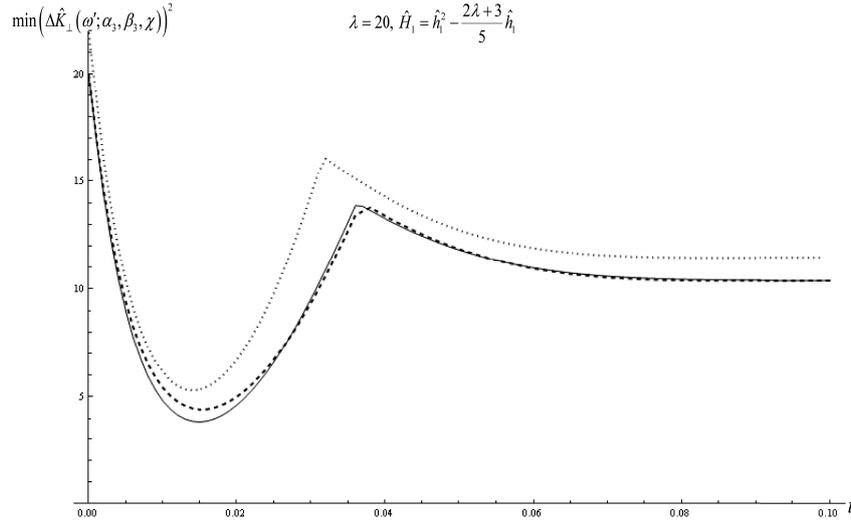
Fig. 5.5: The time evolution of the minimum of $(\Delta\hat{K}_\perp\,(\omega';\alpha_3,\beta_3,\chi))^2$ under the Hamiltonian $\hat{H}_1$ for $\alpha_1' = \beta_1' = \alpha_2' = 0$, $\beta_2' = \arccos(-1/5\,)$ and $\lambda = 20$. The dotted line is plotted using approximate Wigner function in Eq. (5.25), the dashed line is obtained using the exact Wigner functions of Eqs. (4.66), (4.74) and (4.75) and the solid line shows the quantum mechanical calculations.

where A is the normalization factor. This approximation is useful in calculating the variance of $\hat{K}_\perp$ specially for large values of λ.

Fluctuations of $\hat{K}_\perp(\omega';\alpha_3,\beta_3,\chi)$, when evaluated using the initial coherent state evolved under Hamiltonian $\hat{H}_1$, depend on the parameters $\alpha_3,\beta_3,\chi = 6\gamma_1 + \gamma_2$ in such a way that there exist directions, parameterized by $\alpha_3^*,\beta_3^*,\chi^*$ in the tangent hyperplane, where the fluctuations are smaller than the fluctuations in the corresponding coherent state $|\omega'\rangle$. It remains to select from those directions the one along which the fluctuations are smallest to complete our definition of squeezing.

We analytically calculated the fluctuations $(\Delta\hat{K}_\perp\,(\omega';\alpha_3,\beta_3,\chi))^2$ using the standard phase space techniques, *i.e.* integrating the symbols of $\hat{K}_\perp(\omega';\alpha_3,\beta_3,\chi)$ and its square using the time-evolved Wigner function. A sample of the analytical calculations is given in appendix D.

Fig. 5.5 shows the time evolution of the smallest fluctuations of $\hat{K}_\perp(\omega';\alpha_3,\beta_3,\chi)$ with respect to α_3, β_3 and χ for the initial Wigner function of Eq. (4.66) and its approximation in Eq. (5.25) for $\lambda = 20$. The best squeezing direction $(\alpha_3^*,\beta_3^*,\chi^*)$ has been found through numerical minimization. The results are illustrative of a number of calculations performed for irreps of the type $(\lambda, 0)$ with λ ranging between 10 and 30. It is clear from the figure that semiclassical calculations using both the exact Wigner function and its approximate form are able to describe the squeezing up to the first minimum with a good approximation; for longer times the quantum mechanical plot has other dips that are not reproducible with the semiclassical method. This is because for longer times the Wigner function in the semiclassical approximation is not reliable as can be seen in Figs. 4.6 and 4.7. Again similar to the $SU(2)$ case, because of the numerical issues for longer times in the semiclassical approximation we have plotted the graphs in the region that both methods are in agreement.

From Fig. 5.6 we see that the time location of the minimum of $(\Delta\hat{K}_\perp(\omega;\alpha_3^*,\beta_3^*,\chi^*)(t))^2$ scales like $t_{\min} \approx \lambda^{-0.81}$ (right) and the minimum of $(\Delta\hat{K}_\perp(\omega;\alpha_3^*,\beta_3^*,\chi^*)(t))^2$ scales like $\lambda^{+0.67}$ (left). The values are different from the $SU(2)$ case, indicating that the squeezing is different in nature.
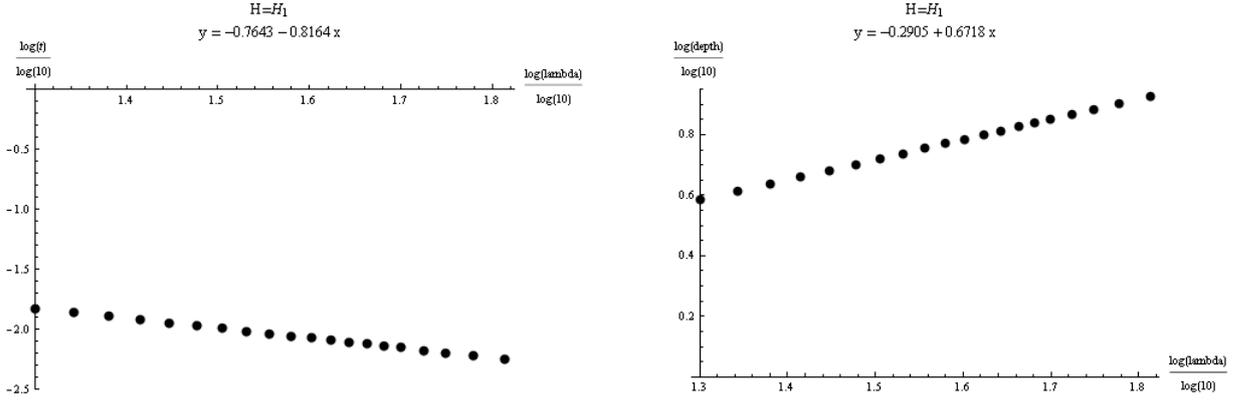
Fig. 5.6: log-log plots of the time location of the minimum of the squeezing versus λ (left) and the minimum versus λ for squeezing generated by the Hamiltonian $\hat{H}_1$

Squeezing generated by $\hat{H}_2$

Now we investigate squeezing under $\hat{H}_2$ Hamiltonian in Eq. (5.18). The symbol for $\hat{H}_2$ is obtained using $W_{h_2^2}$ and W_{h_1} from chapter 4,

$$
\begin{aligned}
W_{H_2} &= \frac{1}{24}\lambda(\lambda+3) + \frac{1}{480}\sqrt{(\lambda-1)\lambda(\lambda+3)(\lambda+4)}\,(3+4\cos\beta_2+5\cos(2\beta_2)) \\
&\quad + \frac{1}{24}\sqrt{(\lambda-1)\lambda(\lambda+3)(\lambda+4)}\,(1+3\cos(2\beta_1))\sin^4\left(\frac{\beta_2}{2}\right).
\end{aligned}
\tag{5.26}
$$

The equation of motion of the Wigner function under this Hamiltonian is

$$
\begin{aligned}
\frac{\partial W_\rho}{\partial t} &= \frac{1}{2\sqrt{\lambda(\lambda+3)}}\left\{W_{H_2}, W_\rho\right\} \\
&= \sqrt{(\lambda-1)(\lambda+4)}\left(\frac{1}{20}(2+5\cos\beta_1(\cos\beta_2-1))\frac{\partial W_\rho}{\partial\alpha_2}\right. \\
&\quad \left. +\cos\beta_1\sin^2\left(\frac{\beta_2}{2}\right)\frac{\partial W_\rho}{\partial\alpha_1}\right),
\end{aligned}
\tag{5.27}
$$

which results in

$$
\alpha_1(t) = \alpha_1 - \sqrt{(\lambda-1)(\lambda+4)}\cos\beta_1\sin^2\left(\frac{\beta_2}{2}\right)t,
\tag{5.28}
$$

$$
\alpha_2(t) = \alpha_2 - \frac{1}{20}\sqrt{(\lambda-1)(\lambda+4)}\,(2+5\cos\beta_1(\cos\beta_2-1))t.
\tag{5.29}
$$

In comparison with the $\hat{H}_1$ Hamiltonian, two angles α_1 and α_2 are time dependent but the evolution still remains solvable.

As before we choose the initial state to sit above the minimum of W_{H_2} which occurs at $\alpha_1' = \alpha_2' = 0, \beta_1' = \frac{1}{2}\pi, \beta_2' = \pi$. Thus the initial state is:

$$
|\omega'\rangle = D(\omega')|\lambda,0,0\rangle = R_{23}\left(0,\tfrac{1}{2}\pi,0\right)R_{12}(0,\pi,0)|\lambda,0,0\rangle,
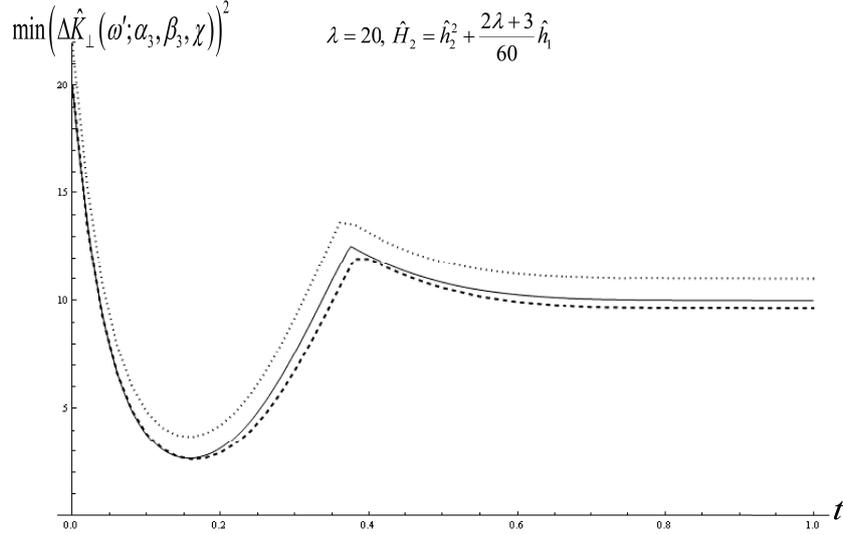\tag{5.30}
$$

Fig. 5.7: The time evolution of the minimum of $(\Delta\hat{K}_\perp(\omega';\alpha_3,\beta_3,\chi))^2$ under the Hamiltonian $\hat{H}_2$ for $\alpha_1' = \alpha_2' = 0$, $\beta_1' = \frac{1}{2}\pi, \beta_2' = \pi$ and $\lambda = 20$. The dotted line is plotted using approximate Wigner function in Eq. (5.25), the dashed line is obtained using the exact Wigner functions of Eqs. (4.66), (4.74) and (4.75) and the solid line shows the quantum mechanical calculations.

from which we obtain

$$\cos\tilde{\beta}_2 = \sin^2\left(\frac{\beta_2}{2}\right) + \cos\alpha_1 \sin\beta_1 \sin^2\left(\frac{\beta_2}{2}\right) - 1 \,. \tag{5.31}$$

Thus for this choice of initial state there is no α_2 dependence in the Wigner function. The evolved Wigner function is then obtained by substituting Eq. (5.31) in Eq. (4.66) where in Eq. (5.31) one must use $\alpha_1(t)$ from Eq. (5.28) instead of α_1.

For the observable in the tangent plane, $\hat{K}_\perp$ we have

$$
\begin{aligned}
&\hat{K}_\perp(\omega';\alpha_3,\beta_3,\chi)\\
&= D(\omega')\,T(\alpha_3,\beta_3,\gamma_1,\gamma_2)\left(\hat{C}_{13}+\hat{C}_{31}\right)T^{-1}(\alpha_3,\beta_3,\gamma_1,\gamma_2)\,D^{-1}(\omega')\\
&= \frac{1}{\sqrt{2}}\left(\hat{C}_{12}+\hat{C}_{21}\right)\cos\left(\alpha_3-\tfrac{1}{2}\chi\right)\sin\left(\tfrac{1}{2}\beta_3\right) + \frac{i}{\sqrt{2}}\left(\hat{C}_{21}-\hat{C}_{12}\right)\sin\left(\alpha_3-\tfrac{1}{2}\chi\right)\sin\left(\tfrac{1}{2}\beta_3\right)\\
&\quad + \frac{1}{\sqrt{2}}\left(\hat{C}_{13}+\hat{C}_{31}\right)\cos\left(\alpha_3-\tfrac{1}{2}\chi\right)\sin\left(\tfrac{1}{2}\beta_3\right) + i\left(\hat{C}_{31}-\hat{C}_{13}\right)\sin\left(\tfrac{1}{2}\beta_3\right)\sin\left(\alpha_3-\tfrac{1}{2}\chi\right)\\
&\quad + i\left(\hat{C}_{32}-\hat{C}_{23}\right)\sin\left(\tfrac{1}{2}\chi\right)\cos\left(\tfrac{1}{2}\beta_3\right) - 2\hat{h}_2\cos\left(\tfrac{1}{2}\chi\right)\cos\left(\tfrac{1}{2}\beta_3\right) \,. \tag{5.32}
\end{aligned}
$$

Thus $W_{K_\perp}$ can be written easily using the symbols of $su(3)$ generators. The Wigner symbol of $\hat{K}_\perp^2$ is given in Eq. (5.23) wherein one must use $\alpha_1' = \alpha_2' = 0, \beta_1' = \frac{1}{2}\pi, \beta_2' = \pi$.

Fig. 5.7 shows the time evolution of the smallest fluctuations of $\hat{K}_\perp(\omega';\alpha_3,\beta_3,\chi)$ for the initial coherent state of Eq. (5.30) for $\lambda = 20$. The solid line is the quantum mechanical calculations, the dashed line is truncated semiclassical calculation using the exact Wigner function in Eq. (4.66) and the dotted line is plotted using the approximate Wigner function in Eq. (5.25). In comparison to Fig. 5.5 we see that the minimum is lower than the $\hat{H}_1$ case. This means we get more squeezing with the $\hat{H}_2$ Hamiltonian. Moreover the minimum occurs at a later time than the $\hat{H}_1$ case. Here again for the first dip in the squeezing graph the agreement between the
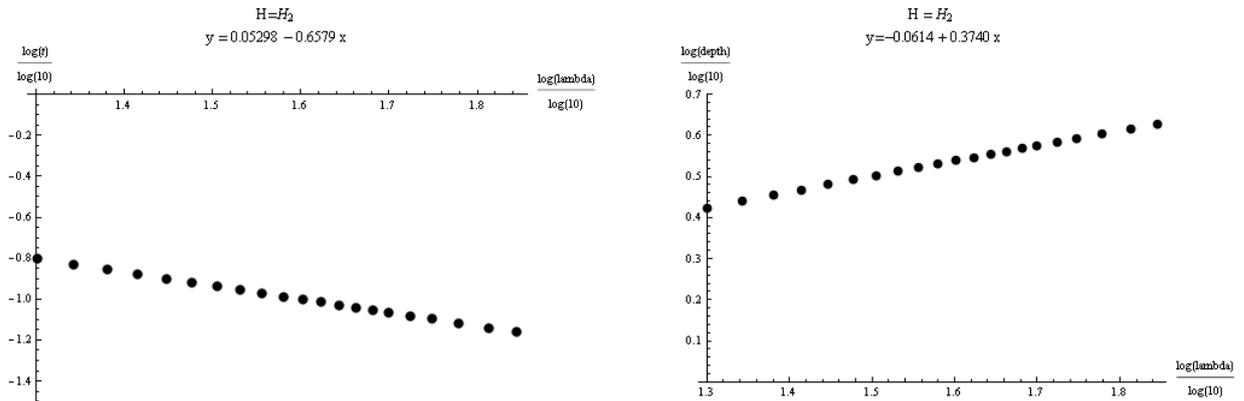
Fig. 5.8: log-log plots of the time location of the minimum of the squeezing versus λ (left) and the minimum versus λ for squeezing generated by the Hamiltonian $\hat{H}_2$

semiclassical method and the quantum mechanical is good but other dips are not reproducible in the semiclassical plots.

We have also found the time location and the minimum of $(\Delta \hat{K}_{\perp}(\omega; \alpha_3^*, \beta_3^*, \chi^*)(t))^2$ for $\lambda = 20$ to $\lambda = 70$ which is plotted in Fig. 5.8. The time location of the minimum scales as $t_{min} \approx \lambda^{-0.65}$ and the minimum of the variance of $\hat{K}_{\perp}(\omega'; \alpha_3, \beta_3, \chi)$ scales as $\lambda^{0.37}$. This is almost the same as the scalings for the $SU(2)$ squeezing, Fig 5.4. This is because $\hat{h}_2$ is the diagonal operator of $su(3)$ that corresponds to $\hat{S}_z$ and also the initial state we chose here is an $SU(2)$ coherent state.

6. CONCLUSION

The objective of this thesis was to investigate squeezing in $SU(3)$ systems in phase space using semiclassical methods. We obtained the corresponding phase space functions of the quantum mechanical observables and also the Poisson bracket on the phase space of the system. These are our main tools to investigate the dynamics in the phase space.

We showed that for $SU(3)$ systems, similar to the previously discussed position-momentum and $SU(2)$ systems, the quantum Liouville equation of the Wigner function for Hamiltonians linear in the generators of the algebra is exactly the classical Liouville equation; for nonlinear Hamiltonians it can be written as Poisson bracket plus other terms which are in fact quantum correction terms.

The quantum correction terms in the case of position-momentum are proportional to $\hbar$ and in the case of $SU(2)$ and $SU(3)$ are inversely proportional to j and λ respectively. For large values of j and λ the quantum correction terms are small and we were able to truncate the Liouville equation to the Poisson bracket and therefore using the classical Liouville equation to discuss the quantum system.

We checked the validity of this approximation by calculating the time evolution of the variance of an observable and comparing the semiclassical plots with the quantum mechanical plots. We showed that the semiclassical plot agrees with the quantum mechanical one for almost half of the full cycle of the evolution.

In the last chapter we showed that squeezing, which is a quantum mechanical effect, can be described in the semiclassical approximation. Squeezed states can be obtained by evolving coherent states of the system under non-linear Hamiltonians. We generalized the squeezing criterion for $SU(2)$ systems to $SU(3)$ systems. We called a state squeezed if the variance of an observable which is a combination of $su(3)$ generators and geometrically lies on the hyperplane tangent to the phase space of the system, perpendicular to the direction of the initial coherent state, be less than the variance of this operator for the coherent state; for the coherent state this variance is λ.

We chose as initial state a $su(3)$ coherent state which sits above the minimum of the phase space symbol of the Hamiltonian. The semiclassical approximation gives better result for this choice of initial state. We then investigated the evolution of the initial state under two nonlinear Hamiltonians: $\hat{H}_1 = \hat{h}_1^2 - \frac{2\lambda+3}{5}\hat{h}_1$ and $\hat{H}_2 = \hat{h}_2^2 + \frac{2\lambda+3}{60}\hat{h}_1$. We showed that although the shape of squeezing for each of these cases is qualitatively similar, the two types of squeezing are different, as can be quantitatively determined by the scaling properties of the time of maximum squeezing and of the actual maximum squeezing as a function of the representation λ. By the evolution under $\hat{H}_2$ Hamiltonian we get more squeezing than what is generated using $\hat{H}_1$, and the time of best squeezing occurs later than the corresponding time in $\hat{H}_1$.

The scaling properties also shows that the squeezing obtained by $\hat{H}_2$ Hamiltonian is almost the same as the $SU(2)$ squeezing. This was not unexpected because $\hat{h}_2$ is the diagonal operator of the $su(2)_{23}$ subalgebra of $su(3)$ and also the initial state that sits above the minimum of W_{H_2} is a $SU(2)$ coherent state.

We have also worked out the generation of squeezing under the Hamiltonian $\hat{H} = \hat{H}_1 + \hat{H}_2$. These result have not presented in this thesis but the quantum mechanical investigation shows that, although our initial state for this case is a true $SU(3)$ coherent state (in contrast with the $\hat{H}_1$ and $\hat{H}_2$ Hamiltonians that we had $SU(2)$ coherent states as initial states) we can't get better squeezing than the $\hat{H}_2$ case. The semiclassical approximation is again able to produce only the first dip in the quantum mechanical curve but it also grasps the main trend of the quantum mechanical curve [63]. The results presented in this thesis could be generalized to other systems of the $SU(n)$ type but the technical challenge of evaluating some integrals will not be easy to manage. Nevertheless, because the qualitative features of squeezing are expected to be well reproduced using a semiclassical evolution, the phase space approach will remain useful in investigating squeezing in $SU(n)$ systems.

At the end we can say that the semiclassical approximation give the qualitative behavior of the system in terms of classical physics. Moreover by comparing semiclassical and quantum mechanical calculations we can identify what part of the problem is really quantum and cannot be understood as a classical effect.

APPENDIX

A. $SU(3)$ POISSON BRACKET

In this appendix we obtain the Poisson bracket on the phase space for $(\lambda, 0)$ irrep of $SU(3)$ which is a four dimensional sphere.

One can show that coherent states for irreps of the type $(\lambda, 0)$, defined in Eq. (4.19), can be written as

$$|\Omega\rangle = N e^{-\tau_1 \hat{C}_{31}} e^{-\tau_2 \hat{C}_{21}} |\lambda, 0, 0\rangle \,, \tag{A.1}$$

where N, τ_1 and τ_2 can be obtained by expanding the exponentials $e^{-\tau_1 \hat{C}_{31}}$ and $e^{-\tau_2 \hat{C}_{21}}$ and comparing the result with Eq. (4.22). We have

$$
\begin{aligned}
\tau_1 &= e^{i(\alpha_1 + \alpha_2)} \sin\left(\frac{\beta_1}{2}\right) \tan\left(\frac{\beta_2}{2}\right), \\
\tau_2 &= e^{i\alpha_2} \cos\left(\frac{\beta_1}{2}\right) \tan\left(\frac{\beta_2}{2}\right), \\
N &= \cos\left(\frac{\beta_2}{2}\right).
\end{aligned}
\tag{A.2}
$$

Using Eq. (A.1) we can write the so-called symplectic 2-form as[37]

$$\omega = i \sum_{k,l} g_{kl} d\tau_k \wedge d\tau_l^* \,, \tag{A.3}$$

where

$$g_{kl} = \frac{\partial^2 F}{\partial \tau_k \partial \tau_l^*}, \quad F = \ln\left(1 + |\tau_1|^2 + |\tau_2|^2\right). \tag{A.4}$$

Defining the following variables:

$$
\begin{aligned}
\eta_1 &= \tau_1, \quad \eta_2 = \tau_1^*, \quad \eta_3 = \tau_2, \quad \eta_4 = \tau_2^*, \\
\xi_1 &= \alpha_1, \quad \xi_2 = \alpha_2, \quad \xi_3 = \beta_1, \quad \xi_4 = \beta_2,
\end{aligned}
\tag{A.5}
$$

the 2-form can be written as

$$\omega = i \sum_{\alpha, \beta} G_{\alpha\beta} d\eta_\alpha \wedge d\eta_\beta \,, \tag{A.6}$$

where

$$G_{\alpha\beta} = \frac{1}{2} \begin{pmatrix} 0 & g_{11} & 0 & g_{12} \\ -g_{11} & 0 & -g_{21} & 0 \\ 0 & g_{21} & 0 & g_{22} \\ -g_{12} & 0 & -g_{22} & 0 \end{pmatrix}. \tag{A.7}$$

The matrix G is antisymmetric. One can easily work out

$$g_{11} = \frac{1 + |\tau_2|^2}{\left(1 + |\tau_1|^2 + |\tau_2|^2\right)^2} = \cos^4\left(\frac{\beta_2}{2}\right)\left(1 + \cos^2\left(\frac{\beta_1}{2}\right)\tan^2\left(\frac{\beta_2}{2}\right)\right),$$

$$g_{12} = g_{21}^* = -\frac{\tau_1^*\tau_2}{\left(1 + |\tau_1|^2 + |\tau_2|^2\right)^2} = -e^{-i\alpha_1}\sin\left(\frac{\beta_1}{2}\right)\cos\left(\frac{\beta_1}{2}\right)\sin^2\left(\frac{\beta_2}{2}\right)\cos^2\left(\frac{\beta_2}{2}\right),$$

$$g_{22} = \frac{1 + |\tau_1|^2}{\left(1 + |\tau_1|^2 + |\tau_2|^2\right)^2} = \cos^4\left(\frac{\beta_2}{2}\right)\left(1 + \sin^2\left(\frac{\beta_1}{2}\right)\tan^2\left(\frac{\beta_2}{2}\right)\right). \tag{A.8}$$

The Poisson bracket given in [37] as

$$\{f, g\} = -i\sum_{i,j} g^{ij}\left(\frac{\partial f}{\partial \tau_i}\frac{\partial g}{\partial \tau_j^*} - \frac{\partial g}{\partial \tau_i}\frac{\partial f}{\partial \tau_j^*}\right), \tag{A.9}$$

can be written in the new variables as

$$\begin{aligned}
\{f, g\} &= -i\sum_{\alpha,\beta} G^{\alpha\beta}\frac{\partial f}{\partial \eta_\alpha}\frac{\partial g}{\partial \eta_\beta} = -i\sum_{i,j}\frac{\partial f}{\partial \xi_i}\left(\sum_{\alpha,\beta}\frac{\partial \xi_i}{\partial \eta_\alpha}G^{\alpha\beta}\frac{\partial \xi_j}{\partial \eta_\beta}\right)\frac{\partial g}{\partial \xi_j} \\
&= -i\sum_{i,j}\frac{\partial f}{\partial \xi_i}G^{ij}\frac{\partial g}{\partial \xi_j}. \tag{A.10}
\end{aligned}$$

Introducing $U_{i\alpha} = \frac{\partial \xi_i}{\partial \eta_\alpha}$ we have $G^{ij} = U_{i\alpha}G^{\alpha\beta}U_{j\beta} = \left(UGU^T\right)^{ij}$. Note that $G^{\alpha\beta}$ is the inverse of $G_{\alpha\beta}$ and $U_{i\alpha}$ is the inverse of $U^{i\alpha} = \frac{\partial \eta_\alpha}{\partial \xi_i}$. Thus we have

$$U^{i\alpha} = \begin{pmatrix}
-\frac{i}{2}e^{-i(\alpha_1+\alpha_2)}\csc\frac{\beta_1}{2}\cot\frac{\beta_2}{2} & \frac{i}{2}e^{i(\alpha_1+\alpha_2)}\csc\frac{\beta_1}{2}\cot\frac{\beta_2}{2} & \frac{i}{2}e^{-i\alpha_2}\sec\frac{\beta_1}{2}\cot\frac{\beta_2}{2} & \frac{-i}{2}e^{i\alpha_2}\sec\frac{\beta_1}{2}\cot\frac{\beta_2}{2} \\
\\
0 & 0 & \frac{-i}{2}e^{-i\alpha_2}\sec\frac{\beta_1}{2}\cot\frac{\beta_2}{2} & \frac{i}{2}e^{i\alpha_2}\sec\frac{\beta_1}{2}\cot\frac{\beta_2}{2} \\
\\
e^{-i(\alpha_1+\alpha_2)}\cos\frac{\beta_1}{2}\cot\frac{\beta_2}{2} & e^{i(\alpha_1+\alpha_2)}\cos\frac{\beta_1}{2}\cot\frac{\beta_2}{2} & -e^{-i\alpha_2}\sin\frac{\beta_1}{2}\cot\frac{\beta_2}{2} & -e^{i\alpha_2}\sin\frac{\beta_1}{2}\cot\frac{\beta_2}{2} \\
\\
e^{-i(\alpha_1+\alpha_2)}\sin\frac{\beta_1}{2}\cos^2\frac{\beta_2}{2} & e^{i(\alpha_1+\alpha_2)}\sin\frac{\beta_1}{2}\cos^2\frac{\beta_2}{2} & e^{-i\alpha_2}\sin\frac{\beta_1}{2}\cos^2\frac{\beta_2}{2} & e^{i\alpha_2}\sin\frac{\beta_1}{2}\cos^2\frac{\beta_2}{2}
\end{pmatrix} \tag{A.11}$$

and

$$G^{ij} = \begin{pmatrix}
0 & 0 & 4i\csc\beta_1\csc^2\left(\frac{\beta_2}{2}\right) & 0 \\
\\
0 & 0 & -2i\tan\frac{\beta_1}{2}\csc^2\left(\frac{\beta_2}{2}\right) & 4i\csc\beta_2 \\
\\
-4i\csc\beta_1\csc^2\left(\frac{\beta_2}{2}\right) & 2i\tan\frac{\beta_1}{2}\csc^2\left(\frac{\beta_2}{2}\right) & 0 & 0 \\
\\
0 & -4i\csc\beta_2 & 0 & 0
\end{pmatrix}, \tag{A.12}$$

from which we obtain Poisson bracket

$$\begin{aligned}
\{f, g\} &= \frac{4}{\sin\beta_1\sin^2\left(\frac{\beta_2}{2}\right)}\left(\frac{\partial f}{\partial \alpha_1}\frac{\partial g}{\partial \beta_1} - \frac{\partial f}{\partial \beta_1}\frac{\partial g}{\partial \alpha_1}\right) + \frac{2\tan\left(\frac{\beta_1}{2}\right)}{\sin^2\left(\frac{\beta_2}{2}\right)}\left(\frac{\partial f}{\partial \beta_1}\frac{\partial g}{\partial \alpha_2} - \frac{\partial f}{\partial \alpha_2}\frac{\partial g}{\partial \beta_1}\right) \\
&+ \frac{4}{\sin\beta_2}\left(\frac{\partial f}{\partial \alpha_2}\frac{\partial g}{\partial \beta_2} - \frac{\partial f}{\partial \beta_2}\frac{\partial g}{\partial \alpha_2}\right). \tag{A.13}
\end{aligned}$$

B. SOME USEFUL SYMBOLS OF $SU(3)$ OBSERVABLES

In this appendix we obtain the phase space symbol of $\left(\hat{C}_{12} + \hat{C}_{21}\right)^2$ which is needed in chapter 4 and we also obtain the symbol of $\left(\hat{C}_{13} + \hat{C}_{31}\right)^2$ needed in chapter 5.

We have $\left(\hat{C}_{12} + \hat{C}_{21}\right)^2 = \hat{C}_{12}^2 + \hat{C}_{21}^2 + \hat{C}_{12}\hat{C}_{21} + \hat{C}_{21}\hat{C}_{21}$. It is easier to obtain the symbols of each of the terms in the expansion. We start by writing each term in terms of tensors. For $\hat{C}_{12}^2$ and $\hat{C}_{21}^2$ we have

$$
\begin{aligned}
\hat{C}_{12}^2 &= N\,\hat{T}^\lambda_{(2,2),(4,0,2);1},\\
\hat{C}_{21}^2 &= N\,\hat{T}^\lambda_{(2,2),(0,4,2);1},\\
N &= \frac{1}{6\sqrt{5}}\sqrt{(\lambda-1)\,\lambda\,(\lambda+1)\,(\lambda+2)\,(\lambda+3)\,(\lambda+4)},
\end{aligned}
\tag{B.1}
$$

and the other two terms can be written as

$$
\begin{aligned}
\hat{C}_{12}\hat{C}_{21} &= \gamma_0\hat{T}^\lambda_{(0,0);(0,0,0),0} + \gamma_{10}\hat{T}^\lambda_{(1,1);(1,1,1),0} + \gamma_{11}\hat{T}^\lambda_{(1,1);(1,1,1),1} + \gamma_{20}\hat{T}^\lambda_{(2,2);(2,2,2),0} + \gamma_{21}\hat{T}^\lambda_{(2,2);(2,2,2),1},\\
\hat{C}_{21}\hat{C}_{12} &= \eta_0\hat{T}^\lambda_{(0,0);(0,0,0),0} + \eta_{10}\hat{T}^\lambda_{(1,1);(1,1,1),0} + \eta_{11}\hat{T}^\lambda_{(1,1);(1,1,1),1} + \eta_{20}\hat{T}^\lambda_{(2,2);(2,2,2),0} + \eta_{21}\hat{T}^\lambda_{(2,2);(2,2,2),1}.
\end{aligned}
\tag{B.2}
$$

To obtain the factors we need to know how tensors $\hat{T}^\lambda_{(2,2),(2,2,2);I}$, $I = 0, 1, 2$ can be written in terms of states. We have the following expressions for them,

$$
\hat{T}^\lambda_{(2,2);(2,2,2),0} = \frac{N_2}{\sqrt{30}}\sum_{n_1=0}^{\lambda}\sum_{n_2=0}^{\lambda-n_1}\left(3n_1^2 + (n_2 + n_3)(n_2 + n_3 - 1) - 3n_1(2n_2 + 2n_3 + 1)\right)
$$
$$
\times |n_1, n_2, n_3\rangle\langle n_1, n_2, n_3|
\tag{B.3}
$$

$$
\hat{T}^\lambda_{(2,2);(2,2,2),1} = \frac{N_2}{\sqrt{10}}\sum_{n_1=0}^{\lambda}\sum_{n_2=0}^{\lambda-n_1}(4n_1 - n_2 - n_3 + 1)(n_3 - n_2)|n_1, n_2, n_3\rangle\langle n_1, n_2, n_3|
\tag{B.4}
$$

$$
\hat{T}^\lambda_{(2,2);(2,2,2),2} = \frac{N_2}{\sqrt{6}}\sum_{n_1=0}^{\lambda}\sum_{n_2=0}^{\lambda-n_1}\left(n_2^2 - 4n_3n_2 - n_2 + n_3^2 - n_3\right)|n_1, n_2, n_3\rangle\langle n_1, n_2, n_3|
\tag{B.5}
$$

$$
N_2 = \sqrt{\frac{180}{(\lambda-1)\,\lambda\,(\lambda+1)\,(\lambda+2)\,(\lambda+3)\,(\lambda+4)}}
\tag{B.6}
$$

where

$$\gamma_0 = \eta_0 = \frac{\sqrt{2}}{24}\lambda(\lambda+3)\sqrt{(\lambda+1)(\lambda+2)},$$

$$\gamma_{10} = \frac{1}{60}(\lambda+9)\sqrt{\lambda(\lambda+1)(\lambda+2)(\lambda+3)},$$

$$\eta_{10} = \frac{1}{60}(\lambda-6)\sqrt{\lambda(\lambda+1)(\lambda+2)(\lambda+3)},$$

$$\gamma_{11} = -\frac{\sqrt{3}}{60}(\lambda-1)\sqrt{\lambda(\lambda+1)(\lambda+2)(\lambda+3)},$$

$$\eta_{11} = -\frac{\sqrt{3}}{60}(\lambda+4)\sqrt{\lambda(\lambda+1)(\lambda+2)(\lambda+3)},$$

$$\gamma_{20} = \eta_{20} = -\frac{\sqrt{6}}{120}\sqrt{(\lambda-1)\lambda(\lambda+1)(\lambda+2)(\lambda+3)(\lambda+4)},$$

$$\gamma_{21} = \eta_{21} = -\frac{\sqrt{2}}{60}\sqrt{(\lambda-1)\lambda(\lambda+1)(\lambda+2)(\lambda+3)(\lambda+4)}. \tag{B.7}$$

The symbols are then obtained as:

$$W_{\hat{C}_{12}^2} = \frac{1}{4}\sqrt{(\lambda-1)\lambda(\lambda+3)(\lambda+4)}\,e^{-2i\alpha_2}\cos^2\left(\frac{\beta_1}{2}\right)\sin^2(\beta_2), \tag{B.8}$$

$$W_{\hat{C}_{21}^2} = \frac{1}{4}\sqrt{(\lambda-1)\lambda(\lambda+3)(\lambda+4)}\,e^{2i\alpha_2}\cos^2\left(\frac{\beta_1}{2}\right)\sin^2(\beta_2), \tag{B.9}$$

$$\begin{aligned}
W_{\hat{C}_{12}\hat{C}_{21}} = {} & \frac{1}{12}\lambda(\lambda+3) + \frac{1}{60}(\lambda+9)\sqrt{\lambda(\lambda+3)}\,(1+3\cos(\beta_2)) \\
& +\frac{1}{10}(\lambda-1)\sqrt{\lambda(\lambda+3)}\cos(\beta_1)\sin^2\left(\frac{\beta_2}{2}\right) \\
& -\frac{1}{80}\sqrt{(\lambda-1)\lambda(\lambda+3)(\lambda+4)}\,(3+4\cos(\beta_2)+5\cos(2\beta_2)) \\
& +\frac{1}{20}\sqrt{(\lambda-1)\lambda(\lambda+3)(\lambda+4)}\cos\beta_1(3+5\cos\beta_2)\sin^2\left(\frac{\beta_2}{2}\right),
\end{aligned} \tag{B.10}$$

$$\begin{aligned}
W_{\hat{C}_{21}\hat{C}_{12}} = {} & \frac{1}{12}\lambda(\lambda+3) + \frac{1}{60}(\lambda-6)\sqrt{\lambda(\lambda+3)}\,(1+3\cos(\beta_2)) \\
& +\frac{1}{10}(\lambda+4)\sqrt{\lambda(\lambda+3)}\cos(\beta_1)\sin^2\left(\frac{\beta_2}{2}\right) \\
& -\frac{1}{80}\sqrt{(\lambda-1)\lambda(\lambda+3)(\lambda+4)}\,(3+4\cos(\beta_2)+5\cos(2\beta_2)) \\
& +\frac{1}{20}\sqrt{(\lambda-1)\lambda(\lambda+3)(\lambda+4)}\cos\beta_1(3+5\cos\beta_2)\sin^2\left(\frac{\beta_2}{2}\right).
\end{aligned} \tag{B.11}$$

To obtain the phase space symbol of $\left(\hat{C}_{13}+\hat{C}_{31}\right)^2$ we write $\left(\hat{C}_{13}+\hat{C}_{31}\right)^2 = \hat{C}_{13}^2+\hat{C}_{31}^2+\hat{C}_{13}\hat{C}_{31}+$

$\hat{C}_{31}\hat{C}_{13}$ and find the symbol of each term. These terms can be written in terms of tensors as

$$\hat{C}_{13}^2 = N\hat{T}_{(2,2);(4,2,0),1}^\lambda,$$

$$\hat{C}_{31}^2 = N\hat{T}_{(2,2);(0,2,4),1}^\lambda,$$

$$\hat{C}_{13}\hat{C}_{31} = \gamma_0\hat{T}_{(0,0);(0,0,0),0}^\lambda + \gamma_{10}\hat{T}_{(1,1);(1,1,1),0}^\lambda - \gamma_{11}\hat{T}_{(1,1);(1,1,1),1}^\lambda + \gamma_{20}\hat{T}_{(2,2);(2,2,2),0}^\lambda - \gamma_{21}\hat{T}_{(2,2);(2,2,2),1}^\lambda,$$

$$\hat{C}_{31}\hat{C}_{13} = \eta_0\hat{T}_{(0,0);(0,0,0),0}^\lambda + \eta_{10}\hat{T}_{(1,1);(1,1,1),0}^\lambda - \eta_{11}\hat{T}_{(1,1);(1,1,1),1}^\lambda + \eta_{20}\hat{T}_{(2,2);(2,2,2),0}^\lambda - \eta_{21}\hat{T}_{(2,2);(2,2,2),1}^\lambda,$$

$$\text{(B.12)}$$

where the factors γ, η and N are given in Eqs.(B.1) and (B.7). The symbols are then as follows:

$$W_{\hat{C}_{13}^2} = \frac{1}{4}\sqrt{(\lambda-1)\lambda(\lambda+3)(\lambda+4)}\,e^{-2i(\alpha_1+\alpha_2)}\sin^2\left(\frac{\beta_1}{2}\right)\sin^2(\beta_2), \qquad \text{(B.13)}$$

$$W_{\hat{C}_{31}^2} = \frac{1}{4}\sqrt{(\lambda-1)\lambda(\lambda+3)(\lambda+4)}\,e^{2i(\alpha_1+\alpha_2)}\sin^2\left(\frac{\beta_1}{2}\right)\sin^2(\beta_2), \qquad \text{(B.14)}$$

$$\begin{aligned}
W_{\hat{C}_{13}\hat{C}_{31}} = {}& \frac{1}{12}\lambda(\lambda+3) + \frac{1}{60}(\lambda+9)\sqrt{\lambda(\lambda+3)}(1+3\cos(\beta_2)) \\
& -\frac{1}{10}(\lambda-1)\sqrt{\lambda(\lambda+3)}\cos(\beta_1)\sin^2\left(\frac{\beta_2}{2}\right) \\
& -\frac{1}{80}\sqrt{(\lambda-1)\lambda(\lambda+3)(\lambda+4)}(3+4\cos(\beta_2)+54\cos(2\beta_2)) \\
& -\frac{1}{20}\sqrt{(\lambda-1)\lambda(\lambda+3)(\lambda+4)}\cos\beta_1(3+5\cos\beta_2)\sin^2\left(\frac{\beta_2}{2}\right), \qquad \text{(B.15)}
\end{aligned}$$

$$\begin{aligned}
W_{\hat{C}_{31}\hat{C}_{13}} = {}& \frac{1}{12}\lambda(\lambda+3) + \frac{1}{60}(\lambda-6)\sqrt{\lambda(\lambda+3)}(1+3\cos(\beta_2)) \\
& -\frac{1}{10}(\lambda+4)\sqrt{\lambda(\lambda+3)}\cos(\beta_1)\sin^2\left(\frac{\beta_2}{2}\right) \\
& -\frac{1}{80}\sqrt{(\lambda-1)\lambda(\lambda+3)(\lambda+4)}(3+4\cos(\beta_2)+5\cos(2\beta_2)) \\
& -\frac{1}{20}\sqrt{(\lambda-1)\lambda(\lambda+3)(\lambda+4)}\cos\beta_1(3+5\cos\beta_2)\sin^2\left(\frac{\beta_2}{2}\right). \qquad \text{(B.16)}
\end{aligned}$$

C. QUANTUM MECHANICAL TIME EVOLUTION OF THE WIGNER FUNCTION

In this appendix we obtain the quantum mechanical evolution of the $SU(2)$ and $SU(3)$ Wigner function.

C.1 $SU(2)$

Our initial state is the $SU(2)$ coherent state $|\varphi', \theta'\rangle$ which we write as

$$|\varphi', \theta'\rangle = \sum_{m=-j}^{j} D_{m,j}^{j}(\varphi', \theta', 0) |j, m\rangle. \tag{C.1}$$

The time evolution of the initial density operator $\hat{\rho} = |\varphi', \theta'\rangle \langle \varphi', \theta'|$ under the Hamiltonian $\hat{H} = \hat{S}_{z}^{2}$,

$$\hat{\rho}(t) = e^{-iHt} |\varphi', \theta'\rangle \langle \varphi', \theta'| e^{iHt}, \tag{C.2}$$

thus can be written as

$$\hat{\rho}(t) = \sum_{m,m'=-j}^{j} D_{m,j}^{j}(\varphi', \theta', 0) \left(D_{m',j}^{j}(\varphi', \theta', 0)\right)^{*} e^{i\left(m'^2 - m^2\right)t} |j, m\rangle \langle j, m'|. \tag{C.3}$$

The Wigner function of the evolved density operator $\hat{\rho}(t)$ can be written using Eqs. (3.24), (3.25) and (C.3):

$$
\begin{aligned}
W_{\rho}(\varphi, \theta, t) \;=\; & Tr\left(\hat{\rho}(t)\,\hat{w}(\varphi, \theta)\right) \\
\;=\; & \sum_{m,m'=-j}^{j} D_{m,j}^{j}(\varphi', \theta', 0) \left(D_{m',j}^{j}(\varphi', \theta', 0)\right)^{*} e^{i\left(m'^2 - m^2\right)t} \langle j, m'| \Lambda(\varphi, \theta) \hat{P} \Lambda^{-1}(\varphi, \theta) |j, m\rangle,
\end{aligned}
\tag{C.4}
$$

where we write

$$\langle j, m'| \Lambda(\varphi, \theta) \hat{P} \Lambda^{-1}(\varphi, \theta) |j, m\rangle = \sum_{n,n'=-j}^{j} \langle j, m'| \Lambda(\varphi, \theta) |j, n\rangle \langle j, n| \hat{P} |j, n'\rangle \langle j, n'| \Lambda^{-1}(\varphi, \theta) |j, m\rangle. \tag{C.5}$$

Using Eqs. (3.28) and (3.31) we have

$$\hat{P} = \sum_{L=0}^{2j} \sqrt{\frac{2L+1}{2j+1}} T_{L0}^{j} = \sum_{L=0}^{2j} \sqrt{\frac{2L+1}{2j+1}} \sum_{m''=-j}^{j} C_{j,m'';j,-m''}^{L,0}(-1)^{j-m''} |j, m''\rangle \langle j, m''|. \tag{C.6}$$

Thus

$$
\begin{aligned}
W_\rho(\varphi,\theta,t) &= \sum_{m,m'=-j}^{j} D_{m,j}^{j}(\varphi',\theta',0)\left(D_{m',j}^{j}(\varphi',\theta',0)\right)^* e^{i(m'^2-m^2)t} \\
&\times \sum_{m''=-j}^{j} D_{m',m''}^{j}(\varphi,\theta,0)\left(D_{m,m''}^{j}(\varphi,\theta,0)\right)^* \sum_{L=0}^{2j} \sqrt{\frac{2L+1}{2j+1}}(-1)^{j-m''} C_{j,m'';j,-m''}^{L,0},
\end{aligned}
$$

(C.7)

where for the case of the initial state of chapter 3, $\varphi'=0, \theta'=\pi/2$, we can use

$$
D_{m,j}^{j}\left(\varphi'=0,\theta'=\frac{\pi}{2},0\right) = \frac{1}{2^j}\sqrt{\frac{(2j)!}{(j+m)!\,(j-m)!}}.
$$

(C.8)

C.2 $SU(3)$

Now let us calculate the time evolution of the $SU(3)$ Wigner function under the Hamiltonian $\hat{H} = \hat{h}_1^2 - \frac{2\lambda+3}{5}\hat{h}_1$. Our initial state is the $SU(3)$ coherent state $R_{12}(0,\beta'_2,0)|\lambda,0,0\rangle$,

$$
\begin{aligned}
|\psi(0)\rangle &= R_{12}(0,\beta'_2,0)|\lambda,0,0\rangle \\
&= \sum_{p=0}^{\lambda}|\lambda-p,p,0\rangle\langle\lambda-p,p,0|R_{12}(0,\beta'_2,0)|\lambda,0,0\rangle \\
&= \sum_{p=0}^{\lambda} D_{\frac{1}{2}(\lambda-2p),\frac{1}{2}\lambda}^{\frac{1}{2}\lambda}(0,\beta_2',0)|\lambda-p,p,0\rangle,
\end{aligned}
$$

(C.9)

(C.10)

where we can use

$$
D_{M,J}^{J}(\alpha,\beta,\gamma) = \sqrt{\frac{(2J)!}{(J+M)!\,(J-M)!}}\left(\cos\frac{\beta}{2}\right)^{J+M}\left(\sin\frac{\beta}{2}\right)^{J-M} e^{-i(M\alpha+J\gamma)}.
$$

(C.11)

The time-evolved state, $|\psi(t)\rangle = e^{-i\hat{H}t}|\psi(0)\rangle$, is

$$
\begin{aligned}
|\psi(t)\rangle &= \sum_{p=0}^{\lambda} \sqrt{\frac{\lambda!}{(\lambda-p)!p!}}\cos^{\lambda-p}\left(\frac{\beta'_2}{2}\right)\sin^{p}\left(\frac{\beta'_2}{2}\right) e^{-it\left[(2\lambda-3p)^2-\frac{2\lambda+3}{5}(2\lambda-3p)\right]}|\lambda-p,p,0\rangle \\
&= \sum_{p=0}^{\lambda} C_p(t)|\lambda-p,p,0\rangle.
\end{aligned}
$$

(C.12)

Thus the Wigner function of the time-evolved density operator,

$$
\hat{\rho}(t) = \sum_{p,r=0}^{\lambda} C_p(t)C_r^*(t)|\lambda-p,p,0\rangle\langle\lambda-r,r,0|,
$$

(C.13)

is

$$
W_\rho(\omega,t) = \sum_{p,r=0}^{\lambda} C_p(t)C_r^*(t)\langle\lambda-r,r,0|\hat{\Lambda}(\omega)\hat{P}\Lambda^{-1}(\omega)|\lambda-p,p,0\rangle
$$

(C.14)

with $\Lambda(\omega) = R_{23}(\omega_1) R_{12}(\omega_2)$. The operator $\hat{P}$ is

$$\hat{P} = \sum_\sigma \sqrt{\frac{\dim(\sigma,\sigma)}{\dim(\lambda,0)}} \sum_{\mu,\nu} |\lambda-\mu,\mu-\nu,\nu\rangle \langle\lambda-\mu,\mu-\nu,\nu| \tilde{C}^{\lambda(\sigma,\sigma)(\sigma,\sigma,\sigma)0}_{(\lambda-\mu,\mu-\nu,\nu)(\lambda-\mu,\mu-\nu,\nu)} \,. \tag{C.15}$$

Inserting Eq. (C.15) into Eq. (C.14) we obtain $\langle\lambda-r,r,0|\Lambda(\omega)|\lambda-\mu,\mu-\nu,\nu\rangle$, which can be written as

$$\sum_\eta \langle\lambda-r,r,0| R_{23}(\omega_1)|\lambda-r,r-\eta,\eta\rangle \langle\lambda-r,r-\eta,\eta| R_{12}(\omega_2)|\lambda-\mu,\mu-\nu,\nu\rangle \,. \tag{C.16}$$

In terms of $SU(2)$ D-functions we have

$$\langle\lambda-r,r,0| R_{23}(\omega_1)|\lambda-r,r-\eta,\eta\rangle = D^{\frac{1}{2}r}_{\frac{1}{2}r,\frac{1}{2}(r-2\nu)}(\alpha_1,\beta_1,-\alpha_1) \tag{C.17}$$

and

$$\langle\lambda-r,r-\eta,\eta| R_{12}(\omega_2)|\lambda-\mu,\mu-\nu,\nu\rangle = D^{\frac{1}{2}(\lambda-\nu)}_{\frac{1}{2}(\lambda-2r+\nu),\frac{1}{2}(\lambda-2\mu+\nu)}(\alpha_2,\beta_2,-\alpha_2) \,. \tag{C.18}$$

Thus

$$W_\rho(\omega,t) = \sum_{p,r} C_p(t)C_r^*(t) \sum_\sigma \sqrt{\frac{\dim(\sigma,\sigma)}{\dim(\lambda,0)}} \sum_{\mu,\nu} \tilde{C}^{\lambda(\sigma,\sigma)(\sigma,\sigma,\sigma)0}_{(\lambda-\mu,\mu-\nu,\nu)(\lambda-\mu,\mu-\nu,\nu)} D^{\frac{1}{2}r}_{\frac{1}{2}r,\frac{1}{2}(r-2\nu)}(\omega_1) \left(D^{\frac{1}{2}p}_{\frac{1}{2}p,\frac{1}{2}(p-2\nu)}(\omega_1)\right)^*$$

$$\times D^{\frac{1}{2}(\lambda-\nu)}_{\frac{1}{2}(\lambda-2r+\nu),\frac{1}{2}(\lambda-2\mu+\nu)}(\omega_2) \left(D^{\frac{1}{2}(\lambda-\nu)}_{\frac{1}{2}(\lambda-2p+\nu),\frac{1}{2}(\lambda-2\mu+\nu)}(\omega_2)\right)^* \,. \tag{C.19}$$

Finally, one can additionally use the closed form expression

$$D^J_{J,M}(\alpha,\beta,\gamma) = \sqrt{\frac{(2J)!}{(J+M)!(J-M)!}}\left(\cos\frac{\beta}{2}\right)^{J+M}\left(-\sin\frac{\beta}{2}\right)^{J-M} e^{-i(J\alpha+M\gamma)} \,, \tag{C.20}$$

to produce a slightly more explicit form of the final Wigner function.

D. ANALYTICAL CALCULATIONS OF SEMICLASSICAL VARIANCE OF $\hat{K}_\perp$

In this appendix we show a sample calculation of one of the integrals that appears in calculating the variance of $\hat{K}_\perp$ in chapter 5. Specifically here we show how we analytically calculated the following integral

$$
\left\langle \hat{C}_{12} + \hat{C}_{21} \right\rangle = \frac{\dim(\lambda, 0)}{4\pi^2} \int_0^{2\pi} d\alpha_1 \int_0^{2\pi} d\alpha_2 \int_0^\pi d\beta_1 \sin\beta_1
$$
$$
\times \int_0^\pi d\beta_2 \frac{1 - \cos\beta_2}{4} \sin\beta_2 W_{\hat{C}_{12}+\hat{C}_{21}} W_\rho\left(\Omega(t)\right) \tag{D.1}
$$

where

$$
W_{\hat{C}_{12}+\hat{C}_{21}} = \sqrt{\lambda(\lambda+3)} \cos\alpha_2 \cos\left(\frac{\beta_1}{2}\right) \sin\beta_2 \tag{D.2}
$$

and $W_\rho\left(\Omega(t)\right)$ is the time evolved Wigner function given in Eq. (4.64)

$$
W_\rho\left(\Omega(t)\right) = W_{|\lambda,0,0\rangle\langle\lambda,0,0|}\left(\tilde{\Omega}(t)\right) = \sum_{\sigma=0}^\lambda \sqrt{\frac{\dim(\sigma,\sigma)}{\dim(\lambda,0)}} \tilde{C}^{\lambda(\sigma,\sigma)(\sigma,\sigma,\sigma)0}_{\lambda00;\lambda00} D^{(\sigma,\sigma)}_{(\sigma,\sigma,\sigma)0;(\sigma,\sigma,\sigma)0}\left(\tilde{\Omega}(t)\right). \tag{D.3}
$$

The $SU(3)$ D-function, $D^{(\sigma,\sigma)}_{(\sigma,\sigma,\sigma)0;(\sigma,\sigma,\sigma)0}\left(\tilde{\Omega}\right)$, can be written in terms of Legendre polynomials as

$$
D^{(\sigma,\sigma)}_{(\sigma,\sigma,\sigma)0;(\sigma,\sigma,\sigma)0}\left(\tilde{\Omega}\right) = \frac{1}{(\sigma+1)^2} \sum_{p=0}^\sigma (2p+1) P_p\left(\cos\tilde{\beta}_2\right)
$$
$$
= \frac{1}{\left(\cos\tilde{\beta}_2 - 1\right)(\sigma+1)} \left(P_{\sigma+1}\left(\cos\tilde{\beta}_2\right) - P_\sigma\left(\cos\tilde{\beta}_2\right)\right) \tag{D.4}
$$

and the Legendre polynomial $P_p(x)$ is given explicitly by

$$
P_p(x) = \sum_{k=0}^p (-1)^k \binom{p}{k}\binom{-p-1}{k}\left(\frac{1-x}{2}\right)^k. \tag{D.5}
$$

Thus we can write the Wigner function as

$$
W_\rho\left(\tilde{\Omega}(t)\right) = \sum_{\sigma=0}^\lambda \sqrt{\frac{\dim(\sigma,\sigma)}{\dim(\lambda,0)}} \tilde{C}^{\lambda(\sigma,\sigma)(\sigma,\sigma,\sigma)0}_{\lambda00;\lambda00} \frac{1}{(\sigma+1)^2}
$$
$$
\times \sum_{n_1=0}^\sigma \sum_{n_2=0}^{n_1} \sum_{n_3=0}^{n_2} (2n_1+1)\left(\frac{1}{2}\right)^{n_2}\binom{n_1}{n_2}\binom{-n_1-1}{n_2}\binom{n_2}{n_3}(-1)^{n_3}\left(\cos\tilde{\beta}_2\right)^{n_3}, \tag{D.6}
$$

or, more compactly, as

$$W_\rho\left(\tilde{\Omega}(t)\right) = \sum_{q=0}^{\lambda} A_q^\lambda\left(\cos\tilde{\beta}_2\right)^q.$$ (D.7)

As discussed in chapter 4, for $\hat{H}_1 = \hat{h}_1^2 - \frac{2\lambda+3}{5}\hat{h}_1$ we have

$$
\begin{aligned}
\cos\tilde{\beta}_2 &= -\sin^2\left(\tfrac{1}{2}\beta_2{}'\right)\sin^2\left(\tfrac{1}{2}\beta_1\right) + \cos\beta_2\left(\cos^2\left(\tfrac{1}{2}\beta_2{}'\right) - \cos^2\left(\tfrac{1}{2}\beta_1\right)\sin^2\left(\tfrac{1}{2}\beta_2{}'\right)\right) \\
&\quad + \left(\cos\left(\tfrac{1}{2}\beta_1\right)\sin\beta_2{}'\sin\beta_2\right)\cos\left(\alpha_2(t)\right) \\
&= C + B\cos\left(\alpha_2(t)\right),
\end{aligned}
$$ (D.8)

where

$$
\begin{aligned}
\alpha_2(t) &= \alpha_2 - \frac{9}{5}\sqrt{(\lambda-1)(\lambda+4)}\,(1+5\cos\beta_2)\,t \\
&= \alpha_2 + At + \bar{A}t\cos\beta_2 = \alpha_2 + R.
\end{aligned}
$$ (D.9)

Writing

$$\left(\cos\tilde{\beta}_2\right)^q = \sum_{n_4=0}^{q}\binom{q}{n_4}C^{q-n_4}B^{n_4}\cos^{n_4}\left(\alpha_2+R\right),$$ (D.10)

we get

$$
\begin{aligned}
\left\langle \hat{C}_{12} + \hat{C}_{21}\right\rangle &= \frac{\dim(\lambda,0)}{4\pi^2}2\pi\sqrt{\lambda(\lambda+3)} \\
&\quad \times \sum_{q=0}^{\lambda} A_q^\lambda \int d\beta_1 \int d\beta_2 \cos\left(\tfrac{1}{2}\beta_1\right)\sin\beta_2\sin\beta_1\cos\left(\tfrac{1}{2}\beta_2\right)\sin^3\left(\tfrac{1}{2}\beta_2\right) \\
&\quad \times \sum_{n_4=0}^{(q-1)/2}\binom{q}{2n_4+1}C^{q-(2n_4+1)}B^{2n_4+1}\int_0^{2\pi}d\alpha_2\cos^{2n_4+1}\left(\alpha_2+R\right)\cos\alpha_2,
\end{aligned}
$$ (D.11)

where the integration over α_1 yields 2π since there is no α_1 dependence in the integrand.

Writing $\cos\alpha_2 = \cos\left(\alpha_2 + R - R\right)$ the integral on α_2 turns out to be

$$\cos R\int_0^{2\pi}d\alpha_2\cos^{2n_4+2}\left(\alpha_2+R\right) = \frac{(2n_4+1)!!2\pi}{(n_4+1)!2^{n_4+1}}\cos R.$$ (D.12)

Using trigonometric identities we can write

$$
\begin{aligned}
C &= \tfrac{1}{2}\sin^2\left(\tfrac{1}{2}\beta_2{}'\right) + \cos\beta_2\left(\cos^2\left(\tfrac{1}{2}\beta_2{}'\right) - \tfrac{1}{2}\sin^2\left(\tfrac{1}{2}\beta_2{}'\right)\right) + \left(\tfrac{1}{2}\sin^2\left(\tfrac{1}{2}\beta_2{}'\right)(1-\cos\beta_2)\right)\cos\beta_1 \\
&= X + Y\cos\beta_1.
\end{aligned}
$$ (D.13)

Thus

$$C^{q-(2n_4+1)} = \sum_{n_5=0}^{q-2n_4-1}\binom{q-2n_4-1}{n_5}Y^{n_5}\cos^{n_5}(\beta_1)X^{q-2n_4-1-n_5}$$ (D.14)

and the β_1 integral in fact is

$$\int_0^\pi d\beta_1\cos^{2n_4+2}\left(\frac{\beta_1}{2}\right)\cos^{n_5}(\beta_1)\sin(\beta_1) = \left(\tfrac{1}{2}\right)^{n_4+1}\sum_{n_6=0}^{n_4+1}\binom{n_4+1}{n_6}\frac{(-1)^{n_5+n_6}+1}{n_5+n_6+1},$$ (D.15)

Hence

$$
\begin{aligned}
\left\langle \hat{C}_{12} + \hat{C}_{21} \right\rangle &= \sqrt{\lambda(\lambda+3)}\,\frac{\dim(\lambda,0)}{4\pi^2}\,2\pi \\
&\quad \times \sum_{q=0}^{\lambda} A_q^\lambda \int_0^\pi d\beta_2 \sin(\beta_2) \cos\left(\frac{1}{2}\beta_2\right) \sin^3\left(\frac{1}{2}\beta_2\right) \cos(R) \\
&\quad \times \sum_{n_4=0}^{(q-1)/2} \binom{q}{2n_4+1} \sin^{2n_4+1}(\beta'_2)\left(\frac{1}{2}\right)^{n_4+1}\frac{(2n_4+1)!!2\pi}{(n_4+1)!2^{n_4+1}} \sum_{n_5=0}^{q-2n_4-1}\binom{q-2n_4-1}{n_5} \\
&\quad \times Y^{n_5} X^{q-2n_4-1-n_5}\left(\frac{1}{2}\right)^{n_5}\sin^{2n_5}\left(\frac{1}{2}\beta'_2\right)\frac{1}{4}\sum_{n_6=0}^{n_4+1}\binom{n_4+1}{n_6}\frac{(-1)^{n_5+n_6}+1}{n_5+n_6+1}
\end{aligned}
\tag{D.16}
$$

The β_2 integral is then

$$
\frac{1}{4}\int_{-1}^{1} d\xi\left(1-\xi^2\right)^{n_4+1}(1-\xi)^{n_5+1}(F+G\xi)^{q-2n_4-n_5-1}\cos\left(At+\bar{A}t\xi\right),
\tag{D.17}
$$

where we have used $\xi = \cos\beta_2$. We now expand,

$$
(F+G\xi)^{q-2n_4-n_5-1} = \sum_{n_7=0}^{q-2n_4-n_5-1}\binom{q-2n_4-n_5-1}{n_7}G^{n_7}F^{q-2n_4-n_5-1-n_7}\xi^{n_7},
\tag{D.18}
$$

$$
\left(1-\xi^2\right)^{n_4+1} = \sum_{n_8=0}^{n_4+1}\binom{n_4+1}{n_8}\xi^{2n_8}(-1)^{n_8},
\tag{D.19}
$$

$$
(1-\xi)^{n_5+1} = \sum_{n_9=0}^{n_5+1}\binom{n_5+1}{n_9}\xi^{n_9}(-1)^{n_9},
\tag{D.20}
$$

The integral on ξ is then

$$
\cos(At)\underbrace{\int_{-1}^{1}d\xi\cos\left(\bar{A}t\xi\right)\xi^{2n_8+n_9+n_7}}_{\kappa_c} - \sin(At)\underbrace{\int_{-1}^{1}d\xi\sin\left(\bar{A}t\xi\right)\xi^{2n_8+n_9+n_7}}_{\kappa_s},
\tag{D.21}
$$

where

$$
\kappa_c = (2n_8+n_9+n_7)!\sum_{n_{10}=0}^{2n_8+n_9+n_7}\frac{\sin\left(\bar{A}t+\frac{1}{2}n_{10}\pi\right)+(-1)^{2n_8+n_9+n_7-n_{10}}\sin\left(\bar{A}t-\frac{1}{2}n_{10}\pi\right)}{(2n_8+n_9+n_7-n_{10})!\left(\bar{A}t\right)^{n_{10}+1}}
\tag{D.22}
$$

and

$$
\kappa_s = -(2n_8+n_9+n_7)!\sum_{n_{10}=0}^{2n_8+n_9+n_7}\frac{\sin\left(\bar{A}t+\frac{1}{2}n_{10}\pi\right)-(-1)^{2n_8+n_9+n_7-n_{10}}\cos\left(\bar{A}t-\frac{1}{2}n_{10}\pi\right)}{(2n_8+n_9+n_7-n_{10})!\left(\bar{A}t\right)^{n_{10}+1}}.
\tag{D.23}
$$

Finally we obtain

$$
\begin{aligned}
\left\langle \hat{C}_{12} + \hat{C}_{21} \right\rangle \;=\;\; & \sqrt{\lambda(\lambda+3)}\, \frac{\dim(\lambda,0)}{4\pi^2}\, 2\pi \\[2mm]
& \times \sum_{q=0}^{\lambda} A_q^\lambda \sum_{n_4=0}^{(q-1)/2} \begin{pmatrix} q \\ 2n_4+1 \end{pmatrix} \sin^{2n_4+1}(\beta'_2)\left(\tfrac{1}{2}\right)^{n_4+1} \frac{(2n_4+1)!!\,2\pi}{(n_4+1)!\,2^{n_4+1}} \\[2mm]
& \times \sum_{n_5=0}^{q-2n_4-1} \begin{pmatrix} q-2n_4-1 \\ n_5 \end{pmatrix}\left(\tfrac{1}{2}\right)^{n_5}\sin^{2n_5}\left(\tfrac{1}{2}\beta'_2\right)\frac{1}{4}\sum_{n_6=0}^{n_4+1} \begin{pmatrix} n_4+1 \\ n_6 \end{pmatrix}\frac{(-1)^{n_5+n_6+1}-1}{n_5+n_6+1} \\[2mm]
& \times \sum_{n_7=0}^{q-2n_4-n_5-1} \begin{pmatrix} q-2n_4-n_5-1 \\ n_7 \end{pmatrix} G^{n_7} F^{q-2n_4-n_5-1-n_7}\sum_{n_8=0}^{n_4+1}\begin{pmatrix} n_4+1 \\ n_8 \end{pmatrix}(-1)^{n_8} \\[2mm]
& \times \sum_{n_9=0}^{n_5+1}\begin{pmatrix} n_5+1 \\ n_9 \end{pmatrix}(-1)^{n_9}\left(\cos(At)\,\kappa_c - \sin(At)\,\kappa_s\right)\,. \qquad\text{(D.24)}
\end{aligned}
$$

BIBLIOGRAPHY

[1] J. E. Moyal, "Quantum mechanics as a statistical theory", Proc. Camb. Phil. Soc. **45**, 99 (1949).

[2] H. Weyl, "Quantenmechanik und Gruppentheorie", Z. Phys. **46**, 1 (1927).

[3] E. Wigner, "On the quantum correction for thermodynamic equilibrium", Phys. Rev. **40**, 749 (1932).

[4] D. Leibfried, D. M. Meekhof, B. E. King, C. Monroe, W. M. Itano and D. J. Wineland, "Experimental determination of the motional quantum state of a trapped atom", Phys. Rev. Lett. **77**, 4281 (1996).

[5] A. Royer, "Wigner function as the expectation value of a parity operator", Phys. Rev. A **15**, 449 (1977).

[6] E. Schrödinger, " The constant crossover of micro-to macro-mechanics", Naturwissenschaften **14**, 664 (1926).

[7] R. J. Glauber, "Coherent and incoherent states of the radiation field", Phys. Rev. **131**, 2766 (1963).

[8] J. Maa, X. Wanga, C. P. Suna and F. Nori, "Quantum spin squeezing" ,Physics Reports **509**, 89 (2011).

[9] M. Kitagawa, Y. Yamamoto, "Number-phase minimum-uncertainty state with reduced number uncertainty in a Kerr nonlinear interferometer",Phys. Rev. A **34**, 3974 (1986).

[10] E. S. Polzik, J. Carri, and H. J. Kimble, "Spectroscopy with squeezed light", Phys. Rev. Lett. **68**, 3020 (1992).

[11] M. Xiao, L-A Wu and H. J. Kimble, "Precision measurement beyond the shot-noise limit", Phys. Rev. Lett. **59**, 278 (1987).

[12] C. M. Caves, "Quantum-mechanical noise in an interferometer", Phys. Rev. D **23**, 1693 (1981).

[13] Y. Yamamoto, H. A. Haus, "Preparation, measurement and information capacity of optical quantum states", Rev. Mod. Phys. **58**, 1001 (1986).

[14] K. Goda, O. Miyakawa, E. E. Mikhailov, S. Saraf, R. Adhikari, K. McKenzie, R. Ward, S. Vass, A. J. Weinstein and N. Mavalvala, "A quantum-enhanced prototype gravitational-wave detector", Nature Phys. **4**, 472 (2008).

[15] W. P. Schleich, "Quantum Optics in Phase Space", Wiley-VCH, (2001).

[16] P. D. Drummond and J. F. Corney, "Quantum noise in optical fibers. I. Stochastic equations", J. Opt. Soc. Am. B **18**, 139 (2001).

[17] G. Drobny, A. Bandilla and I. Jex, "Quantum description of nonlinearly interacting oscillators via classical trajectories", Phys. Rev. A **55**, 78 (1997).

[18] D. Dragoman, "I: The Wigner Distribution Function in Optics and Optoelectronics", Progress in Optics, **37**, 1 (1997).

[19] D. J. Tannor, "Introduction to Quantum Mechanics: A Time-Dependent Perspective", University Science Books (2007).

[20] M. Testorf, B. Hennelly, J. Ojeda-Castaneda, "Phase-Space Optics: Fundamentals and Applications", McGraw-Hill Professional (2009).

[21] M. A. Alonso, "Wigner functions in optics: describing beams as ray bundles and pulses as particle ensemblesb", Advances in Optics and Photonics **3**, 272 (2011).

[22] D. Dragoman, "Applications of the Wigner Distribution Function in Signal Processing", EURASIP Journal on Applied Signal Processing **10**, 1520 (2005).

[23] L. Cohen, "Time-Frequency Distributions-A Review", Proceedings of the IEEE, **77**(7), 941 (1989).

[24] W Martin and P Flandrin, "Wigner-Ville Spectral Analysis of Nonstationary Processes", IEEE Transactions on Acoustic, Speech and Signal Processing, **ASSP-33**(6), 1461 (1985).

[25] D. Rainton and S. J. Young, "Time-frequency spectral estimation of speech", Computer Speech and Language **6**, 15 (1992).

[26] R. A. Earnshaw, C. Lei, J. Li, S. Mugassabi and A. Vourdas, "Large-scale data analysis using the Wigner function", Physica A **391**, 2401 (2012).

[27] M. A. Alonso, G. S. Pogosyan and K. B. Wolf, "Wigner functions for curved spaces. I. On hyperboloids", J. Math. Phys. **43**, 5857 (2002).

[28] M. A. Alonso, G. S. Pogosyan and K. B. Wolf, "Wigner functions for curved spaces. II. On spheres", J. Math. Phys. **44**, 1472 (2003).

[29] H-W Lee, "Theory and application of the quantum phase-space distribution functions", Physics Reports **259**, 147 (1995).

[30] M. Hillery, R. F. O'Connell, M. O. Scully and E. P. Wigner, "Distribution functions in physics: fundamentals", Physics Reports, **106**, 121 (1984).

[31] Y. S. Kim and M. E. Noz "Phase space picture of quantum mechanics: group theoretical approach", World Scientific (1991).

[32] C. Zachos, D. Fairlie and T. Curtright, "Quantum mechanics in phase space: an overview with selected papers", World Scientific (2005).

[33] A. B. Klimov, H. Tavakoli Dinani, Z. E. D. Medendrop and H. de Guise, "Qutrit squeezing via semiclassical evolution", New J. Phys. **13**, 113033 (2011).

[34] A. B. Klimov and H. de Guise, "General approach to $SU(n)$ quasi-distribution functions", J. Phys. A. **43**, 402001 (2010).

[35] M. Kitagawa and M. Ueda, "Squeezed spin states", Phys. Rev. A **47**, 5138 (1993).

[36] A. M. Perelomov, "Coherent states for arbitrary Lie group", Commun. Math. Phys. **26**, 222 (1972).

[37] W. M. Zhang, D. H. Feng, R. Gilmore, "Coherent states: theory and some applications", Rev. Mod. Phys. **62**, 867 (1990).

[38] E. Onofri, " A note on coherent state representations of Lie groups", J. Math. Phys. **16**, 1087 (1975).

[39] M. Nakahara, "Geometry, Topology and Physics", IOP Publishing, 2nd Edition (2003).

[40] R. L. Stratonovich, "On distributions in representation space", Zh. Eksp. Teor. Fiz. **31**, 1012 (1956); R. L. Stratonovich, "A gauge invariant analog of the Wigner distribution", Sov. Phys.JETP **31**, 1012 (1956).

[41] J. C. Varilly and J. M. Gracia-Bondia, "The moyal representation for spin", Ann. Phys. (N.Y.) **190**, 107 (1989).

[42] K. B. Wolf and G. Krtzsch, "Geometry and dynamics of squeezing in finite systems", J. Opt. Soc. Am. A **24**, 2871 (2007).

[43] S. M. Chumakov, A. B. Klimov, and K. B. Wolf, "On the connection of two Wigner functions for spin systems", Phys. Rev. A **61**, 034101 (2000).

[44] J. J. Sakurai and J. Napolitano "Modern Quantum Mechanics", Addison Wesley, 2nd Edition (2010).

[45] F. T. Arecchi, E. Courtens, R. Gilmore and H. Thomas, "Atomic coherent states in quantum optics", Phys. Rev. A **6**, 2211 (1972).

[46] D. A. Varshalovich, A. N. Moskalev and V. K. Khersonskii, "Quantum Theory of Angular Momentum", World Scientific, (1988).

[47] A. B. Klimov and S. M. Chumakov, "On the $SU(2)$ Wigner function dynamics", Revista Mexicana de Fisica, **48**(4), 317 (2002).

[48] G. S. Agarwal, R. R. Puri and R. P. Singh, "Atomic Schrdinger cat states", Phys. Rev. A **56**, 2249 (1997).

[49] S. M. Chumakov, A. Frank and K. B. Wolf, "Finite Kerr medium: macroscopic quantum superposition states and Wigner functions on the sphere", Phy. Rev. A **60**, 1817 (1999).

[50] A. B. Klimov and P. Espinoza, "Moyal-like form of the star product for generalized $SU(2)$ Stratonovich-Weyl symbols", J. Phys. A **35**, 8435 (2002).

[51] H. de Guise, "Boson realizations of $su(n)$ algebras", private publication.

[52] D. J. Rowe, B. C. Sanders and H. de Guise, " Representations of the Weyl group and Wigner functions for $SU(3)$", J. Math. Phys. **40**, 3604 (1999).

[53] M. S. M. Wesslen, "Tensor product decompositions for $su(3)$ of an irreducible representation with itself and with its conjugate", J. Phys.: Conf. Ser. **175**, 01201, (2009).

[54] J. Sherson, B. Julsgaard and E. S. Polzik, "Deterministic atom light quantum interface", Adv. Atom. Mol. Opt. Phys. **54**, 81 (2006).

[55] A. Sorensen, L-M. Duan , J. I. Cirac and P. Zoller, "Many-particle entanglement with BoseEinstein condensates", Nature **409**, 63K (2001).

[56] A. B. Klimov and P. Espinoza, "Classical evolution of quantum fluctuations in spin-like systems: squeezing and entanglement", J. Opt. B: Quantum Semiclass. Opt. **7**, 183 (2005).

[57] M. F. Riedel, P. Boehi, Y. Li, T. W. Haensch, A. Sinatra and P. Treutlein, "Atom-chip-based generation of entanglement for quantum metrology", Nature **464** 1170 (2010).

[58] G. I. Mias, N. R. Cooper, and S. M. Girvin, "Quantum noise, scaling, and domain formation in a spinor Bose-Einstein condensate", Phys. Rev. A **77**, 023616 (2008).

[59] O. E. Mustecaphoglu, M. Zhang, and L. You, "Spin squeezing and entanglement in spinor condensates", Phys. Rev. A **66**, 033611 (2002).

[60] J. D. Sau, S. R. Leslie, M. L. Cohen and D. M. Stamper-Kurn, "Spin squeezing of high-spin, spatially extended quantum fields", New J. Phys. **12**, 085011 (2010).

[61] G. Vitagliano, P. Hyllus, I. L. Egusquiza and G. Toth, "Spin squeezing inequalities for arbitrary spin", Phys. Rev. Lett. **107**, 240502 (2011).

[62] C. D. Hamley, C. S. Gerving, T. M. Hoang, E. M. Bookjans and M. S. Chapman, "Spin-nematic squeezed vacuum in a quantum gas", Nature Phys. **8**, 305 (2012).

[63] A. B. Klimov, H. Tavakoli Dinani and H. de Guise, "Semiclassical approach to squeezing-like transformations in quantum systems with higher symmetries", in preperation.

where $(\varphi(s), t(s))$ is the characteristic. By the chain rule we have

$$\frac{dW_\rho}{ds} = \frac{\partial W_\rho}{\partial \varphi}\frac{d\varphi}{ds} + \frac{\partial W_\rho}{\partial t}\frac{dt}{ds}. \qquad (3.56)$$

Now if we set $dt/ds = 1, d\varphi/ds = 1$ we obtain $\partial W_\rho/\partial t + \partial W_\rho/\partial \varphi$ which, according to Eq. (3.54), equals to zero. Thus, along the characteristic the original partial differential equation becomes the ordinary differential equation $dW_\rho/ds = F\left(W_\rho, \varphi(s), t(s)\right) = 0$. That is to say: along the characteristics, the solution is constant. Therefore if we set $t(0) = 0$ we have $t = s$ and $\varphi(t) = t + \varphi(0)$. This means that if $W_\rho(0) = f(\varphi(0))$ then $W_\rho(\varphi(t), t) = f(\varphi - t)$. In other words the evolved Wigner function is obtained by replacing φ with $\varphi - t$. This corresponds to a rotation of Wigner function around $\hat{z}$ axis as illustrated in Fig. 3.1.

To check the validity of our solution one can compare, for example, the variance (as a function of time) of the observable $\hat{S}_x$,

$$(\Delta S_x)^2 = \langle S_x^2 \rangle - \langle S_x \rangle^2, \qquad (3.57)$$

calculated using the usual quantum mechanical evolution

$$\langle \hat{S}_x \rangle = \langle 0, \frac{\pi}{2}|e^{i\hat{H}t}\hat{S}_x e^{-i\hat{H}t}|0, \frac{\pi}{2}\rangle, \qquad (3.58)$$

and calculated using the phase space formulation,

$$\langle \hat{S}_x \rangle = \frac{2j+1}{4\pi}\int_0^\pi \sin\theta d\theta \int_0^{2\pi} d\varphi W_{S_x}(\varphi, \theta) W_\rho(\varphi - t, \theta). \qquad (3.59)$$

This is done on the left of Fig. 3.2. Since the classical evolution in phase space is exact for linear Hamiltonians, both semiclassical and quantum mechanical evolutions give the same result: the two curves on the left of Fig. 3.2 cannot be distinguished.
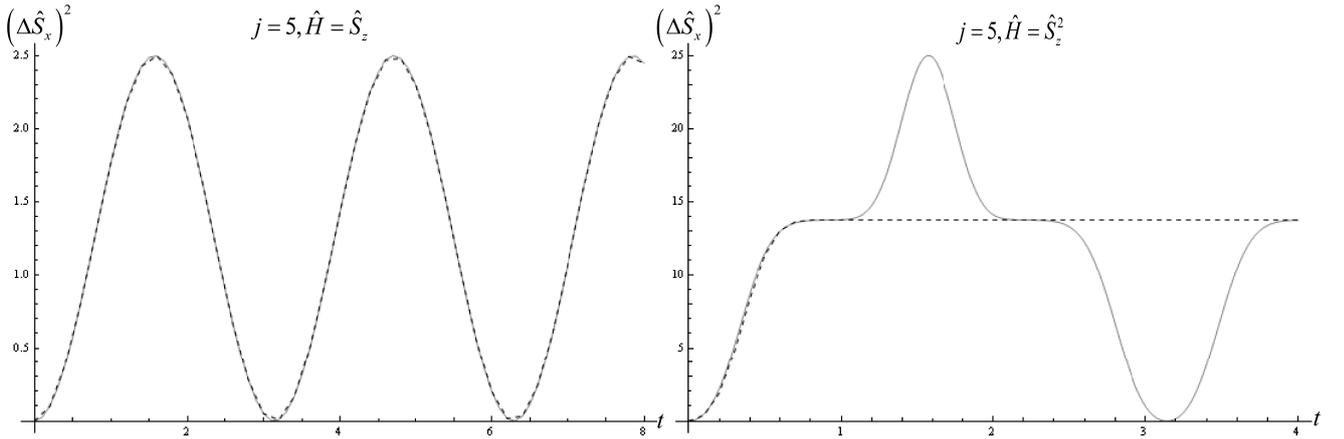

Fig. 3.2: Time evolution of the variance of $\hat{S}_x$, $\left(\Delta\hat{S}_x\right)^2$, calculated semiclassically using Eq. (3.59) (dashed line) and quantum mechanically using Eq. (3.58) (solid line) for $j = 5$. Left plot is the time evolution under linear Hamiltonian $\hat{H} = \hat{S}_z$ and right plot is the time evolution under nonlinear Hamiltonian $\hat{H} = \hat{S}_z^2$
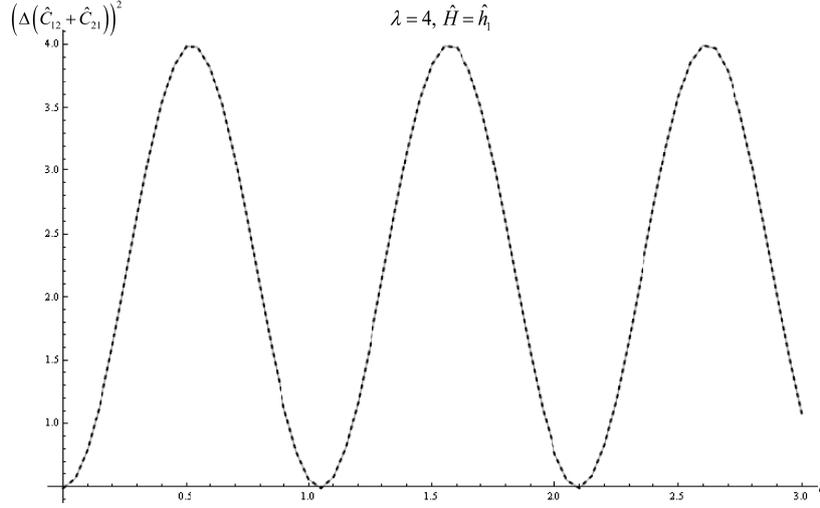
Fig. 4.4: The time evolution of the variance of $\hat{C}_{12} + \hat{C}_{21}$ calculated using phase space method, Eq. (4.69) (dashed line) and Hilbert space quantum mechanical method, (4.71) (solid line) for $\lambda = 4$. Since we haven't used any approximation in the phase space calculations both methods give the same result.

and is obtained by substituting α_2 with $\alpha_2(t) = \alpha_2 - 3t$ in Eq. (4.67).

In Fig 4.3 slices of the Wigner function are plotted for $\lambda = 20$ at $t = 0$, $t = 0.35$ and $t = 0.7$. The figure shows the projection of the Wigner functions in the (α_2, β_2) plane, with slices taken at $(\alpha_1 = 0, \beta_1 = 0)$. It is clear from figure that Wigner function is just translated without any deformation.

Knowing the time-evolution of the Wigner function, we can calculate the time evolution of the expectation value of an operator $\hat{X}$ by

$$\langle \hat{X}(t) \rangle = \frac{(\lambda + 1)(\lambda + 2)}{8\pi^2} \int d\Omega W_X(\Omega) W_\rho(\Omega(t)), \qquad (4.69)$$

where

$$\int d\Omega = \int_0^{2\pi} d\alpha_1 \int_0^{2\pi} d\alpha_2 \int_0^{\pi} d\beta_1 \sin\beta_1 \int_0^{\pi} d\beta_2 \sin\beta_2 \left(\frac{1 - \cos\beta_2}{4}\right). \qquad (4.70)$$

This will be compared to the expectation value computed from the quantum mechanical evolution:

$$\langle \hat{X}(t) \rangle = \langle \lambda, 0, 0 | \Lambda^\dagger(\Omega') e^{i\hat{H}t} \hat{X} e^{-i\hat{H}t} \Lambda(\Omega') | \lambda, 0, 0 \rangle. \qquad (4.71)$$

Fig. 4.4 shows the variance of $\hat{X}$, $\left(\Delta\hat{X}\right)^2 = \langle \hat{X}^2 \rangle - \langle \hat{X} \rangle^2$, for $\hat{X} = \hat{C}_{12} + \hat{C}_{21}$. The dashed line has been plotted using Eq. (4.69) and the solid line has been plotted using Eq. (4.71); as expected both methods give the same result. For calculating the variance by using Eq. (4.69) we need the phase space symbol of $\hat{C}_{12} + \hat{C}_{21}$ which is Eq. (4.39) plus its complex conjugate. We also need the symbol of $\left(\hat{C}_{12} + \hat{C}_{21}\right)^2$ given in Eqs. (B.8) to (B.11).

4.3.2   Nonlinear dynamics

Now let us consider the evolution generated by a simple non-linear Hamiltonian like $\hat{h}_1^2$. From Eq. (4.44), we see that $\hat{h}_1^2$ decomposes into a sum of tensors, including a tensor in the $(1, 1)$ representation, and a constant term in the $(0, 0)$ representation. The constant term can be safely
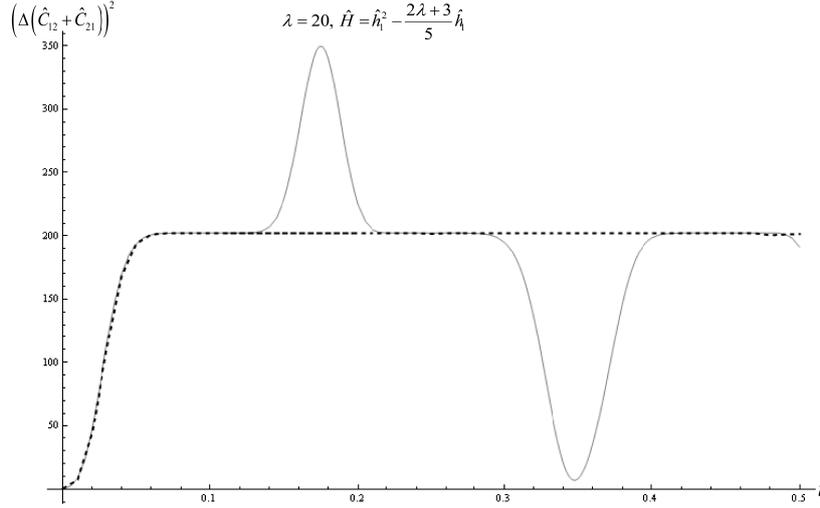
Fig. 4.5: Time evolution of the variance of $\hat{C}_{12} + \hat{C}_{21}$ under the Hamiltonian $H = \hat{h}_1^2 - \frac{2\lambda+3}{5}\hat{h}_1$ plotted using semiclassical method using Eq. (4.69) (dashed line) and quantum mechanical method using (4.71) (solid line) for $\lambda = 20$.

ignored as it plays no role in the evolution (its bracket with any other function is zero). The part proportional to $(1,1)$ is in fact a multiple of the generator $\hat{h}_1$. As we have just seen, the evolution generated by $\hat{h}_1$ simply produces a rigid displacement of the Wigner function. The new effects arise out of the $(2,2)$ term in $\hat{h}_1^2$. We can highlight this by removing the linear terms and look instead at the Hamitonian $\hat{H} = \hat{h}_1^2 - \frac{2\lambda+3}{5}\hat{h}_1$, which produces no rigid displacement of the distribution but will generate the same deformation as $\hat{h}_1^2$. The symbol for this Hamiltonian is

$$W_H = \frac{1}{2}\lambda(\lambda+3) + \frac{9}{40}\sqrt{(\lambda-1)\lambda(\lambda+3)(\lambda+4)}\,(3 + 4\cos(\beta_2) + 5\cos(2\beta_2)) \,. \tag{4.72}$$

Using Eq. (4.59) and ignoring the quantum correction term we obtain

$$\partial_t W_\rho = \frac{1}{2\sqrt{\lambda(\lambda+3)}}\{W_H, W_\rho\} = \frac{9}{5}\sqrt{(\lambda-1)(\lambda+4)}\,(1 + 5\cos(\beta_2))\frac{\partial W_\rho}{\partial\alpha_2} \,, \tag{4.73}$$

with solution

$$\alpha_2(t) = \alpha_2 - \frac{9}{5}\sqrt{(\lambda-1)(\lambda+4)}\,(1 + 5\cos(\beta_2))\,t \,. \tag{4.74}$$

Here again we choose our initial state to be a coherent state located above the minimum of the symbol of the Hamiltonian. W_H is minimized by $\alpha_1' = \alpha_2' = \beta_1' = 0$ and $\beta_2' = \arccos(-1/5)$. This set of angles leads to an expression for $\cos\left(\tilde{\beta}_2\right)$ given by

$$\cos\left(\tilde{\beta}_2\right) = -1 + 2\cos^2\left(\tfrac{1}{2}\beta_2'\right)\cos^2\left(\tfrac{1}{2}\beta_2\right) + 2\cos^2\left(\tfrac{1}{2}\beta_1\right)\sin^2\left(\tfrac{1}{2}\beta_2\right)\sin^2\left(\tfrac{1}{2}\beta_2'\right)$$
$$+ \cos(\alpha_2)\cos\left(\tfrac{1}{2}\beta_1\right)\sin(\beta_2)\sin(\beta_2') \,. \tag{4.75}$$

By substituting this into Eq. (4.66) we get the initial Wigner function and by replacing α_2 with $\alpha_2(t)$ given in Eq. (4.74), we obtain the time-evolved Wigner function.

We can now compare the quantum mechanical evolution and the truncated semiclassical evolution of the variance of an observable as a function of time. The variance of $\hat{C}_{12} + \hat{C}_{21}$
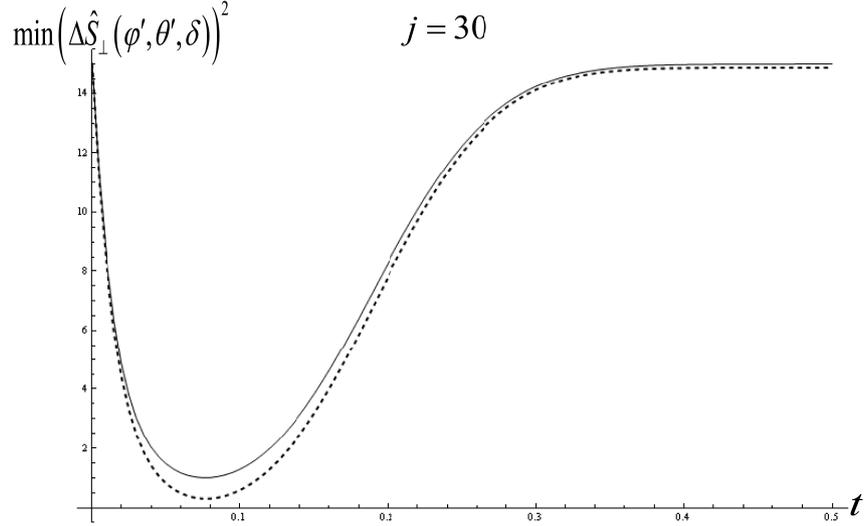
$$\min\left(\Delta\hat{S}_\perp\left(\varphi',\theta',\delta\right)\right)^2 \qquad j=30$$

Fig. 5.3: The time evolution of the minimum of $(\Delta\hat{S}_\perp(\varphi',\theta',\delta))^2$ at $\varphi' = 0$ and $\theta' = \pi/2$ for $j = 30$. The solid line is plotted using quantum mechanical calculations and the dashed line is plotted using the approximate form of the Wigner function in Eq. (5.7).

The log-log graph on the left side of Fig. (5.4) shows that the time location of the minimum of $(\Delta\hat{S}_\perp(\varphi' = 0, \theta' = \pi/2, \delta))^2$ scales as $t_{min} \approx j^{-0.65}$ and the log-log graph on the right side of the Fig. (5.4) shows that the minimum of $(\Delta\hat{S}_\perp(\varphi' = 0, \theta' = \pi/2, \delta))^2$ scales like $j^{+0.35}$. This scaling behavior will be compared with the similar behaviors in $SU(3)$ case.
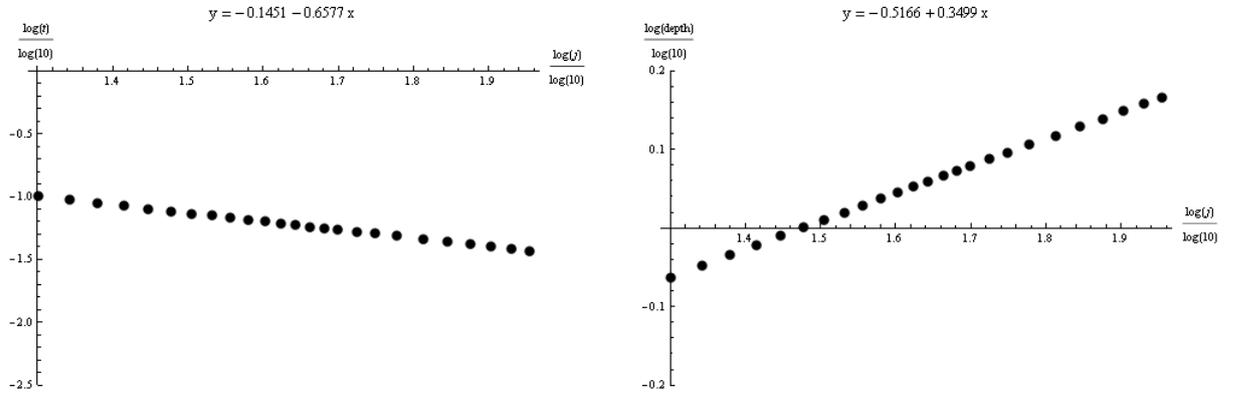

Fig. 5.4: log-log plots of the time location of the minimum of the $SU(2)$ squeezing versus j (left) and the minimum versus j

5.1.2   Experimental implementation

An example of a spin squeezing experiment using condensates of ^{87}Rb atoms has been reported in [57]. The hyperfine states $|+\rangle \equiv |f = 2, m_f = 1\rangle$ and $|-\rangle \equiv |f = 1, m_f = -1\rangle$ of ^{87}Rb form a two level system. The Hamiltonian of the interaction of these levels with a microwave radiation can be expressed in terms of spin operators as

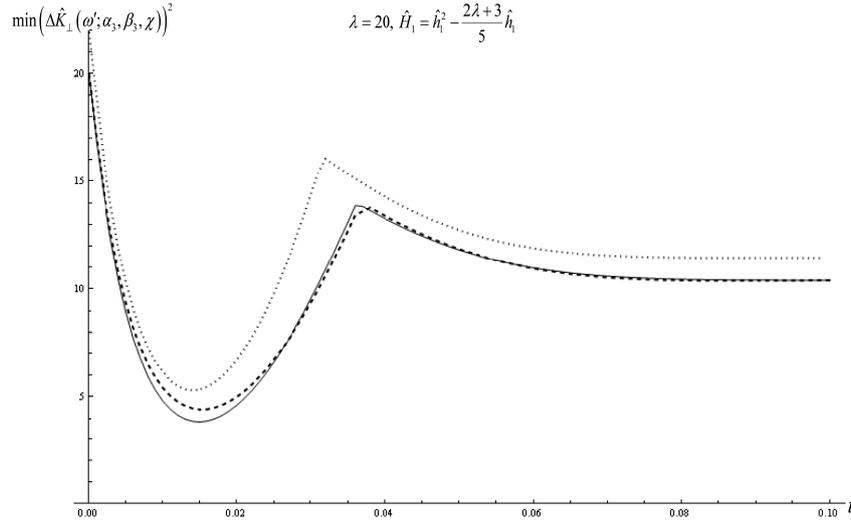$$\hat{H} = \omega_0\hat{S}_z + \Omega\hat{S}(\delta) + \chi\hat{S}_z^2 \tag{5.10}$$

Fig. 5.5: The time evolution of the minimum of $(\Delta\hat{K}_\perp(\omega';\alpha_3,\beta_3,\chi))^2$ under the Hamiltonian $\hat{H}_1$ for $\alpha_1' = \beta_1' = \alpha_2' = 0$, $\beta_2' = \arccos(-1/5)$ and $\lambda = 20$. The dotted line is plotted using approximate Wigner function in Eq. (5.25), the dashed line is obtained using the exact Wigner functions of Eqs. (4.66), (4.74) and (4.75) and the solid line shows the quantum mechanical calculations.

where A is the normalization factor. This approximation is useful in calculating the variance of $\hat{K}_\perp$ specially for large values of λ.

Fluctuations of $\hat{K}_\perp(\omega';\alpha_3,\beta_3,\chi)$, when evaluated using the initial coherent state evolved under Hamiltonian $\hat{H}_1$, depend on the parameters $\alpha_3,\beta_3,\chi = 6\gamma_1 + \gamma_2$ in such a way that there exist directions, parameterized by $\alpha_3^*,\beta_3^*,\chi^*$ in the tangent hyperplane, where the fluctuations are smaller than the fluctuations in the corresponding coherent state $|\omega'\rangle$. It remains to select from those directions the one along which the fluctuations are smallest to complete our definition of squeezing.

We analytically calculated the fluctuations $(\Delta\hat{K}_\perp(\omega';\alpha_3,\beta_3,\chi))^2$ using the standard phase space techniques, *i.e.* integrating the symbols of $\hat{K}_\perp(\omega';\alpha_3,\beta_3,\chi)$ and its square using the time-evolved Wigner function. A sample of the analytical calculations is given in appendix D.

Fig. 5.5 shows the time evolution of the smallest fluctuations of $\hat{K}_\perp(\omega';\alpha_3,\beta_3,\chi)$ with respect to α_3, β_3 and χ for the initial Wigner function of Eq. (4.66) and its approximation in Eq. (5.25) for $\lambda = 20$. The best squeezing direction $(\alpha_3^*,\beta_3^*,\chi^*)$ has been found through numerical minimization. The results are illustrative of a number of calculations performed for irreps of the type $(\lambda, 0)$ with λ ranging between 10 and 30. It is clear from the figure that semiclassical calculations using both the exact Wigner function and its approximate form are able to describe the squeezing up to the first minimum with a good approximation; for longer times the quantum mechanical plot has other dips that are not reproducible with the semiclassical method. This is because for longer times the Wigner function in the semiclassical approximation is not reliable as can be seen in Figs. 4.6 and 4.7. Again similar to the $SU(2)$ case, because of the numerical issues for longer times in the semiclassical approximation we have plotted the graphs in the region that both methods are in agreement.

From Fig. 5.6 we see that the time location of the minimum of $(\Delta\hat{K}_\perp(\omega;\alpha_3^*,\beta_3^*,\chi^*)(t))^2$ scales like $t_{\min} \approx \lambda^{-0.81}$ (right) and the minimum of $(\Delta\hat{K}_\perp(\omega;\alpha_3^*,\beta_3^*,\chi^*)(t))^2$ scales like $\lambda^{+0.67}$ (left). The values are different from the $SU(2)$ case, indicating that the squeezing is different in nature.
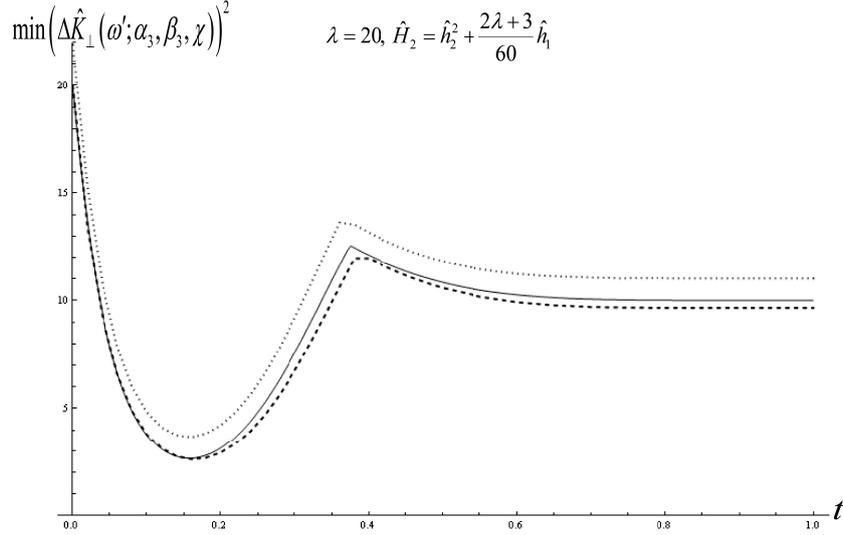
$$\min\left(\Delta\hat{K}_\perp\left(\omega';\alpha_3,\beta_3,\chi\right)\right)^2 \qquad \lambda=20,\ \hat{H}_2=\hat{h}_2^2+\frac{2\lambda+3}{60}\hat{h}_1$$

Fig. 5.7: The time evolution of the minimum of $(\Delta\hat{K}_\perp\,(\omega';\alpha_3,\beta_3,\chi))^2$ under the Hamiltonian $\hat{H}_2$ for $\alpha_1' = \alpha_2' = 0$, $\beta_1' = \frac{1}{2}\pi, \beta_2' = \pi$ and $\lambda = 20$. The dotted line is plotted using approximate Wigner function in Eq. (5.25), the dashed line is obtained using the exact Wigner functions of Eqs. (4.66), (4.74) and (4.75) and the solid line shows the quantum mechanical calculations.

from which we obtain

$$\cos\tilde{\beta}_2 = \sin^2\left(\frac{\beta_2}{2}\right) + \cos\alpha_1\sin\beta_1\sin^2\left(\frac{\beta_2}{2}\right) - 1\,. \tag{5.31}$$

Thus for this choice of initial state there is no α_2 dependence in the Wigner function. The evolved Wigner function is then obtained by substituting Eq. (5.31) in Eq. (4.66) where in Eq. (5.31) one must use $\alpha_1(t)$ from Eq. (5.28) instead of α_1.

For the observable in the tangent plane, $\hat{K}_\perp$ we have

$$\hat{K}_\perp\left(\omega';\alpha_3,\beta_3,\chi\right)$$
$$= D\left(\omega'\right)T\left(\alpha_3,\beta_3,\gamma_1,\gamma_2\right)\left(\hat{C}_{13}+\hat{C}_{31}\right)T^{-1}\left(\alpha_3,\beta_3,\gamma_1,\gamma_2\right)D^{-1}\left(\omega'\right)$$
$$= \frac{1}{\sqrt{2}}\left(\hat{C}_{12}+\hat{C}_{21}\right)\cos\left(\alpha_3-\tfrac{1}{2}\chi\right)\sin\left(\tfrac{1}{2}\beta_3\right)+\frac{i}{\sqrt{2}}\left(\hat{C}_{21}-\hat{C}_{12}\right)\sin\left(\alpha_3-\tfrac{1}{2}\chi\right)\sin\left(\tfrac{1}{2}\beta_3\right)$$
$$+\frac{1}{\sqrt{2}}\left(\hat{C}_{13}+\hat{C}_{31}\right)\cos\left(\alpha_3-\tfrac{1}{2}\chi\right)\sin\left(\tfrac{1}{2}\beta_3\right)+i\left(\hat{C}_{31}-\hat{C}_{13}\right)\sin\left(\tfrac{1}{2}\beta_3\right)\sin\left(\alpha_3-\tfrac{1}{2}\chi\right)$$
$$+i\left(\hat{C}_{32}-\hat{C}_{23}\right)\sin\left(\tfrac{1}{2}\chi\right)\cos\left(\tfrac{1}{2}\beta_3\right)-2\hat{h}_2\cos\left(\tfrac{1}{2}\chi\right)\cos\left(\tfrac{1}{2}\beta_3\right)\,. \tag{5.32}$$

Thus $W_{K_\perp}$ can be written easily using the symbols of $su(3)$ generators. The Wigner symbol of $\hat{K}_\perp^2$ is given in Eq. (5.23) wherein one must use $\alpha_1' = \alpha_2' = 0, \beta_1' = \frac{1}{2}\pi, \beta_2' = \pi$.

Fig. 5.7 shows the time evolution of the smallest fluctuations of $\hat{K}_\perp(\omega';\alpha_3,\beta_3,\chi)$ for the initial coherent state of Eq. (5.30) for $\lambda = 20$. The solid line is the quantum mechanical calculations, the dashed line is truncated semiclassical calculation using the exact Wigner function in Eq. (4.66) and the dotted line is plotted using the approximate Wigner function in Eq. (5.25). In comparison to Fig. 5.5 we see that the minimum is lower than the $\hat{H}_1$ case. This means we get more squeezing with the $\hat{H}_2$ Hamiltonian. Moreover the minimum occurs at a later time than the $\hat{H}_1$ case. Here again for the first dip in the squeezing graph the agreement between the